THE FUNCTIONAL IMPACT OF RETINOIC ACID AND RIP140 IN MACROPHAGES: FROM CHROMATIN TO PHYSIOLOGY

A DISSERTATION
SUBMITTED TO THE FACULTY OF
UNIVERSITY OF MINNESOTA
BY

BOMI LEE

IN PARTIAL FULFILLMENT OF THE REQUIREMENTS
FOR THE DEGREE OF
DOCTOR OF PHILOSOPHY

LI-NA WEI, ADVISOR

August 2016

Acknowledgements

First, I would like to thank my advisor, Dr. Li-Na Wei, for providing the mentorship to support me as an independent scientist in all aspects during my Ph.D training. I appreciate all her guidance, advice and support that allow me to develop my scientific thinking and skillsets.

I also feel thankful and grateful for that I worked with wonderful former and current graduate students and post-docs in Dr. Wei's lab. Working and discussing with them were delightful and great experiences for me to learn scientifically and personally. Without their assistance, all my thesis work would not have been possible to accomplish.

One of my projects about "RIP140 in osteoclasts" would not have been possible without the expertise of Dr. Anne Gingery in Mayo Clinic (Rochester) and other collaborators in Mayo Clinic and Oregon State University. I appreciate all the effort and hard work done by Dr. Gingery and collaborators.

I would like to thank Drs. Timothy Walseth, Hiroshi Hiasa, Kristin Hogquist for taking the time to serve on my committee and for the guidance they provided over the course of my thesis work.

Lastly, I thank my family and friends in Korea and here in Minnesota for their heartful love and support. Without their support, it must have been more challenging to accomplish my Ph.D training.

Abstract

Innate immunity consists of two systems; humoral and cellular systems. The humoral system includes anti-microbial peptides and opsonins while the cellular system involves specialized cells including phagocytes. The major functions of phagocytes are scavenging toxic compounds and producing inflammatory mediators to destroy infectious organisms and to transfer signals to other immune cells. Dysregulation of the phagocytic system by various conditions including the defect of immune cells and insufficient nutrition can lead to inflammatory diseases. Therefore, understanding the characteristics of phagocytes and the molecular mechanism in response to extracellular stimulations is critical for the development of therapeutics for inflammatory diseases. The focus of my thesis was to evaluate cellular signaling and its pathophysiological relationship in one type of phagocytes, macrophages.

All-*trans* retinoic acid (RA) and its derivatives have been proved as potent therapeutics for inflammatory diseases, but the molecular mechanism of RA action in macrophages was not well established. In order to shed light on the functional role of RA in macrophages, I first found that topical application of RA significantly improved wound healing and the co-stimulation with RA and IL-4 synergistically activated Arginase-1 (Arg1), a critical gene for tissue repair, in macrophages. This involves feed forward regulation of Raldh2, a rate-limiting enzyme for RA biosynthesis, and requires Med25 to remodel the +1 nucleosome of *Arg1* for transcription initiation and to facilitate transcriptional initiation-elongation coupling by recruiting elongation factor TFIIS. This

study demonstrated RA's modulatory activity in IL-4-induced anti-inflammatory macrophages, which involves synergistic activation of Arg1 by RA and IL-4 and a functional role of Med25 in chromatin remodeling of this gene promoter.

In macrophage activation, there are two well-established phenotypes; classically activated (M1, pro-inflammatory) and alternatively activated (M2, anti-inflammatory) macrophages. The switch from M1 to M2 is critical for the control of inflammatory responses including wound repair. Previously, it has been found that Receptor-interacting Protein 140 (RIP140) is an enhancer of M1 by acting as a co-activator for NF-κB. Related to this, my research has uncovered that RIP140 delays the wound healing process by suppressing the macrophage phenotype switch from M1 to M2. With regards to mechanism, IL-4 treatment stimulates RIP140 export from the nucleus to the cytoplasm to form a complex with calpain regulatory subunit (CAPNS1) to activate calpain1/2 that enhances the activity of PTP1B, a negative regulator for STAT6 in M2 macrophages. Together, these results have established a new modulatory role of RIP140 in macrophage phenotype switch during wound healing by regulating both M1 and M2 activations (enhancing M1 and suppressing M2 activation).

Another new finding I discovered about RIP140 was its repressive effect on osteoclast (OC) differentiation. OCs are derived from monocyte/macrophage lineage of hematopoietic cells and are responsible for bone resorptive activity. OCs maintain a balance in bone remodeling with osteoblasts (OB) that are involved in bone formation. RIP140 forms a complex with orphan nuclear receptor TR4 in pre-osteoclastic cells to suppress OC differentiation. Receptor Activator of Nuclear factor Kappa-B Ligand

(RANKL) induces RIP140 protein degradation and represses TR4 mRNA level, which terminates the repressive activity of TR4/RIP140 complex in OC differentiation. In vivo micro CT analysis of macrophage/monocyte-specific RIP140 KD (mϕRIP140KD) mice showed an osteopenia phenotype with reduced OB function and increased OC activity, indicating uncoupling between OC and OB. This study demonstrated RIP140's additional role in OC differentiation and bone diseases such as osteoporosis.

Taken all together, these studies have established fine-tuning molecular mechanisms in macrophages, including their phenotypic switch and polarization/maturation. Specifically, we uncovered additional pathways of signal inputs and stimuli that regulate these processes such as RA, IL-4 and RANKL, and determined their physiological relevance in wound healing, inflammation and osteoclastogenesis. Differential activation of macrophages by these biological cues further confirms the plastic nature of macrophages. These findings contribute to our understanding of signaling mechanisms in macrophage polarization and their impact on diseases.

Table of Contents

List of Figures

Chapter I

Introduction

Macrophages and wound healing

Macrophages belong to an innate immune group with well-established roles in pathogen elimination and housekeeping in a wide range of organisms. Macrophages have crucial roles in various physiological and pathological processes, such as embryo development and inflammatory diseases where tissue remodeling and repair dynamically occur[1-3]. One of essential characteristics of macrophages is the functional and phenotypic diversity that allows their dynamic roles in appropriate tissues and organs. There are two well-established phenotypes, classically activated macrophages (pro-inflammatory, M1) and alternatively activated macrophages (anti-inflammatory, M2)[4]. M1 phenotype is characterized by the production of pro-inflammatory cytokines and reactive oxygen intermediates for their microbicidal and tumoricidal activities. In contrast, M2 activation involves tissue repair, parasite containment and the resolution of inflammatory responses.

Wound healing or tissue repair after injury is one of fine-tuned protective mechanisms that occurs in our healthy organs and tissues. Wound healing consists of several essential processes including inflammation, proliferation and remodeling[5,6]. Disruption of each phase can lead to tissue destruction and fibrosis. During the inflammatory process, primary line of immune cells, such as neutrophils, macrophages and mast cells, infiltrate into wound sites in response to cytokines released from platelets mainly working on removing foreign organisms and damaged materials. In the proliferation step, transforming growth factor beta (TGF-β) secreted from macrophages and T cells stimulates fibroblasts to produce collagen, proteoglycans and fibronectin for the new matrix. Lastly, proteolytic enzymes produced by fibroblasts, neutrophils and

macrophages degrade collagen in the remodeling step. Notably, macrophages are involved in all the phases of complicated wound repair with crucial roles, such as host defense, phagocytosis and paracrine cytokine secretion.

Macrophages found at different stages of wound repair show functionally different phenotypes, and this phenotypic switch is critically regulated during wound healing[7]. At the early phase of wound repair, macrophages are mainly M1 macrophages characterized with pathogen killing, while M2 macrophages are predominant at the later phases of wound healing. Although this macrophage phenotypic switch, from M1 to M2, in wound healing processes is first confirmed in vitro, more studies have sought to determine macrophage phenotypes at wound sites in vivo by measuring phenotypic marker gene expression. Still, molecular mechanisms or key molecules involved in modulating macrophage phenotype switch have not been well established.

Retinoic Acid in Immunity

During the last 100 years, many studies have proved that vitamin A is one of essential dietary components for our body. All-*trans* retinoic acid (RA), the active metabolite of vitamin A, has essential roles in various biological functions including embryonic development, vision and brain function[8-10]. The crucial role of vitamin A in immune system has been implicated from the recognition that vitamin A deficiency has a positive correlation with increased susceptibility to infectious diseases. The effect of RA has been found in innate immune cells including monocytes/macrophages and dendritic cells (DCs) as well as adaptive immune cells, such as T cells and B cells[11,12]. For

example, RA induces DCs migration to support antigen-presenting role of DCs[13]. RA is also a key mediator in T-cell homing by inducing gut-homing receptors, α4β7 and CCR9, and in $CD4^+$ regulatory T cell differentiation by enhancing Foxp3 expression[14,15]. More importantly, antigen-presenting cells (APCs) including DCs and macrophages can produce RA by expressing RALDHs, key rate-limiting enzymes in retinoid metabolism, to target other immune cells[16,17]. Among APCs, functional role of RA in macrophages has been reported mostly as an inducer for Th2-type cells to establish anti-inflammatory environment[17,18]. However, the exact mechanism by which RA modulates anti-inflammatory macrophages remains to be studied.

Receptor Interacting Protein 140

Receptor interacting protein 140 (RIP140, also known as Nrip1) has been known as a co-repressor or co-activator for a number of nuclear receptors and transcription factors including ER, TR2, PPARs, RAR/RXR and NF-κB[19-22] with imperative roles in gene regulation related to various biological processes, such as development, metabolism and inflammation[23,24]. RIP140 is widely expressed, and its expression is controlled by hormones or biological ligands, such as estrogen, retinoic acid and cholesterol[25-27]. Proteomic analyses of RIP140 revealed various post-translational modifications including methylation, acetylation, phosphorylation, PLP conjugation and sumoylation, which subsequently modulate RIP140's subcellular localization, functional activity, interacting proteins and protein stability[28-33]. RIP140 knockout mice exhibit two major phenotypes, female infertility and impaired energy homeostasis, implicating its crucial roles in ovary,

adipose tissue, muscle and liver[34,35].

Recent studies demonstrate that RIP140 is a positive regulator for inflammatory responses by acting as a co-activator for NF-κB[22], which is a master transcription factor in inflammatory genes. RIP140 deletion in macrophages abrogated lipopolysaccharide (LPS)-induced pro-inflammatory cytokine production suggesting RIP140's role in M1 macrophage activation. Interestingly, RIP140 mRNA and protein levels are upregulated by cholesterol via lowering miRNA-33 that can target 3'UTR of RIP140 mRNA in macrophages resulting in increased RIP140 coactivator activity for NF-κB in inflammatory responses[27]. Furthermore, it has been found that NF-κB-mediated signaling degrades RIP140 protein, which allows the resolution of inflammatory responses and endotoxin tolerance by reducing inflammatory target gene expression[36]. Macrophage-specific RIP140 knockdown mice show improved systemic insulin sensitivity and white adipose tissue browning under a high-fat diet challenge. The mechanism is through the regulation of circulating monocyte population and altered adipose tissue macrophage profile, increasing M2 activation and decreasing M1 macrophages, in white adipose tissue[37]. These results prompted us to speculate about RIP140's functional roles in M2 activation and in the macrophage phenotype switch, which is critically regulated in inflammatory processes, such as wound healing.

Osteoclast Differentiation and Osteopenia/Osteoporosis

Osteoclasts are tissue-specific macrophages derived from the monocyte/macrophage lineage of hematopoietic cells[38]. The major function of osteoclasts

is degrading bone matrix by secreting acid and lytic enzymes in extracellular compartments, in which osteoblasts synthesize bone to replace the amount of degraded bone[39,40]. The balance between bone resorption by osteoclasts and bone formation by osteoblasts has been known to be critical in maintaining bone structure and bone mass. This process is so called bone remodeling that occurs throughout life replacing about 5-10% of the adult human skeleton every year[41]. Disruption of bone remodeling can trigger skeletal diseases including osteoporosis and rheumatoid arthritis, which are characterized by markedly enhanced osteoclast activity and bone resorption[42]. Therefore, understanding molecular mechanisms in osteoclast biology, such as differentiation and the coupling process of osteoclasts with osteoblasts, will provide evidence to support the development of therapeutic strategy in skeletal diseases with bone loss.

There are two major triggers in osteoclast differentiation, macrophage colony-stimulating factor (M-CSF) and receptor activator of nuclear factor κB ligand (RANKL)[43,44], both produced by mesenchymal cells, such as osteoblasts and stromal cells. M-CSF binds to its receptor, c-FMS, and transmits its signals to downstream molecules including PI3K and Akt to activate the proliferation and survival of pre-osteoclasts[45]. RANKL binds to its receptor, RANK in osteoclasts, which then activates various signaling cascades including NF-κB, mitogen-activated protein kinase (MAPK) pathways and calcium signaling[46]. At the end of these signaling cascades, major transcription factors that activate osteoclast marker genes are NFATc1, NF- κB, PU.1, MITF and c-fos [47-50]. Among these factors, NFATc1 (Nuclear factor of activated T cells, cytoplasmic 1) is the master regulator for osteoclast differentiation by self-activation and

targeting broad range of osteoclast marker genes, such as cathepsin K (CtsK) and tartrate-resistant acid phosphatase (TRAP, Acp5)[51]. Recent studies demonstrated repressive mechanisms of RANK signaling cascades and downstream transcriptional regulations that inhibit osteoclast differentiation and bone resorption activity through negative regulators including NF- κB p100, Ids, MafB and IRF-8[52-55]. It is also crucial to identify endogenous molecules that play critical roles in the maintenance of bone homeostasis, remodeling and the coupling of osteoclasts and osteoblasts, thereby providing potential therapeutics for a variety of pathological conditions where bone homeostatic control is disrupted, such as osteoporosis, osteopenia and rheumatoid arthritis.

With an understanding of macrophage biology and regulatory signals such as RA and modulation of RIP140 function, I aimed to uncover their functional roles, molecular mechanisms of action and physiological impact. My three objectives were to understand i) RA in anti-inflammatory macrophage activation and wound healing, ii) the role of RIP140 in macrophage phenotype switch, and iii) RIP140 in osteoclast biology and bone health.

Preface

This chapter has been published:

Bomi Lee, Cheng-Ying Wu, Yi-Wei Lin, Sung Wook Park and Li-Na Wei (2016) Synergistic activation of Arg1 gene by retinoic acid and IL-4 involves chromatin remodeling for transcription initiation and elongation coupling.

Nucleic Acids Research, doi: 10.1093/nar/gkw392

*Contribution: B.L. designed the experiments and analyzed the data. B.L., C.Y.W. and Y.W.L. performed the experiments. B.L., C.Y.W. and S.W.P. discussed the results and commented on the discussion. The manuscript was written by B.L. and L.N.W.. L.N.W. provided financial support.

Chapter II

Synergistic activation of Arg1 gene by retinoic acid and IL-4 involves chromatin remodeling for transcription initiation and elongation coupling

Introduction

All-trans Retinoic acid (RA), the principal active ingredient of vitamin A, plays crucial roles in a wide spectrum of biological processes, such as development, vision, reproduction, cell proliferation/differentiation and immune function [9,56-58]. It is one of the most potent therapeutics for diseases like acute promyelocytic leukemia, inflammatory diseases, psoriasis and wound repair for its anti-tumor and potent immune-modulatory effects [59,60]. Studies have shown that retinoids can enhance wound healing in preoperative use, but clinical application for tissue repair has remained contradictory due to toxicity elicited by their prolonged use [61,62]. This has been suggested to involve an alteration in arginine metabolism [63]. The molecular mechanism by which RA affects wound healing remains unclear.

Nutritional studies have established that RA deficiency is frequently associated with elevated susceptibility to infectious diseases, and that RA is important to the development and functions of multiple immune cells such as dendritic cells, T cells and B cells [11,64,65]. RA is particularly critical for promoting mucosal immunity by inducing gut-homing effector T cells and IgA-producing B cells. RA is also known to regulate Foxp3+ regulatory T cell and Th17 effector T cell differentiation [15,66,67]. Endogenously, RA can be synthesized in various cell types particularly antigen presenting cells (APCs), such as macrophages and dendritic cells. APCs are principal players in innate immunity, and are active in RA biosynthesis [17,68]. These cells express rate-limiting enzymes in RA biosynthesis, retinal dehydrogenases (Raldhs) that catalyze the conversion of retinal to RA. In APCs, RA is known to regulate Raldhs gene expression in conjunction with inputs

from pro- or anti-inflammatory cytokines [69-71], resulting in functional amplification of immune responses. However, the physiological relevance remains to be elucidated.

RA binds to nuclear RA receptors (RARs) that act as transcription factors and interact with co-regulators to regulate target gene transcription. The Mediator complex is a multi-unit co-regulator that recruits RNA Pol II and basal transcriptional machinery [72,73]. Certain subunits, such as, MED1, MED17 and MED25, are known as RAR or RXR-interacting proteins [74-76]. IL-4, an anti-inflammatory cytokine, binds to its receptor, IL-4R, which is then auto-phosphorylated and activates JAK1/3. The phosphorylated JAK1/3 recruits and phosphorylates signal transducer and activator of transcription 6 (STAT6), which is then translocated to the nucleus as a homodimer and acts as a master transcription activator for M2 macrophage gene expression [77]. It is believed that signal integration between RA and various cytokines contributes to RA's potent actions in immune modulation [17,69,70].

Macrophages are the principal innate immune cells and play a central role in inflammation, host defense and resolution of inflammation. Upon activation, macrophages exhibit, mainly, classical, pro-inflammatory activation (M1) or alternative, anti-inflammatory activation (M2) [4]. M1 macrophages are characterized by high levels of pro-inflammatory cytokines, reactive nitrogen and oxygen intermediates, and harbor strong microbicidal and tumoricidal activities. M2 macrophages are involved in the resolution of inflammation and parasite containment and promote wound healing, tissue remodeling and fibrosis. Arginase-1 (Arg1) is a cytosolic enzyme which catalyzes arginine hydrolysis to urea and ornithine [78]. The production of urea allows excess

nitrogen to be removed from the body, and ornithine can be used to generate polyamines and proline, which is important for collagen synthesis and wound healing. As such, Arg1 is a prototypic marker for M2 activation, and its gene regulation involves multiple transcription factors (STAT6, C/EBPβ, KLF4, PU.1 and nuclear receptors RAR, RXR and PPARγ) [79]. Among these, a cytokine responsive enhancer for STAT6 binding, located 3 kb upstream [80] and an RA response element located 1 kb upstream of the proximal promoter [70] are most noticeable. But how these hormones/cytokines coordinately regulate Arg1 expression on the chromatin level is unclear.

In this study, we found that RA and IL-4 synergistically facilitate wound healing in mice and dampen inflammatory responses. On the genome level, the synergism occurs rapidly and specifically, which is to robustly activate Arg1 expression in M2 macrophage. This involves RA feed forward regulation of Raldh2 and dual functions of Med25. Mechanistically, Med25 coordinates the remodeling of a specific nucleosome spanning the transcription initiation site of Arg1 gene and facilitates elongation by recruiting transcription elongation factor TFIIS. Feed forward regulation of Raldh2 provides endogenous RA source to sustain prolonged Arg1 activation that is required for wound healing.

Materials and Methods

Reagents

Reagent sources: all-trans RA (Sigma, R-2625), 0.1% Tretinoin cream (Boynton Health Service at the University of Minnesota), IL-4 (Cell signaling #5208), AGN 193109 (pan-

RAR antagonist, Santa Cruz CAS 171746-21-7), LPS (lipopolysaccharide, Sigma, L4391). Antibodies for STAT6 (M-20, sc-981), RAR (M-454, sc-773), RARβ (C-19, sc-552), RNA Pol II (sc-899), Brg1 (H-88, sc-10768), TFIIS (B-6, sc-393520), β-actin (C4, sc-47778) are from Santa Cruz. Antibodies for MED25 (Aviva systems biology, OAAB00209), H3.3 (Abcam, ab62642), H3k36me3 (Active motif, 61101), Arginase-1 (Cell signaling, #9819) are from indicated companies.

Animals

All studies were carried out using male C57BL/6J mice from The Jackson Laboratory and maintained in the animal facility of the University of Minnesota. Animal studies were approved by the University of Minnesota Institutional Animal Care and Use Committee.

In vivo wound healing assay

As described in [81], cutaneous wounds were made on both sides of the shaved mice back (2 wounds per animal, n=6) with a 5 mm round biopsy punch under anesthesia. Wound size was recorded daily, and reagents (control cream or 0.1% Tretinoin cream) were applied on wounds until day 5. Wound size were measured and analyzed by Image J (NIH).

Cell culture, lentivirus production and transduction

RAW264.7 cells were cultured in Dulbecco's Modified Eagle Medium (DMEM) supplemented with 10% fetal bovine serum (FBS) and 1% antibiotics. STAT6 KD and Med25 KD lentivirus were produced in 293TN cells using lentivirus packing system (System Biosciences). Lentivirus constructs and package plasmids were transfected using Lipofectamine 2000 (Thermo Fisher Scientific) and incu- bated for 3 days. Cell culture

medium containing virus soup was collected and concentrated with Lenti-X Concentrator (Clontech) overnight. Viruses were centrifuged and mixed with fresh medium, stored in −80◦ freezer. STAT6 and Med25 shRNA lentivirus constructs were purchased from Genomic Center at the University of Minnesota:

-Full hairpin sequence for STAT6 KD:

#1-CCGGGCCACCTTATGATCTTGGAATCTCGA

GATTCCAAGATCATAAGGTGGCTTTTTG

#2-CCGGCGGCTGATCATTGGCTTTATTCTCGA

GAATAAAGCCAATGATCAGCCGTTTTTG

#3-CCGGCCACAGTCCATCCACTCATTTCTCGA

GAAATGAGTGGATGGACTGTGGTTTTTG

#4-CCGGCGGTTCAGATGCTTTCTGTTACTCGA

GTAACAGAAAGCATCTGAACCGTTTTTG

-Full hairpin sequence for Med25 KD:

#1-TGCTGTTGACAGTGAGCGACCAGGTCATCA

CCAACCACAATAGTGAAGCCACAGATGT

ATTGTGGTTGGTGATGACCTGGCTGCCTACTG CCTCGGA

#2-TGCTGTTGACAGTGAGCGCCCGGAACTCAA

GAATGGTTCATAGTGAAGCCACAGATG

TATGAACCATTCTTGAGTTCCGGATGCCTACT GCCTCGGA

#3-TGCTGTTGACAGTGAGCGACTCAGGCTCTC

TGCAGACCAATAGTGAAGCCACAGATGT

ATTGGTCTGCAGAGAGCCTGAGGTGCCTACTG CCTCGGA

#4-TGCTGTTGACAGTGAGCGCCTCAAGAATGG

TTCAGTTCCATAGTGAAGCCACAGATGT

ATGGAACTGAACCATTCTTGAGTTGCCTACTG CCTCGGA

RNA isolation, gene expression analyses and Immunoblotting

Total RNA was isolated using TRIzol (Invitrogen). Reverse transcription (RT) was performed by using High-Capacity cDNA Reverse Transcription Kit (Applied Biosystems). Quantitative real-time PCR (qPCR) was performed with SYBR enzyme mix (Applied Biosystems). Each gene ex- pression experiment was performed in triplicate. Expression levels were normalized to β-actin mRNA level. For the immunoblotting, cells were lysed in radioimmunoprecipitation assay (RIPA) buffer. Protein was quantified with Brad- ford method and separated by 10% SDS-PAGE gel.

Chromatin-immunoprecipitation (ChIP) assay

RAW264.7 cells were cross-linked with 1% formaldehyde. Cell pellets were lysed with NP40-lysis buffer. Nuclear extracts were sonicated and immunoprecipitated with antibodies and protein A/G beads overnight. Beads were washed, and DNA-protein complex was eluted from beads. Following reverse-crosslinking, DNA was isolated and DNA enrichment was analyzed by qPCR with primer sets for the indicated regions of Arg1 gene.

-Arg1 enhancer STAT6 binding site: (F) TGAACA GGCTGTAGCCAACA,

(R) AGCACCCTCAACCCA AAGTG,

-Arg1 RARE: (F) CAGGTTGCAGAAGAATCGAA,

(R) TGACACTCTGCTGGTGTGTAGA,

-Arg1 +1 Nucleosome: (F) GAAAAAGATGTGCC CTCTGT,

(R) AGAGAGACCCAAGGTCGCCG.

Nucleosome positioning assay

As described in [82], RAW264.7 cells nuclear extracts were digested with 30U of MNase at 37◦C for 30 min, and digested genomic DNA was purified. The specific DNA regions were amplified with 20 primer sets by using qPCR. The nucleosome positions were determined by the ratio of digested/undigested DNA. Each primer set amplified about 100 bp product with an average of ~60 bp overlap to achieve mononucleosome resolution. Data represent average gene amplification signal protected against MNase digestion from three biological replicates.

The measurement of pre-mRNA synthesis

As modified from[83], RAW264.7 cells were treated with DRB (5,6-Dichloro-1-β-D-ribofuranosylbenzimidazole, Sigma D-1916) for 3 h, and cells were treated with IL-4 or IL-4/RA. Cells were collected every 10 min after the stimulation. Total RNA was extracted with High Pure RNA isolation kit (Roche), and newly synthesized pre-mRNAs were measured with primer sets that can detect Arg1 intron 7-exon 8 by using qRT-PCR.

In vitro arginase activity

RAW264.7 cells were lysed with RIPA buffer, and arginase activity from each sample was measured according to manufacturer's instruction (Sigma, MAK112). Arginase catalyzes arginine to urea and ornithine, and the urea reacts with the substrate to generate a colored product, which is proportional to the arginase activity. The arginase activity of

a sample was determined by measuring the absorbance at 430 nm.

Statistical analysis

Experiments were performed at least three times and results were presented as means ± SD. Student's t-test was used. P values of 0.05 or less were considered statistically significant (*P < 0.05; **P < 0.01; ***P < 0.001).

Results

RA enhances wound healing in mice and promotes anti- inflammatory macrophage activation by synergizing with IL- 4 to activate Arg1 expression

Although RA can regulate both pro- and anti-inflammatory genes in APCs, in general, RA signaling ultimately establishes an anti-inflammatory environment [12]. We first employed a wound-healing model in the mouse to determine how RA affects the healing process, which involves, mainly, the anti-inflammatory (alternative, or M2, macrophage activation) response. Wounds were created on both sides of the back of the mouse, and monitored for 5 days with or without topical RA application (0.1% Tretinoin cream). As shown in Fig. 2-1A, RA-treated mice exhibited significantly improved wound closure (57.7%) as compared to control mice (21.9%) as early as 1 day after wound creation. During wound healing, alternative (M2) macrophage activation is crucial following initial inflammatory (classical, or M1 macrophage activation) response [84]. Therefore, we examined Arg1 mRNA expression, a key M2 marker, in wounded tissues. Indeed, Arg1 mRNA level was significantly elevated in RA cream-treated animals, indicating in-creased M2 activation by RA treatment (Fig. 2-1A right). M2 activation is typically

triggered by anti-inflammatory cytokines such as IL-4 and IL-13 [78]. To examine whether RA and anti-inflammatory cytokines individually or combinatorially affect gene expression in macrophage activation, we profiled gene expression in cultured macrophages during pro- and anti-inflammatory responses (Fig. 2-1B and 2-2A).

It appeared that, for LPS-stimulated macrophages (for pro-inflammatory M1 response), supplement with conditioned medium (CM) derived from IL-4/RA co-treated RAW264.7 macrophages (M2 macrophage) dampened their expression of inflammatory cytokine genes such as TNF-α and IL-6 genes (Fig. 2-1B). These results demonstrate the suppression of inflammation by RA/IL-4 stimulated M2 (anti-inflammatory) macrophage activation. To comprehensively examine changes in gene expression during the anti-inflammatory phase, which is most critical to wound healing, we first employed microarrays to profile genes synergistically induced by IL-4/RA co-treatment. These were further validated quantitatively by qRT-PCR (Fig. 2-2A). Very interestingly, only the Arg1 gene exhibited a robust synergistic induction by IL-4/RA (about 140- fold higher than control treatment) in M2 activation. This result revealed that IL-4 and RA synergize to robustly activate Arg1 gene, a gene most critical to tissue repair, which can lead to an important functional outcome, i.e. enhanced wound healing. Arg1 gene regulation by IL-4, RA or IL- 4/RA co-treatment was further validated in experiments using primary macrophages (Fig. 2-2B). Interestingly, Arg1 activation by IL-4/RA co-treatment was sustained over a period of 24 h (Supplementary Fig.2-S1A). Western blot data confirmed synergistic elevation in Arg1 protein level stimulated by IL-4/RA co-treatment (Fig. 2-2C). Sustained Arg1 expression would require continuous supply of RA

in M2 polarized macrophages, which is supported by the finding of significant activation of Raldh2, a rate-limiting enzyme for RA biosynthesis, as demonstrated using primary bone marrow-derived macrophages (BMDM). For a comparison (Fig. 2-2D), we found that LPS enhanced Raldh2 expression for a 31-fold in M1 macrophages, but IL- 4 and RA co-treatment robustly (for a 671-fold) induced its expression in M2 macrophages. This synergism was reduced by AGN (a pan RAR antagonist), suggesting activation elicited by a canonical, RAR-mediated event. It appeared that synergistic activation of Raldh2 by IL-4 and RA was sustained over 24 h (data not shown), indicating that this positive feed forward mechanism could be critical for maintaining enhanced Arg1 activation for a longer period during the healing process. These data show robust induction of Arg1 by RA and IL-4 co-treatment in M2 macrophages, which involves RA's feed forward regulation of Raldh2 that contributes to sustained Arg1 expression and enhanced wound healing.

STAT6 and RAR are required for the synergistic effect of IL- 4 and RA on Arg1 expression

To determine whether synergistic activation of Arg1 gene by RA and IL-4 was mediated by canonical pathways, i.e. through the actions of RAR and STAT6, we employed both pharmacological and genetic approaches. RAW264.7 macrophages were pre-treated with a RAR pan-antagonist, AGN to block the actions of RARs (Fig. 2-3A), which indeed dampened the synergistic induction of Arg1 expression in a concentration-dependent manner. The synergism was also significantly reduced in two independent STAT6 stably knockdown (STAT6 KD-1,2) clones as compared to control knockdown (Ctrl KD) clones

(Fig. 2-3B and Supplementary Fig. 2-S1B). Furthermore, a combination of AGN pre-treatment and STAT6 KD almost completely abolished the induction of Arg1 gene by IL-4 and RA (Fig. 2-3C). Interestingly, among the three RAR isoforms (RARα, β, γ), only RARβ responded to RA or RA/IL-4 treatment in this cellular context (Fig. 2-3D), indicating that RARβ may be the one mediating RA activation of Arg1 gene in macrophages. To determine the targets on the Arg1 gene promoter responding to RA and IL-4, we employed a luciferase reporter system to dissect STAT6 binding sites in the upstream enhancer (for responding to IL-4) and RARE near the promoter (for responding to RA). As shown in Fig. 2-3E, the reporter construct containing both the IL-4-responsive enhancer and the RARE showed a synergistic effect of IL-4 and RA whereas constructs deleted in either the enhancer or the RARE exhibited no synergistic effect. Therefore, the canonical signaling pathways of IL-4 and RA, mediated through their corresponding genetic elements (STAT6 binding site and RARE), are responsible for the synergistic activation of Arg1 in IL-4 stimulated M2 macrophages co-treated with RA.

Med25 plays dual functional roles in synergistic activation of Arg1 by IL-4 and RA, involving remodeling +1 nucleosome for transcription initiation and enhancing transcription elongation

To examine the molecular events mediating the robust synergism of IL-4 and RA on Arg1 gene, we first validated that RARβ and STAT6 were indeed recruited to the endogenous chromatin regions of Arg1 gene upon RA/IL-4 co-treatment using chromatin immunoprecipitation (ChIP) assay (Fig. 2-4A). The data showed similar levels of recruitment of RARβ and STAT6 by RA/IL-4 co-treatment as compared to single

treatment, ruling out the possibility of enhanced transcription factor recruitment by co-treatment. Given that the enhancer and RARE are separated by a relatively long (~2 kb) distance, we speculated a role for the Mediator complex that might act to bridge RARE and the enhancer. It appeared that among several reported RAR-interacting Mediator components, only Med25 recruitment was increased on the enhancer and the +1 nucleosome regions in IL-4/RA co-stimulated cells (Fig. 2-4B). Since Med25 recruitment occurred after the recruitment of STAT6 and RARβ (Supplementary Fig. 2-S2A), Med25 is likely to be recruited by RARβ or STAT6. This was confirmed in the two following findings: IL-4/RA-induced Med25 enrichment to the +1 nucleosome region was dampened by AGN-pretreatment (Fig. 2-4C, left), and its recruitment to the enhancer region was reduced by STAT6 KD (Fig. 2-4C, right). Finally, the functional role for Med25 was validated in the experiments using loss- of-function (Med25 KD) (Fig. 2-4D) and gain-of-function (over-expression, Supplementary Fig. 2-S3A) approaches.

Med25 belongs to the Mediator complex that recruits general transcription machinery including RNA Pol II to the target promoter. To investigate whether Med25 may also regulate other M2 genes, we monitored M2 markers' mRNA expression patterns in control KD and Med25 KD macrophages upon IL-4 stimulation. As shown in Supplementary Fig. 2-S3B, most M2 genes were not affected by Med25 KD, such as Chi3l3, Retnla and Pparg, except for Mrc1 gene. Thus, RA/IL-4 synergism during M2 activation, which requires the Med25, seems to occur only on selected M2 genes, such as the Arg1 gene. Interestingly, MED1, also a RAR-interacting Mediator component [74], is not involved in the synergistic induction of Arg1 by IL-4 and RA (Supplementary Fig. 2-

S3C), suggesting a unique role for Med25 in mediating synergism of RA and IL-4 on Arg1 gene. Sequential ChIP (Re-ChIP) assay revealed that Med25 forms a complex with STAT6, most evidently on the +1 nucleosome region and the enhancer region (Fig. 2-4E); whereas STAT6 and RARβ complex formation occurred mainly on the enhancer region (Supplementary Fig. 2-S4A). These data show that Med25, recruited by RARβ and STAT6, is required for the synergistic activation of Arg1 gene by IL-4 and RA through enhanced transcription factor-Mediator complex formation on the initiation site covered by the first (+1) nucleosome. Thus, transcription factors/cofactors recruitment on the Arg1 gene regulatory region occurs sequentially, with each transcription factor first recruited to its own corresponding DNA element upon stimulation, which then alters the recruitment of other co-activators such as the Mediator complex to transcription initiation site to stimulate transcription initiation.

It is known that nucleosomes spanning the gene promoter region affect RNA pol II recruitment for transcription initiation [85]. To survey nucleosome occupancy on Arg1 gene, we employed MNase-digestion to generate mono- nucleosomes and scanned nucleosome occupancy on the Arg1 gene regulatory regions (nucleosome array, Fig. 2-5A). Interestingly, the intensity of the nucleosome spanning exon 1 region was most robustly reduced in cells stimulated by RA or IL-4/RA. This result suggests that this +1 nucleosome is destabilized mainly by RA treatment (Fig. 2-5B). Consistently, this effect was blocked by AGN pre-treatment (Fig. 2-5C, upper). In Med25 KD stable clones, we found that Med25 KD also mainly affected this +1 nucleosome (Fig. 2-5C, bottom). We then determined which of the two ATP-dependent chromatin remodelers, Brg1 and Brm,

was involved and found that the recruitment of Brg1, but not Brm, on +1 nucleosome region was significantly enhanced upon IL-4 and RA co-treatment. Further, this was dampened by Med25 KD (Fig. 2-6A, left, Supplementary Fig. 2-S4B). Together, the data show that IL-4/RA stimulation destabilizes, specifically, the +1 nucleosome, which involves RAR- and STAT6-recruited Med25 and its subsequent recruitment of the ATPase chromatin remodeler Brg1.

Among various steps of the transcription process, we found that Med25 KD reduced the recruitment of RNA Pol II, a major component of transcriptional pre-initiation complex, and the expected histone variants/post-translational modifications (PTM) (Fig. 2-6A, second left). Among the histone variants, H3.3, known as an active histone variant with H2A.Z [86], was most dramatically augmented by IL-4/RA co-treatment, which was reversed by Med25 KD (Fig. 2-6A, middle). Surprisingly, H3K36me3 enrichment, a histone marker related to transcription elongation [87], was also significantly enhanced upon IL-4/RA co-treatment, which was also abolished by Med25 KD (Fig. 2-6A, second right). This result suggests an extended Med25 function in transcription elongation, which was supported by the finding of enhanced recruitment of TFIIS, an elongation complex component and an inducer of catalytic mode of promoter-bound Pol II [88]. Importantly, this was also abolished by Med25 KD (Fig. 2-6A. right). To further substantiate the synergistic effects of RA/IL-4 on transcription elongation of Arg1, we monitored newly synthesized pre-mRNA of Arg1 every 10 min by removing pre-existing pre-mRNA through blocking transcription with 5,6-Dichloro-1-β-D-ribofuranosylbenzimidazole (DRB), a RNA Pol II-dependent elongation inhibitor, for 3 h

before the stimulation (Fig. 2-6B, left) [83]. Primers spanning intron 7 and exon 8 regions were used in qRT-PCR to quantify pre-mRNA accumulation. Indeed, the relative level of pre-mRNA in cells co-stimulated with IL-4 and RA was much higher than when stimulated with IL-4 alone, and the difference was readily evident in 30 min (Fig. 2-6B, right). These data indicate that co-stimulation of IL-4 and RA accelerates RNA Pol II release from pausing for transcription initiation and also enhances progression from initiation to elongation possibly by Med25-dependent recruitment of elongation factors such as TFIIS (as shown in Fig. 2-6A). Finally, we validated the functional role of Med25 in IL-4/RA's synergistic activation of Arg1 enzyme activity as shown in Fig. 2-6C.

Discussion

Vitamin A deficiency has long been associated with delayed wound healing and delayed recovery following inflammation [56]. Therefore, retinoids have been very useful in dermatology. Preoperative use of retinoids to enhance wound healing has been clinically documented, which involves stimulation of collagen synthesis, epithelialization and angiogenesis [62,89-91]. Our current study unambiguously demonstrates the molecular and cellular bases underlying a robust synergism of RA and anti-inflammatory cytokine IL-4 on Arg1, a gene critical to the wound healing processes. Importantly, this involves RA feed forward regulation of Raldh2 and requires dual functions of Med25, which accelerates nucleosome remodeling for transcription initiation and enhances transcription elongation.

There are two distinct isoforms of arginase in mammalian cells. Arginase 1

(encoded by Arg1) is a widely expressed cytosolic enzyme with a principal role in the hepatic urea cycle; whereas arginase 2 (encoded by Arg2) is a mitochondrial enzyme with limited expression only in certain organs such as kidney, brain and liver. Importantly, Arg1 has been known to play important roles in anti-inflammation, tumor immunity, fibrosis and immunosuppression-related diseases mainly because of its activity in regulating L-arginine metabolism in immune cells including macrophages [92-94]. As such, controlling Arg1 expression levels through the synergism of RA with anti-inflammatory cytokine IL-4 can provide a potential therapeutic strategy in treating inflammatory diseases that may be further exploited clinically.

Interestingly, the synergism of IL-4 and RA co-treatment yielded a 4-fold increase in Arg1 enzyme activity, whereas the effect on Arg1 mRNA levels was detected for hundreds- to thousands-fold higher than control treatment. This suggests that while the enhanced capacity to produce Arg1 enzyme is critical for wound healing, there are additional regulations needed to control the level of this enzyme activity in the very dynamic process of wound healing, such as by regulation at translational/post-translational levels. This requires further investigation in future studies. In our animal wound healing experiments (Fig. 2-1 and Supplementary Fig. 2-S1), elevation of the Arg1 mRNA level, stimulated by RA/IL-4 co-treatment, was sustained for longer than 1 day (Supplementary Fig. 2-S1 shows sustained elevation after 24 h, and our unpublished data show sustained elevation can be as long as 3 days). In order to monitor direct effects of RA and IL-4 on endogenous Raldh2 expression, we have routinely measured Raldh2 mRNA levels at early time points, such as 6 h post-stimulation (Fig. 2-2D); however, it

appears that Raldh2 regulation by RA can last as long as 24 h (data not shown). Presumably, this is to en- sure the endogenous supply of RA, which would be required for prolonged activation of Arg1 gene during wound healing without pharmacological intervention. An interesting question arises as to the dampening of this feed forward regulation of Raldh2 by RA in a physiological context. Since efficient Raldh2 activation in M2 macrophages requires IL-4 stimulation, reduction in immune cytokines, including IL-4, in the wounded tissues as the healing process occurs would likely provide a break to prevent continuous activation of Raldh2 gene later after healing has completed and RA is no longer needed.

MED25 was originally identified as a PTOV1 relative [95] and is also identical to ARC92/ACID1, which is a direct target of the activator VP16 [96]. The Mediator complex is highly conserved from yeast to humans [97]. There may be an evolutionary advantage of MED25 in higher eukaryotes given that it is not found in Caenorhabditis elegans or yeast. Although MED25 has similar features with MED1 in its domains and the action on nuclear receptor (NR)-mediated transcription, MED25 possesses distinct functions separated from MED1 upon different environmental signals in different cells [76,98]. Our data provide evidence for unique functional roles for Med25, such as in regulating Arg1 gene expression in M2 macrophage that is critically needed for wound healing.

In gene transcription, the formation of pre-initiation complex (PIC) and the initiation steps were considered to be most critical. However, it has become increasingly clear that post-recruitment steps, including RNA Pol II release from promoter-proximal pausing and transcription elongation, are also important in the control of transcriptional

rate [99,100]. Our data show elongation-related histone marker, H3K36me3 and elongation factor TFIIS are enhanced by IL-4 and RA co-stimulation, which were blocked by Med25 KD. This is in line with a recent study showing cooperation of the Mediator complex and TFIIS in altering intrinsic catalytic properties of RNA Pol II transit across the +1 nucleosome [101].

Figures

Figure 2-1.

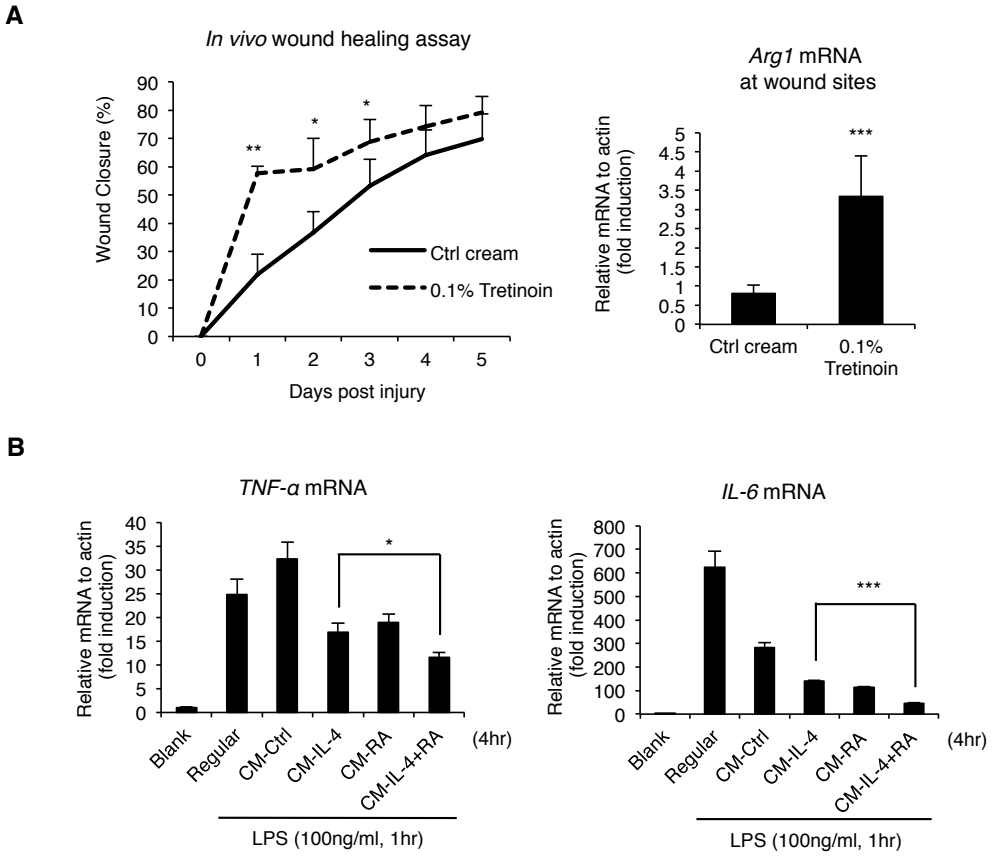

Figure 2-1. RA enhances wound healing and represses inflammatory responses.

(A) In vivo wound healing assay. The wounds were created and treated with a control or 0.1% Tretinoin cream for 5 days. The size of wound was monitored daily by recording wound closure (%) (n = 6 per each group) (left). qRT-PCR analyses of Arg1 mRNA at wound sites (right). Each wound tissue was collected at day 5 for mRNA extraction. (B) qRT-PCR analyses of LPS-induced (100 ng/ml, 1 h) pro-inflammatory cytokine gene (TNF-αand IL-6) mRNA in RAW264.7 cells treated with conditioned medium (CM, 4 h) collected from IL-4, RA or IL-4/RA-treated (6 h) RAW264.7 cells. Cells were treated with IL-4 (10 ng/ml) and/or RA (100 nM) in this figure. Data are representative of three experimental repeats (mean ± s.d), and Student's t-test (n = 3) was used (*P < 0.05; **P < 0.01; ***P < 0.001).

Figure 2-2.

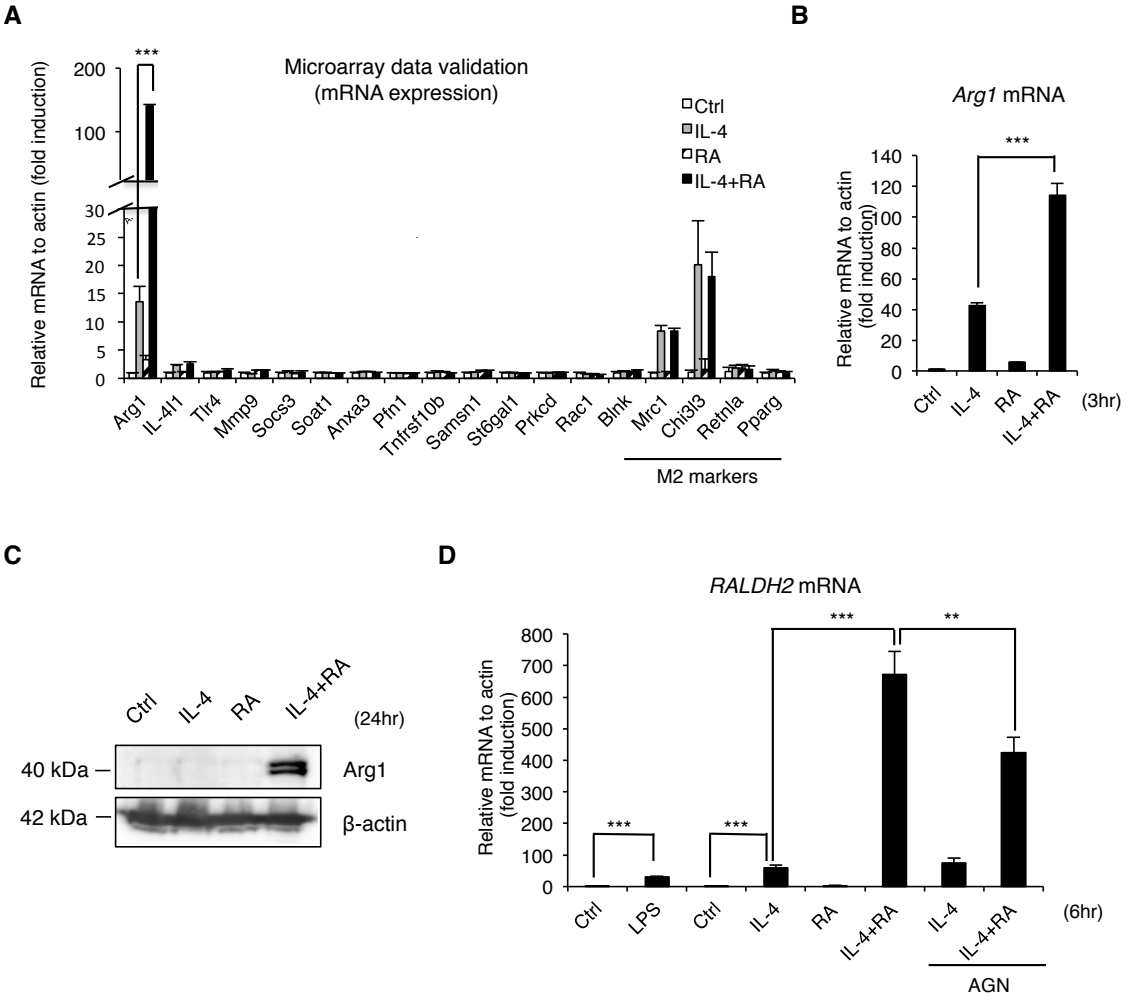
A
Microarray data validation
(mRNA expression)
Relative mRNA to actin (fold induction)
Ctrl
IL-4
RA
IL-4+RA
Arg1
IL-4I1
Tlr4
Mmp9
Socs3
Soat1
Anxa3
Pfn1
Tnfrsf10b
Samsn1
St6gal1
Prkcd
Rac1
Blnk
Mrc1
Chi3l3
Retnla
Pparg
M2 markers
B
Arg1 mRNA
Relative mRNA to actin (fold induction)
Ctrl
IL-4
RA
IL-4+RA
(3hr)
C
Ctrl
IL-4
RA
IL-4+RA
(24hr)
40 kDa
Arg1
42 kDa
β-actin
D
RALDH2 mRNA
Relative mRNA to actin (fold induction)
Ctrl
LPS
Ctrl
IL-4
RA
IL-4+RA
IL-4
IL-4+RA
AGN
(6hr)

Figure 2-2. RA promotes anti-inflammatory macrophage activation by synergizing with IL-4 to activate Arg1 expression.

(A) qRT-PCR for genes selected from microarray analysis of RAW264.7 cells treated with IL-4, RA or IL-4/RA for 3 h. (B) qRT-PCR analyses of Arg1 mRNA in mouse peritoneal macrophages stimulated with IL-4, RA or IL-4/RA for 3 h. (C) Western blot analyses of Arg1 protein from the extract of RAW264.7 cells treated with IL-4, RA or IL-4/RA for 24 h. (D) qRT-PCR analyses of Raldh2 mRNA in mouse bone marrow-derived macrophages treated with indicated ligands and cytokines for 6 h. Cells were treated with IL-4 (10 ng/ml) and/or RA (100 nM) in this figure. Data are representative of three experimental repeats (mean ± s.d), and Student's t-test (n = 3) was used (*$P < 0.05$; **$P < 0.01$; ***$P < 0.001$).

Figure 2-3.

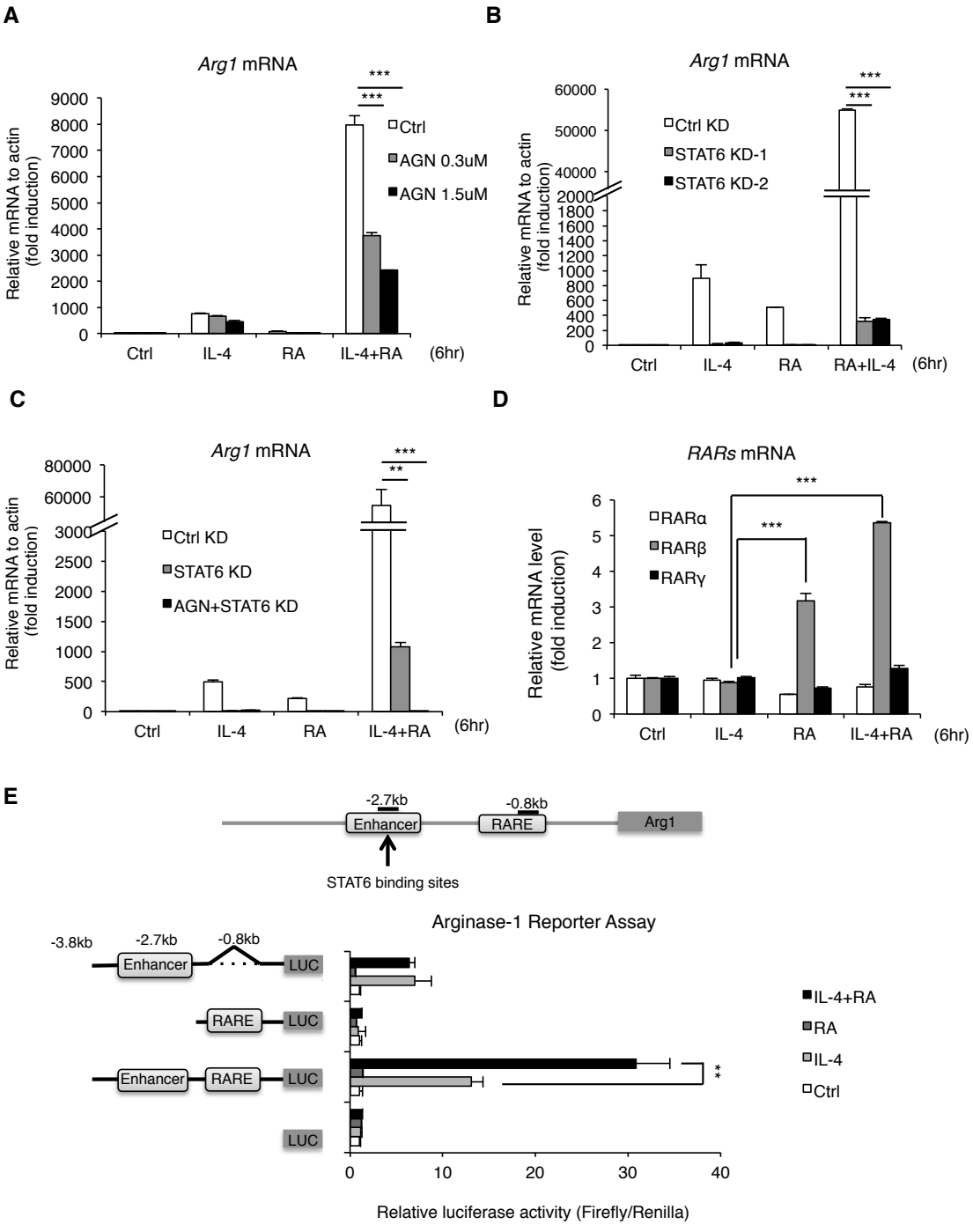
A
Arg1 mRNA
Relative mRNA to actin (fold induction)
Ctrl
AGN 0.3uM
AGN 1.5uM
Ctrl
IL-4
RA
IL-4+RA
(6hr)
B
Arg1 mRNA
Relative mRNA to actin (fold induction)
Ctrl KD
STAT6 KD-1
STAT6 KD-2
Ctrl
IL-4
RA
RA+IL-4
(6hr)
C
Arg1 mRNA
Relative mRNA to actin (fold induction)
Ctrl KD
STAT6 KD
AGN+STAT6 KD
Ctrl
IL-4
RA
IL-4+RA
(6hr)
D
RARs mRNA
Relative mRNA level (fold induction)
RARα
RARβ
RARγ
Ctrl
IL-4
RA
IL-4+RA
(6hr)
E
-2.7kb
-0.8kb
Enhancer
RARE
Arg1
STAT6 binding sites
Arginase-1 Reporter Assay
-3.8kb
-2.7kb
-0.8kb
Enhancer
LUC
RARE
LUC
Enhancer
RARE
LUC
LUC
IL-4+RA
RA
IL-4
Ctrl
Relative luciferase activity (Firefly/Renilla)

Figure 2-3. STAT6 and RAR are required for the synergistic effect of IL-4 and RA on Arg1 activation.

(A–C) qRT-PCR analyses of (A) Arg1 mRNA expression in RAW264.7 cells treated with IL-4, RA or IL-4/RA for 6 h with or without AGN (RAR pan-antagonist, 300 nM) pre-treatment for 30 min (B) Control knockdown (Ctrl KD) or STAT6 knockdown (STAT6 KD) cells treated with IL-4, RA or IL-4/RA for 6 h (C) Control, STAT6 KD or AGN-pretreated STAT6 KD cells treated with IL-4, RA or IL-4/RA for 6 h. (D) qRT-PCR analyses of RAR isoforms mRNA expression in RAW264.7 cells treated with IL-4, RA or IL-4/RA for 6 h. (E) Arg1 gene luciferase reporter assay deleted in enhancer (STAT6-binding sites, −2.7 kb), RARE (RAR- response element, −0.8 kb) or both in RAW264.7 cells treated with IL-4, RA or IL-4/RA 24 h. Cells were treated with IL-4 (10 ng/ml) and/or RA (100 nM) in this figure. Data are representative of three experimental repeats (mean ± s.d), and Student's t-test (n = 3) was used (*$P < 0.05$; **$P < 0.01$; ***$P < 0.001$).

Figure 2-4.

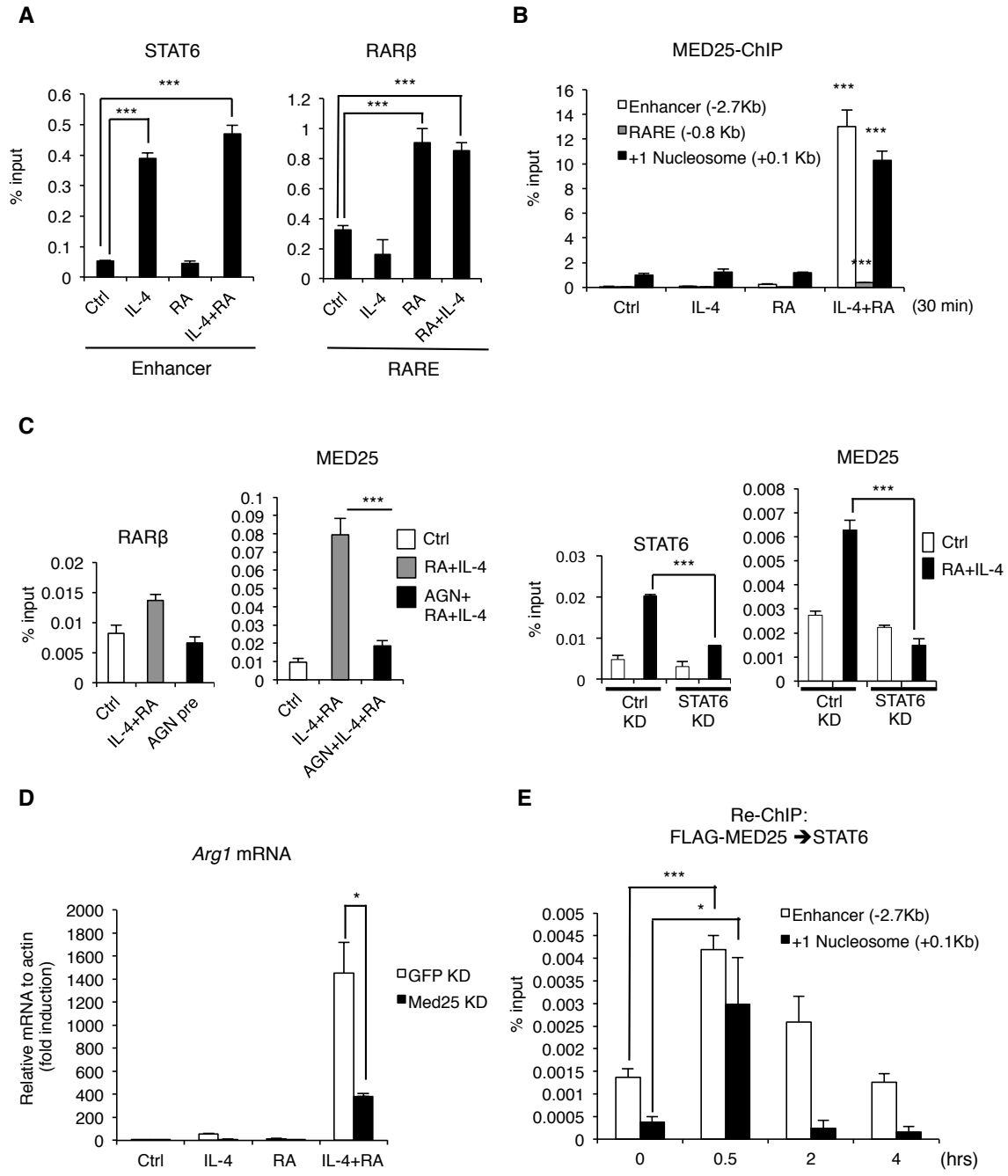
A
STAT6
RARβ
% input
Ctrl
IL-4
RA
IL-4+RA
RA+IL-4
Enhancer
RARE
B
MED25-ChIP
Enhancer (-2.7Kb)
RARE (-0.8 Kb)
+1 Nucleosome (+0.1 Kb)
(30 min)
C
MED25
RARβ
Ctrl
RA+IL-4
AGN+ RA+IL-4
IL-4+RA
AGN pre
AGN+IL-4+RA
STAT6
Ctrl KD
STAT6 KD
D
Arg1 mRNA
Relative mRNA to actin (fold induction)
GFP KD
Med25 KD
E
Re-ChIP:
FLAG-MED25 ➔STAT6
Enhancer (-2.7Kb)
+1 Nucleosome (+0.1Kb)
(hrs)

Figure 2-4. STAT6 and RARβ synergistically recruit Med25 upon IL-4 and RA treatment to enhance Arg1 transcription. (A) ChIP (Chromatin immunopre- cipitation) assay of STAT6 and RARβ in RAW264.7 cells treated with IL-4, RA or IL-4/RA for 30 min. STAT6 and RARβ enrichment on enhancer and RARE, respectively, was measured by qPCR. (B) ChIP assay of Med25 on Arg1 enhancer, RARE or +1 nucleosome region in IL-4, RA or IL-4/RA-treated RAW264.7 cells. (P value: compared with ctrl or single treatment) (C) ChIP assay of RARβ or Med25 on RARE or +1 nucleosome, respectively, upon IL-4 and RA treatment with or without AGN (300 nM) pre-treatment for 30 min (left). ChIP assay of STAT6 or Med25 on the enhancer in Ctrl KD or STAT6 KD RAW264.7 cells upon IL-4 and RA treatment (right). (D) qRT-PCR analyses of Arg1 mRNA expression in Ctrl KD (GFP KD) or Med25 KD RAW264.7 cells upon IL-4, RA or IL-4/RA treatment. (E) Re-ChIP assay of FLAG-MED25 and STAT6 on the enhancer and the +1 nucleosome of Arg1 at indicated time-points after IL-4 and RA treatment. Cells were treated with IL-4 (10 ng/ml) and/or RA (100 nM) in this figure. Data are representative of three experimental repeats (mean ± s.d), and Student's t-test (n = 3) was used (*P < 0.05; **P < 0.01; ***P < 0.001). See also Supplementary Figure S3.

Figure 2-5.

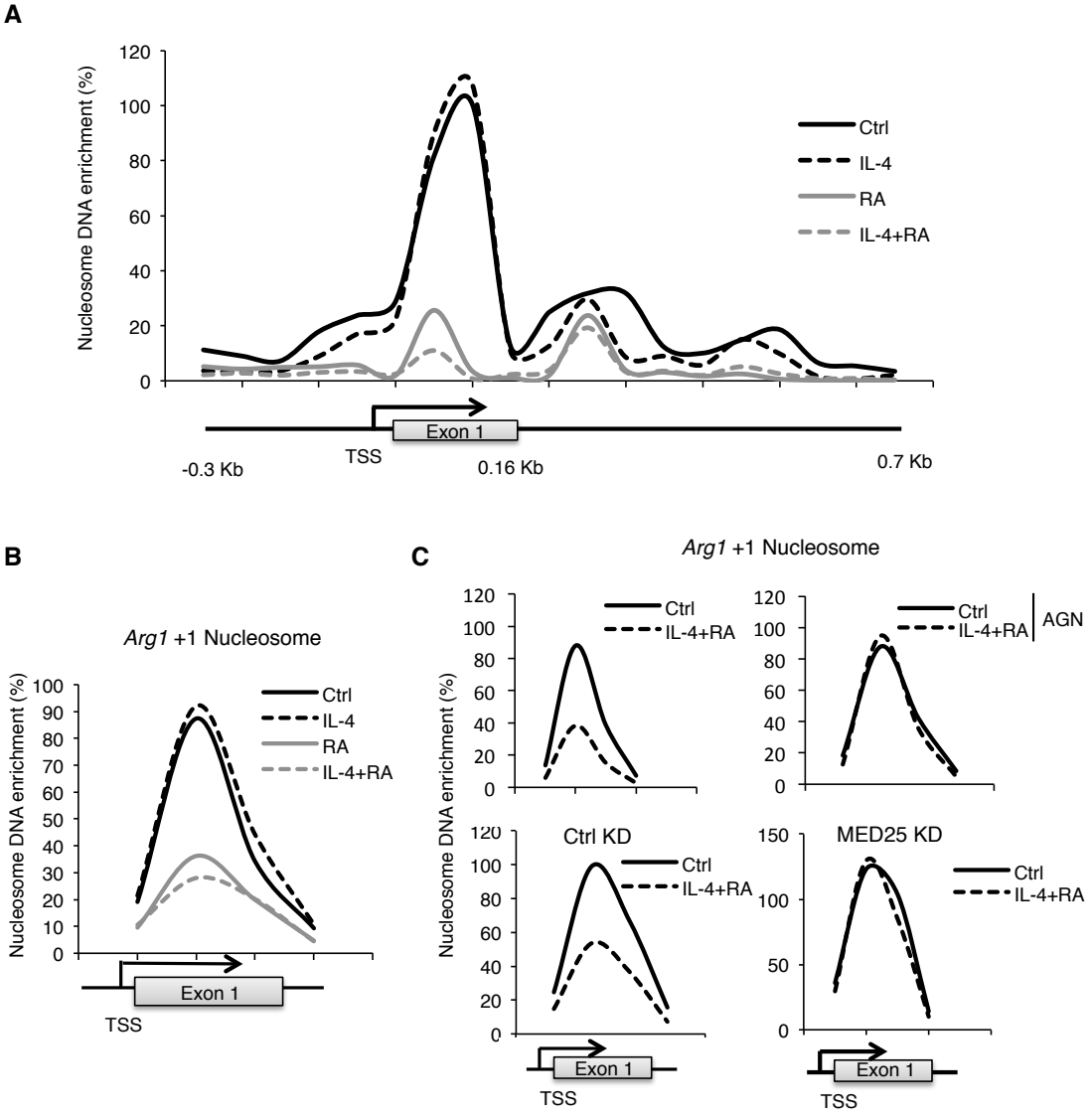
A
Nucleosome DNA enrichment (%)
120
100
80
60
40
20
0
Ctrl
IL-4
RA
IL-4+RA
Exon 1
-0.3 Kb
TSS
0.16 Kb
0.7 Kb
B
Arg1 +1 Nucleosome
Nucleosome DNA enrichment (%)
100
90
80
70
60
50
40
30
20
10
0
Ctrl
IL-4
RA
IL-4+RA
Exon 1
TSS
C
Arg1 +1 Nucleosome
Nucleosome DNA enrichment (%)
Ctrl
IL-4+RA
AGN
Ctrl KD
MED25 KD
Exon 1
TSS

Figure 2-5. Med25 mediates synergistic activation of Arg1 by IL-4 and RA via remodeling +1 nucleosome.

(A) Nucleosome scanning on the Arg1 promoter, the +1 nucleosome and the gene body region in IL-4, RA or IL-4/RA-treated RAW264.7 cells (30 min). (B) The +1 nucleosome occupancy immediately down-stream of Arg1 gene's TSS in RAW264.7 cells treated with IL-4, RA or IL-4/RA. (C) The +1 nucleosome occupancy in RAW264.7 cells with (upper right) or without (upper left) AGN (300 nM) pre-treatment for 30 min, and that in Ctrl KD (bottom left) or Med25 KD (bottom right) RAW264.7 cells. Cells were treated with IL-4 (10 ng/ml) and/or RA (100 nM) in this figure. Data are representative of three experimental repeats.

Figure 2-6.

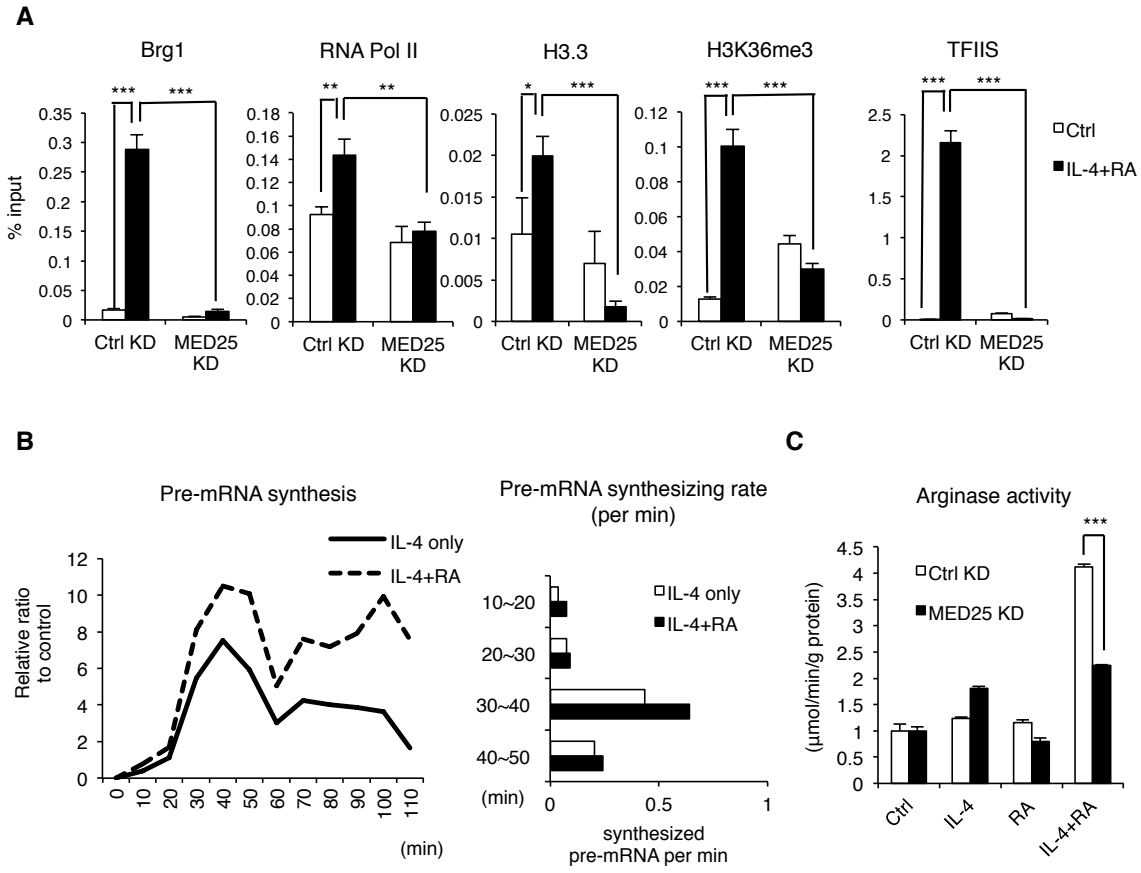
A
Brg1
RNA Pol II
H3.3
H3K36me3
TFIIS
% input
Ctrl KD
MED25 KD
Ctrl
IL-4+RA
B
Pre-mRNA synthesis
IL-4 only
IL-4+RA
Relative ratio to control
(min)
Pre-mRNA synthesizing rate (per min)
10~20
20~30
30~40
40~50
synthesized pre-mRNA per min
C
Arginase activity
Ctrl KD
MED25 KD
(μmol/min/g protein)
Ctrl
IL-4
RA
IL-4+RA

Figure 2-6. IL-4 and RA synergistically induce Med25 recruitment for transcription initiation-elongation coupling on Arg1 gene.

(A) ChIP assay of Brg1, RNA Pol II, H3.3, H3K36me3 and TFIIS on the +1 nucleosome in Ctrl KD or Med25 KD RAW264.7 cells with or without IL-4 and RA treatment for 30 min. (B) The kinetics of Arg1 pre-mature mRNA synthesis. Total RNAs were isolated to monitor Arg1 pre-mRNA level determined with primers spanning intron 7 and exon 8 regions in qRT-PCR (left). Pre-mRNA synthesizing rate was deduced through measuring the differences in relative ratios of synthesized pre-mRNA per min (right) (C) In vitro arginase activity assayed in Ctrl KD or Med25 KD RAW264.7 cells following IL-4, RA or IL-4/RA treatment for 24 h. Cells were treated with IL-4 (10 ng/ml) and/or RA (100 nM) in this figure. Data are representative of three experimental repeats (mean ± s.d), and Student's t-test (n = 3) was used (*P < 0.05; **P < 0.01; ***P < 0.001).

Figure 2-S1.

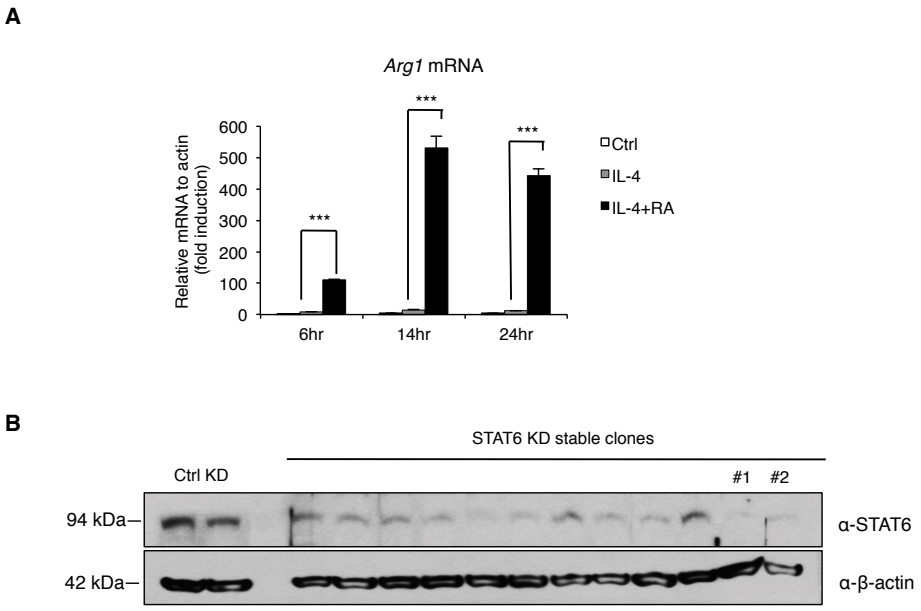

Figure 2-S1.

A. qRT-PCR analyses of Arg1 mRNA in RAW264.7 cells stimulated with IL-4 or IL-4/RA for different time periods. B. Western blot analyses of STAT6 and β-actin in Ctrl KD (GFP KD) and STAT6 KD stable clones from RAW264.7 cells showing knockdown efficiency. Cells were treated with IL-4 (10ng/ml) and/or RA (100nM) in this figure. Data are representative of three experimental repeats (mean ± s.d), and Student's t-test (n=3) was used (*P<0.05; **P<0.01; ***P<0.001).

Figure 2-S2.

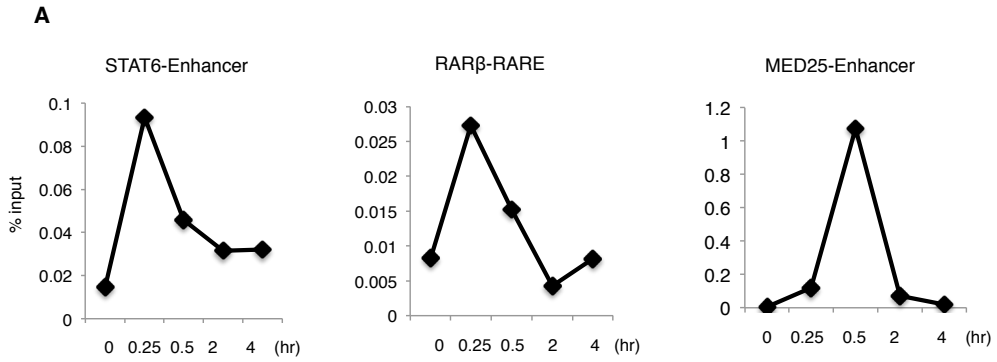

Figure 2-S2.

A. ChIP assay for the kinetics of STAT6, RARβ and MED25 binding on Arg1 gene promoter in RAW264.7 cells. IL-4 and RA-treated cells were collected at the indicated time points, and the enrichment of STAT6, RARβ and MED25 on enhancer and RARE was monitored by qPCR. Cells were treated with IL-4 (10ng/ml) and/or RA (100nM) in this figure. Data are representative of three experimental repeats.

Figure 2-S3.

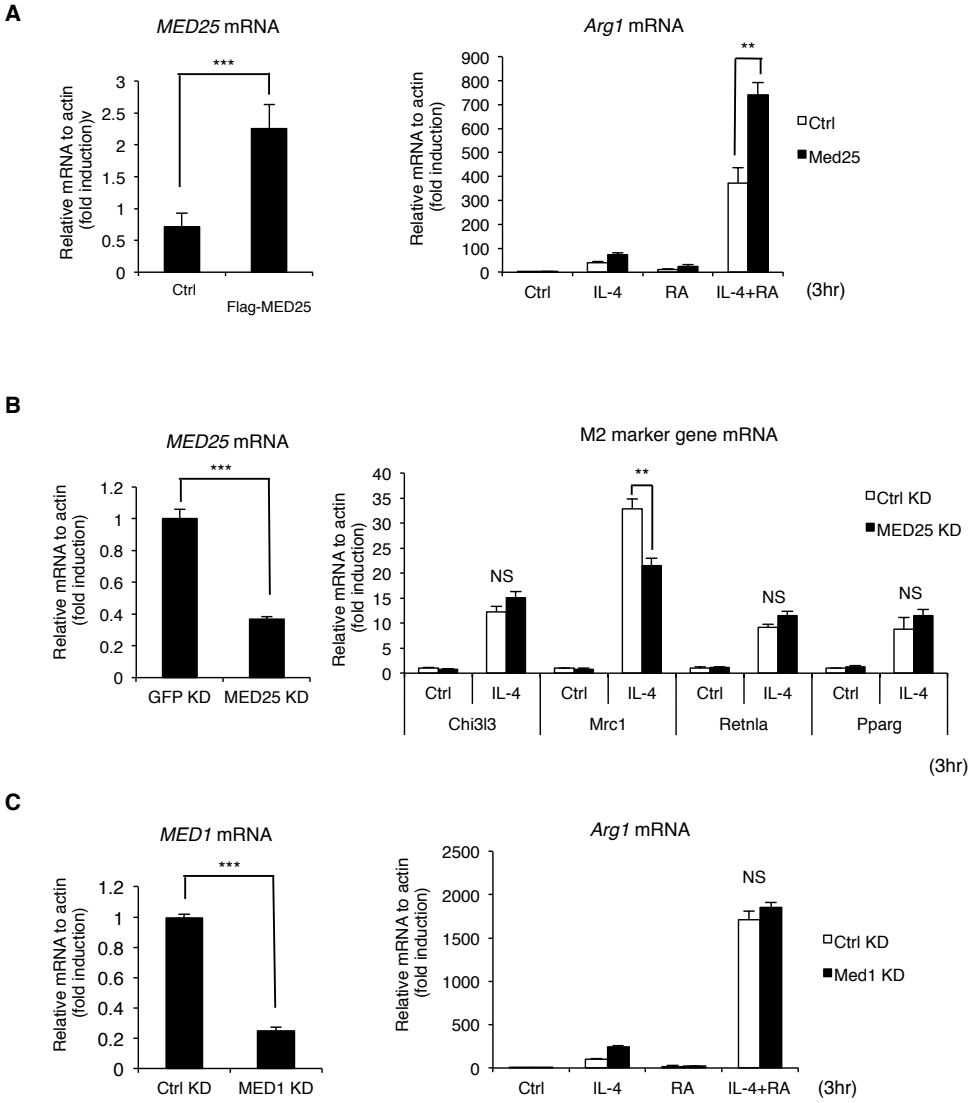
A
MED25 mRNA
Relative mRNA to actin (fold induction)v
***
Ctrl
Flag-MED25
Arg1 mRNA
Relative mRNA to actin (fold induction)
**
Ctrl
Med25
Ctrl
IL-4
RA
IL-4+RA
(3hr)
B
MED25 mRNA
Relative mRNA to actin (fold induction)
***
GFP KD
MED25 KD
M2 marker gene mRNA
Relative mRNA to actin (fold induction)
**
NS
Ctrl KD
MED25 KD
Ctrl
IL-4
Chi3l3
Mrc1
Retnla
Pparg
(3hr)
C
MED1 mRNA
Relative mRNA to actin (fold induction)
***
Ctrl KD
MED1 KD
Arg1 mRNA
Relative mRNA to actin (fold induction)
NS
Ctrl KD
Med1 KD
Ctrl
IL-4
RA
IL-4+RA
(3hr)

Figure 2-S3.

A. qRT-PCR analyses of MED25 (left) and Arg1 (right) mRNA expression in control or MED25 overexpressing RAW264.7 cells treated with IL-4, RA or IL-4/RA. B. qRT-PCR analyses of MED25 (left) and M2 marker genes (right) mRNA expression in Ctrl KD or MED25 KD RAW264.7 cells with or without IL-4 stimulation. C. qRT-PCR analyses of MED1 (left) and Arg1 (right) mRNA expression in Ctrl KD or MED1 KD RAW264.7 cells treated with IL-4, RA or IL-4/RA. Cells were treated with IL-4 (10ng/ml) and/or RA (100nM) for 3hr in this figure. Data are representative of three experimental repeats (mean ± s.d), and Student's t-test (n=3) was used (*P<0.05; **P<0.01; ***P<0.001).

Figure 2-S4.

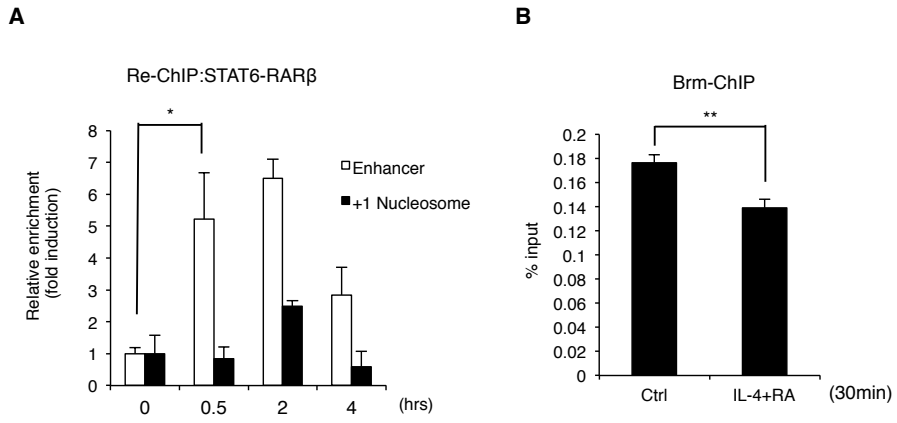

Figure 2-S4.

A. Re-ChIP assay of STAT6 and RARβ on the enhancer and the +1 nucleosome region of Arg1 after IL-4 and RA co-treatment at indicated time points. B. ChIP assay of Brm on the +1 nucleosome region of Arg1 in RAW264.7 cells with or without IL-4 and RA co-treatment. Cells were treated with IL-4 (10ng/ml) and/or RA (100nM) in this figure. Data are representative of three experimental repeats (mean ± s.d), and Student's t-test (n=3) was used (*P<0.05; **P<0.01; ***P<0.001).

Preface

This chapter has been published, and this study was accomplished with other collaborators in Dr. Li-Na Wei laboratory, especially Yi-Wei Lin who is the co-first author with me:

Yi-Wei Lin*, Bomi Lee*, Pu-Ste Liu and Li-Na Wei (2015) Receptor-interacting protein 140 orchestrates the dynamics of macrophages M1/M2 polarization. Journal of Innate Immunity, *doi: 10.1159/000433539. PMID: 26228026*

*Contribution: Y.W.L. and B.L. contributed equally to this work. B.L. designed the experiments and analyzed the data mainly in molecular mechanism study. Y.W.L. and P.S.L. designed the experiments and analyzed the data mainly in animal study. Y.W.L., B.L. and L.N.W. wrote the manuscript. L.N.W. supervised and provided financial support.

Chapter III

Receptor-interacting Protein 140 orchestrates the dynamics of macrophages M1/M2 polarization.

Introduction

Macrophages are innate immune cells and play a central role in inflammation and host defense; they are highly heterogeneous and exhibit diverse functional phenotypes in response to different environmental cues[102,103] . In general, they undergo two types of polarized activation, classic proinflammatory activation (M1) and alternative anti-inflammatory activation (M2) [104,105] . The M1 macrophage produces high levels of proinflammatory cytokines and reactive nitrogen and oxygen intermediates, and it generally harbors strong microbicidal and tumoricidal activities. The M2 macrophage is anti-inflammatory and primarily involved in resolving inflammation, parasite containment and tissue remodeling. When tissues are damaged following infection or injury, inflammatory monocytes are recruited from the circulation and differentiated into macrophages as they migrate into the affectedtissues. These recruited macrophages often first show an M1 phenotype, producing proinflammatory cytokines such as interleukin-1 (IL)-1 and tumor necrosis factor α (TNFα). Subsequently, the recruited macrophages then shift to become more M2-like, producing regulatory cytokines such as IL-10 and transforming growth factor β (TGFβ). It remains unclear whether the M1–M2 phenotype switch occurs in the same macrophage, but it is widely accepted that M1–M2 switch among macrophage populations is an essential process during recovery[106]. This macrophage phenotype switch must be tightly regulated to maintain the homeostasis of innate immunity. Uncontrolled macrophage polarization is frequently implicated in diseases such as sepsis, autoimmune diseases and cancers[104,107-109]. Cytokines that stimulate the M1 or M2 phenotype have been largely uncovered and principal

transcription factors for M1 versus M2 activation have also been well-characterized [110-113]; however, whether the dynamics of the M1–M2 switch or the homeostatic control of this phenotypic switch involve cell-autonomous factors in macrophages is unknown.

Upon infection, inflammation occurs as a defense mechanism, but uncontrolled inflammation leads to dangerous pathological states including septic shock[114,115]. An important host adaptation to protect against septic shock is to establish a state of 'endotoxin tolerance' (ET), where macrophages become transiently unresponsive and fail to produce inflammatory cytokines upon further endotoxin challenge[116,117] . Molecules that may mediate ET by suppressing Toll-like receptor (TLR) signaling have been reported[118-120]. Recently, we have reported that a nuclear coregulator, receptor-interacting protein 140 (RIP140)[24], which is involved in various physiological processes[121], also plays a crucial role in the establishment of ET[36] . We found that RIP140 is the principal nuclear coactivator of NF-κB in endotoxin-challenged M1 macrophages and that upon endotoxin challenge, it is rapidly degraded by Syk-initiated ubiquitination, which renders NF-κB inactive[36]. Thus, reducing the RIP140 protein level facilitates ET and protects against septic shock[36,122]. Other studies have shown that endotoxin-challenged M1 macrophages, while unable to respond to further endotoxin stimulation, can still respond to stimuli for M2 polarization[123,124]. Is a state of ET required for proceeding to M2 polarization? Are there cellular factors regulating the progression of stimulated macrophages from M1, ET and then M2? These are central questions to be addressed in this study.

Numerous disease conditions involve the coordination of inflammatory and anti-

inflammatory responses[125]. Wound healing encompasses macrophage M1 polarization and transition to a state of ET and then to an M2 phenotype. When this transition is out of control, macrophages could be locked into a specific phenotype, leading to chronic inflammation and tissue destruction. In this study, we uncover that RIP140 is not only crucial for M1-ET establishment, but can also negatively regulate the progression of a macrophage switch to an M2 state during recovery. Interestingly, this particular function of RIP140 in M2-stimulated macrophages is executed by its cytosolic form, which activates a specific cytosolic phosphatase that inactivates the master regulator of M2 polarization, pSTAT6. We employ both in vitro and in vivo wound-healing models to demonstrate the dual functions of RIP140 in regulating the dynamics of the macrophage M1–M2 phenotypic switch and to explain, at least partially, the plastic nature of macrophage polarization in various disease conditions.

Materials and Methods

Reagents

Reagent sources are LPS (Sigma-Aldrich #L4391), IFN-γ (Invitrogen #PMC4031), IL-4 and IL-13 (Cell signaling #5208, 5242), antibodies for RIP140 (Abcam ab42126), CAPNS1 (ab28237), pSTAT6 (Cell signaling #9361), PTP1B (Santa Cruz sc-1718), STAT6 (M-20 sc-981), α-Tubulin (B-7 sc-5286), Lamin A/C (346 sc-7293), HA (SC-7392), β-actin (C4, sc-47778), kinase inhibitor Staurosporine (S5921, Sigma), PTP inhibitor I (sc-204220, Santa Cruz), PTP1B inhibitor XXII (593741, Calbiochem), SHP1/2 PTPase inhibitor (565851, Calbiochem), and Calpain inhibitor (03-34-0051,

Calbiochem).

Cell culture, lentivirus production and transduction

RAW264.7 cells were cultured in DMEM medium supplemented with 10% FBS and 1% antibiotics. Cells were transfected using Lipofectamine LTX and PLUS reagent (Invitrogen). WT-RIP140 and Y3F-RIP140 expression and RIP140-shRNA lentivirus were as described[16,17,36]. PTP1B shRNA lentivirus constructs were from Genomic Center at the University of Minnesota: siRNA sequence: #1-GCGGCTATTTACCAGGACATT, #2- CTGCCTCTTACTGATGGACAA.

Cell fractionation, Immunoblotting and Immunofluorescence

Cells were suspended in a hypotonic buffer, lysed with RIPA [17,18,33] and the nuclear fraction was obtained from the pellet. Endoplasmic Reticulum Isolation Kit (Sigma, ER0100) was used for ER and cytosolic fractionation. Whole cell lysates were prepared 3 days after virus transduction or 2 days after transfection in RIPA buffer. Protein was quantified with Bradford, separated by 8% SDS-PAGE and analyzed by immunoblotting. For immunofluorescence, cells fixed on coverslips were permeabilized for 5 min at RT and stained with antibodies, and mounted using a DAPI-contained mounting buffer. The slides were imaged under a confocal microscope (Olympus FluoView 1000 BX2 Upright Confocal).

RNA isolation and gene expression analyses

Total RNA was isolated using TRIzol (Invitrogen). Reverse transcription (RT, 2 μg) was performed using High-Capacity cDNA Reverse Transcription Kit (Applied Biosystems). Quantitative real-time PCR (qPCR) was performed with SYBR enzyme mix (Applied

Biosystems). Each gene expression experiment was performed in triplicate. Expression levels were normalized to β-actin.

Chromatin-immunoprecipitation (ChIP) assay

Raw264.7 cells were cross-linked with 1% formaldehyde, lysed, sonicated and immunoprecipitated with antibodies against STAT6 (Santa Cruz) or RNA Pol II (Millipore) overnight. Following decrosslinking, DNA was isolated and analyzed by qPCR for STAT6-binding and non-binding regions. Arginase 1 promoter STAT6 binding site: (F) TGAACAGGCTGTAGCCAACA, (R) AGCACCCTCAACCCAAAGTG, STAT non-binding site: (F) TCTGATGATGCCAAGTAGCC (R) GGACAAGCCACAGTCAGAGA.

In vitro phosphatase activity assays

RAW264.7 cells were infected with RIP140-trageting shRNA lentivirus followed by IL-4 stimulation. Cell lysates were prepared (50 mM HEPES, 0.1 mM EGTA, 0.1 mM EDTA, 120 mM NaCl and 0.5% NP-40) and incubated with immobilized capture antibody specific to PTP1B bound microplates and washed to remove unbound materials. A synthetic phosphopeptide substrate was added, and the free phosphate generated by PTP1B was detected using malachite green and molybdic acid, and determined by the absorbance at 620 nm.

Animals

All studies were carried out using male C57BL/6J mice from The Jackson Laboratory and maintained in the animal facility of the University of Minnesota. Animal studies were approved by the University of Minnesota Institutional Animal Care and Use Committee.

MφRIP140KD transgenic mice were generated as previously described[19-22,36]. Peritoneal macrophages (PM) isolation and bone marrow transplantation were performed as described[25-27,37].

In vitro Wound healing assay

293TN cells monolayer on 6-well plates at a 90% confluence was scraped using a pipette tip to produce a wound, incubated with conditioned medium of primary macrophages transfected with a control, RIP140-knockdown or RIP140-overepresion vector. After 24h and 48h, photographs were taken and analyzed by Image J (NIH) software to determine wound closure.

Flow Cytometry

Macrophage surface antigens were blocked with Fc block (BD Biosciences), incubated with fluorophore-conjugated or isotype control antibodies for 1 h, washed and centrifuged at 500 g for 5 min and resuspended for FACS Calibur analyses using WinMDI software. The gated CD11b + F4/80 + cells were examined with anti-CD11c (as M1) or anti-CD206 (as M2) antibody.

In vitro Phosphatase Activity Assay

RAW264.7 cell lysate was prepared in 50 m M HEPES, 0.1 m M EGTA, 0.1 m M EDTA, 120 m M NaCl and 0.5% NP-40, incubated with immobilized PTP1B capture antibody-bound microplates and washed, and then synthetic phosphopeptide substrate was added. The generated free phosphate was detected using malachite green and molybdic acid with absorbance at 620 nm.

In vivo Wound-Healing Assay

Cutaneous wounds were made on both sides of the shaved back (2 wounds per mouse), with a 5-mm, round biopsy punch under anesthesia. The wound size was recorded daily and analyzed by Image J.

Statistical Analysis

Experiments were performed at least twice and presented as means ± SD. One-way ANOVA or Student's t test was used. p values ≤ 0.05 were considered statistically significant (* $p < 0.05$; * * $p < 0.01$; * * * $p < 0.001$).

Results

Failure to Establish RIP140 Degradation-Mediated ET Prevents Macrophage M2 Polarization

We previously showed that RIP140 is required for macrophage M1 polarization, but it must then be rapidly degraded in order to establish ET and prevent inflammatory storm such as sepsis. In this study, we first found that under the condition when ET fails to be established and RIP140 cannot be degraded, e.g. following stimulation with IFN-γ[126] , subsequent M2 polarization is severely dampened. Fig. 3-1 a shows that, as predicted, in an LPS-treated M1 macrophage, RIP140 protein is degraded without altering its mRNA level, which is abolished in IFN-γ pretreated cells. Fig. 3-1 b shows that IL-4-stimulated M2 polarization, as shown in LPS-tolerated cells, is dramatically dampened in IFN-γ pretreated cells. We speculated that RIP140 might play a regulatory (negative) role in macrophage polarization for the transition to M2 and, to test this possibility, we employed a nondegradable mutant, RIP140 (Y3F; Tyr364, Tyr418 and

Tyr436 all mutated into phenylalanine to prevent degradation; supplementary Fig. 3-S1)[36]. Fig. 3-1 c shows that expressing this nondegradable RIP140 (Y3F) but not the wild-type RIP140 (WT), indeed significantly diminishes the effect of IL-4-stimulated M2 polarization; this is supported by the significantly reduced expression of M2 markers. These results demonstrate a pivotal role for RIP140, not only in promoting M1 polarization during an inflammatory response but also in controlling the phenotypic switch from the M1 to the M2 state.

Reducing RIP140 Level Promotes Wound Healing by Facilitating M1–M2 Switch

The macrophage M1–M2 phenotype switch is critical for wound healing. We asked whether and how changing RIP140 levels might affect wound-healing efficiency. We first employed a macrophage-specific RIP140 knockdown (MΦRIP140KD) mouse as an in vivo model[36] in which the RIP140 protein level in monocyte-macrophage populations is reduced for 90–95% (supplementary Fig. 3-S2). As shown in Fig. 3-2 a, wound closure in MΦRIP140KD mice (2 independent lines: KD-1 and KD-2) is more efficient than that in WT mice. We then examined the dynamics of M1–M2 switch during the wound-healing process (Fig. 3-2 b). In WT mice (closed markers), M1–M2 switch occurs on approximately the 5th day after the wound whereas in MΦRIP140KD KD (open markers), M1–M2 switch occurs on approximately the 3rd day. Consistently, in the wounds, the levels of all the examined M1 marker genes (TNFα , iNOS and IL-1β) are lower in MΦRIP140KD mice than in WT mice (Fig. 3-2 c) whereas the levels of all the examined M2 marker genes (Arg1 , TGFβ and VEGF) are significantly elevated in MΦRIP140KD mice (Fig. 3-2 d). These data support the notion that the RIP140 protein

level is an important factor that regulates the kinetics of macrophage phenotypic switch in, and thus the efficiency of, the wound-healing process.

We then utilized an in vitro primary macrophage (PM) culture to examine the effects of altering RIP140 protein levels in M2 polarization (supplementary Fig. 3-S3a). Using lentivirus to overexpress or knock down RIP140 in primary PM, we found that IL-4 induction of all characteristic M2 genes is significantly attenuated by overexpressing RIP140, but is significantly elevated by knocking down RIP140. Further, the activity of arginase 1 (Arg1), a critical factor in M2 macrophages, is significantly elevated by knocking down the RIP140 level, and is reduced by elevating the RIP140 level (supplementary Fig. 3-S3b). We further employed an in vitro wound-healing model of 293TN monolayer cultures supplemented with conditioned media of macrophage cultures, where the RIP140 level had been altered (Fig. 3-2 e; supplementary Fig. 3-S4). It appears that the conditioned medium of the RIP140-overexpressing, IL-4-treated macrophage culture suppresses healing in the wounded 293TN culture (Fig. 3-2 e: top panel; supplementary Fig. 3-S4: left panel) whereas the conditioned medium of RIP140 knockdown, IL-4-treated macrophage culture significantly improves wound closure (Fig. 3-2 e: bottom panel; supplementary Fig. 3-S4: right panel). These results support that RIP140 regulates the macrophage M1–M2 switch to affect wound healing both in vivo and in vitro.

Preventing RIP140 Degradation Delays Wound Healing

We next examined whether preventing RIP140 degradation in macrophages would delay wound healing in vivo. In order to specifically monitor the effects elicited by

disturbing the dynamics of macrophage polarization in adult stages, we employed bone marrow transplantation to replace the animal's endogenous macrophages with myeloid cells carrying either green fluorescent protein (GFP) only, WT RIP140-GFP or the nondegradable mutant Y3F RIP140-GFP, and examined their wound healing processes. Comparable BTM efficiency was validated (supplementary Fig. 3-S5). It appears that wound healing in mice receiving myeloid cells carrying WT RIP140 is slightly delayed compared to those receiving GFP only (control), but complete healing (with 100% wound closure) occurs on day 12 for both groups. Interestingly, wound closure in mice receiving Y3F-RIP140 is significantly less efficient; by day 12, their wounds close for only 70% (Fig. 3-3 a). Further, in the wounds of the Y3F-RIP140 group, the M1 population is expanded but the M2 population is reduced, when compared to the WT RIP140 group (Fig. 3-3 b). Consistently, in the wounds of the Y3FRIP140 group, in the course of healing, the expression of all the monitored M1 marker genes (TNFα , iNOS and IL-1β) is significantly elevated and the expression of all the monitored M2 marker genes (Arg1 , TGFβ and VEGF) is significantly lowered (Fig. 3-3 c, d). These data further validate the notion that elevating the RIP140 protein level, e.g. by blunting its degradation in monocytes/macrophages during injury, facilitates and locks these macrophages in their M1 state, resulting in an impaired wound healing process.

RIP140 Suppresses M2 Macrophage Polarization by Inhibiting the Activation of STAT6 (Phosphorylation) in the Cytosol

We noticed that the suppressive effect of RIP140 on M2 gene expression is evident only after treatment with M2 cues such as IL-4 (supplementary Fig. 3-S3), indicating that

RIP140 targets the downstream signaling pathway of IL-4. Interestingly, in IL-4-stimulated cells, endogenous RIP140 is gradually translocated from the nucleus to the cytosol (Fig. 3-4 a, b); this appears to also be true for the RIP140-Y3F mutant protein (supplementary Fig. 3-S6). The nuclear-cytosolic translocation of RIP140 also occurs in macrophages stimulated with other anti-inflammatory cytokines such as IL-13 (supplementary Fig. 3-S7). To understand how RIP140 inhibits the IL-4 signaling pathway, we examined several potential targets and found that RIP140 suppresses the activation of the master signal transducer for M2, STAT6 phosphorylation at Tyr641 (Fig. 3-4 c), resulting in its decreased DNA binding as well as RNA polymerase II recruitment to the promoter of its target genes like Arg1 (Fig. 3-4 d). These results indicate that upon IL-4 stimulation, RIP140 is translocated from the nucleus to the cytosol, where it suppresses the activation of the master regulator STAT6 (phosphorylation at Tyr641). M2 target gene expression is thus dampened.

RIP140 Targets Calpin1/2 to Activate PTP1B to Reduce STAT6 Phosphorylation

To examine how RIP140 suppresses the activation of STAT6, i.e. its phosphorylation at Tyr641, we examined two possibilities – either impairing its kinase or enhancing its phosphatase activity, since RIP140 does not form a complex with STAT6 (data not shown). It appears that RIP140 does not affect the kinase, because silencing RIP140 still affects the induction of pSTAT6 even though kinases are blocked by inhibitors like staurosporine (supplementary Fig. 3-S8a). Instead, it probably targets the dephosphorylation of pSTAT6. PTP1B has been reported as a phosphatase for pSTAT6[127]. Indeed, both a general phosphatase inhibitor and a PTP1B-specific inhibitor,

but not the SHP-1/2 specific inhibitor, block RIP140-triggered reduction in the pSTAT6 level (Fig. 3-5 a). The specificity of RIP140 to PTP1B is further confirmed, because silencing PTP1B abolishes the suppressive effect of RIP140 (Fig. 3-5 b). An in vitro phosphatase enzyme assay substantiated that RIP140 regulates PTP1B activity that inactivates (de-phosphorylates) pSTAT6 (Fig. 3-5 c) without affecting PTP1B mRNA levels (supplementary Fig. 3-S8b).

We found that RIP140 and PTP1B are colocalized in the cytosol of IL-4-treated macrophages (Fig. 3-5 d). Further, the level of 'active' PTP1B, typically cleaved from its precursors on the ER membrane, is increased by overexpressing RIP140 (Fig. 3-5 e). We speculated that in IL-4-treated cells, RIP140 is exported to the cytosol and translocated to ER to facilitate the activation of PTP1B precursors, and performed ER and cytosol fractionation to examine the distribution of the active and inactive forms of PTP1B protein. Elevating the RIP140 level increases the active, cytosolic PTP1B and reduces the inactive, ER-associated PTP1B (Fig. 3-5 f), which supports that RIP140 enhances PTP1B activity by facilitating the cleavage of its precursor. The PTP1B precursor on the ER is cleaved by a calciumdependent protease, calpain. Interestingly, we found that RIP140 forms complexes with the calpain regulatory subunit, CAPNS1, in the presence or absence of IL-4 (Fig. 3-5 h). In addition, calpain inhibitor pretreatment completely blocks RIP140-regulated PTP1B cleavage in IL-4-treated M2 PM (Fig. 3-5 g). These data are consistent with previous reports that PTP1B is one of the targets of caplain1/2[128,129], and CAPNS1 is necessary for calpain1/2 activity[130,131]. All together, the data demonstrate that in IL-4-treated macrophages, RIP140 is increasingly translocated from the nucleus to

become more associated with the calpain regulatory subunit to regulate calpain1/2 activity, which cleaves PTP1B precursor from ER, releasing active PTP1B to inactivate pSTAT6 in the cytosol.

Discussion

In this study, we used ET and wound-healing models to understand the regulation of M1/M2 polarization. While it has been reported that macrophages in the ET state exhibit M2-like features and are more sensitive to M2 cues, the underlying mechanism remained elusive[123,124]. Here, we demonstrate that the level of RIP140 protein is crucial: (1) RIP140 suppresses the activation of the M2 master regulator STAT6 and (2) for inflammatory macrophages to proceed to a state of ET, the RIP140 level must be reduced. As such, ET macrophages generally have low RIP140 levels and are more sensitive to M2 activation.

As the wound healing progresses, the macrophage phenotype switches from M1 to M2[106]. The transition from inflammatory M1 polarization to alternative anti-inflammatory M2 polarization is critical for the healing process. One critical molecular event in this transition is the rapid reduction of the NF-κB coactivator RIP140 protein level, which allows timely dampening of inflammation (via the inactivation of NF-κB). Lowering the RIP140 level by rapid degradation is made possible by the action of a specific SCF E3 ubiquitin ligase that ubiquitinates RIP140[36]. This study extends our previous finding and demonstrates a new function of RIP140, which is to regulate the dynamics of M1 versus M2 polarization. On the cellular level, M1–M2 transition requires

the establishment of ET, at least for TLR-4 mediated stimulation, which is also orchestrated by altering the RIP140 protein level (Fig. 3-2 b). We employed 2 animal models to support this conclusion, an MΦRIP140KD transgenic mouse model where the RIP140 level in macrophages is reduced from birth, and a bone marrow transplant-generated macrophage replacement model where a nondegradable RIP140 mutant protein, Y3F, is introduced only during adult stages. Our data clearly show that the accumulated RIP140 protein level in adults is crucial to the dynamics of macrophage phenotype transition.

An unexpected finding in this in vivo wound experiment is that Arg1 gene expression is higher in Y3F-RIP140 mice than WT mice on day 10 (Fig. 3-3 d). It is important to note that gene regulation, especially in whole animals, can involve more complicated regulatory pathways. Y3FRIP140 could possibly exert additional effects that might have disturbed Arg1 gene regulation, causing a higher level of Arg1 gene expression in certain points of the wound healing process, as was surprisingly observed on day 10 of this experiment. However, the expression of the 2 additional M2 markers, TGFβ and VEGF, and the M2 population analysis from FACS support the notion that preventing RIP140 degradation (to an elevated RIP140 level) indeed delays wound healing, which involves inhibiting M1–M2 switch.

An interesting mechanistic finding is that the new M2-suppressive function of RIP140 is achieved by its cytosolic form, exported from the nuclei in M2 cue-stimulated macrophages. RIP140 was initially identified as a coregulator of numerous transcription factors in the nucleus, but more studies have revealed that, in various cell types and

stimulated by different signal inputs, nuclear RIP140 can be exported to the cytosol to regulate a wide variety of biological processes. Interestingly, all these events are highly cell type-selective and signal-specific. For instance, in mature adipocytes, the lipid signal stimulates its export to the cytosol to regulate AS160 to modulate insulin sensitivity[33]. In differentiated neurons, ER stress stimulates RIP140 export to the cytosol and then to ER, where it interacts with IP3R to modulate ER store calcium release, thereby protecting neurons from apoptosis[132]. In this study, we uncover RIP140 exported to the cytosol in M2 cue-stimulated macrophages to suppress the efficiency of M2 polarization. Clearly, in macrophages, RIP140 modulates the homeostasis of innate immunity via its dual functions in the M1 and M2 states. With this dual control in place, macrophages may not overreact to either stimulus. A fault in this control may result in devastating situations such as sepsis or delayed wound healing (when RIP140 cannot be degraded or exported in time). Surprisingly, the cytosolic RIP140 suppresses the M2 master regulator, pSTAT6, by targeting the regulatory step of a specific phosphatase of STAT6, PTP1B, in the ER/cytosol. This is achieved by its increasing association with calpain's regulatory subunit, CAPNS1, in IL-4-treated cells, to further activate calpain1/2 which cleaves the PTP1B precursor and renders its activation. Whether and how RIP140 association with CAPNS1 would alter calpain1/2 activity must still to be determined. Activated PTP1B then efficiently dephosphorylates pSTAT6, thereby reducing M2 target gene activation.

PTP1B is a negative regulator for the insulin and leptin signaling pathways[133,134]. Currently, a PTP1B inhibitor, trodusquemine, and PTP1B-specific antisense oligonucleotides are in phase 2 clinical trials for treating diabetes or obesity[135,136].

Clearly, in innate immune cells, the expression level of RIP140 protein and its subcellular localization are critical to the maintenance of the functional plasticity of macrophages. The factors and molecules regulating its protein level and subcellular distribution can also be potential therapeutic targets. However, the mechanism underlying the M2 cue-stimulated (e.g. with IL-4 and IL-13) nuclear export of RIP140 has still to be determined. Furthermore, while RIP140 can be associated with the calpain regulatory subunit, CAPNS1, it remains unclear how this affects calpain activity. Rigorous biochemical studies are needed in order to understand the molecular details of activation of this specific protease complex.

Figures

Figure 3-1.

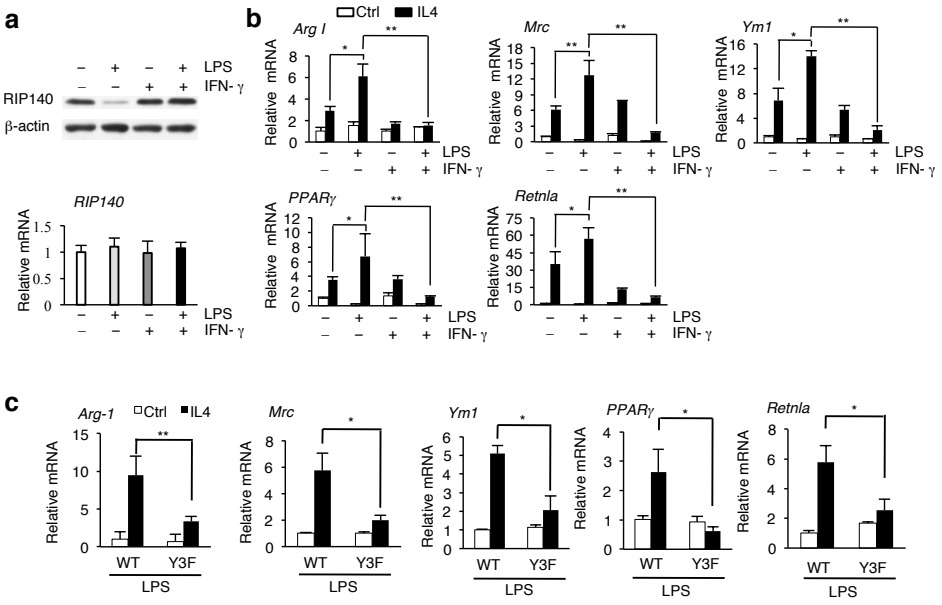

Figure 3-1. ET established by degrading RIP140 facilitates macrophage M2 polarization. a. Western blot (top) and qPCR (bottom) of RIP140 in primary PM with or without IFN-γ pretreatment for 16 h followed by LPS (10 ng/ml) treatment for 24 h. b. qPCR of M2 marker expression in PM with or without IFN-γ pretreatment followed by LPS stimulation, and then treated with (black bars) or without (open bars) IL-4 for 6 h. Results are presented relative to control (neither LPS nor IFN-γ). c qPCR of M2 marker expression in lentinvirus-WT-RIP140 (WT) or lentivirus-Y3F-RIP140 (Y3F) infected (for 48 h) PM that were then challenged with LPS for 18 h, followed by control or IL-4 stimulation for 6 h. Results are presented relative to the control. Data are representative of 3 experiments (means ± SD), and Student's t test (n = 3) was used. * $p < 0.05$; * * $p < 0.01$; * * * $p < 0.001$. Ctrl = Control.

Figure 3-2.

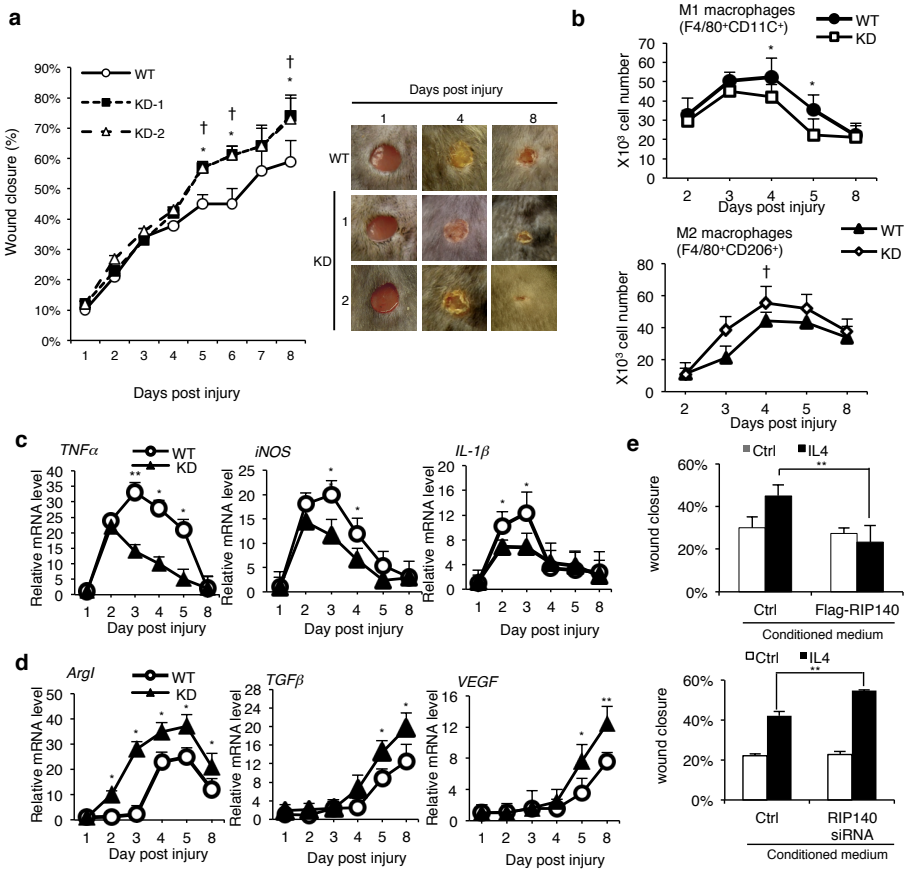
a
Wound closure (%)
WT
KD-1
KD-2
Days post injury
Days post injury
1
4
8
WT
KD
1
2
b
M1 macrophages
(F4/80+CD11C+)
WT
KD
X10³ cell number
Days post injury
M2 macrophages
(F4/80+CD206+)
WT
KD
X10³ cell number
Days post injury
c
TNFα
iNOS
IL-1β
WT
KD
Relative mRNA level
Day post injury
d
Arg1
TGFβ
VEGF
WT
KD
Relative mRNA level
Day post injury
e
Ctrl
IL4
wound closure
Ctrl
Flag-RIP140
Conditioned medium
Ctrl
IL4
wound closure
Ctrl
RIP140 siRNA
Conditioned medium

Figure 3-2. Reducing RIP140 level promotes wound healing by facilitating M1–M2 switch. a. Daily record of wound closure on WT and MΦRIP140KD mice of 3 experiments of 2 independent MΦRIP140KD lines (means ± SD). A one-way ANOVA test was used * $p < 0.05$ (WT vs. KD-1); † $p < 0.05$ (WT vs. KD-2). **b.** FACS evaluation of M1 (F4/80 + CD11C + , top) and M2 (F4/80 + CD206 + , bottom) populations in the wounds of 3 experiments. M1 and M2 numbers are normalized to wound mass (cell numbers/mg). Student's t test (n = 3) was used. * $p < 0.05$ (WT-M1 vs. KD-M1); † $p < 0.05$ (WT-M2 vs. KD-M2). **c , d.** qPCR of M1 and M2 marker expression in the wounds. **e.** In vitro wound healing results of 3 experiments. Student's t test (n = 3) was used. * $p < 0.05$; * * $p < 0.01$; * * * $p < 0.001$. Ctrl = Control.

Figure 3-3.

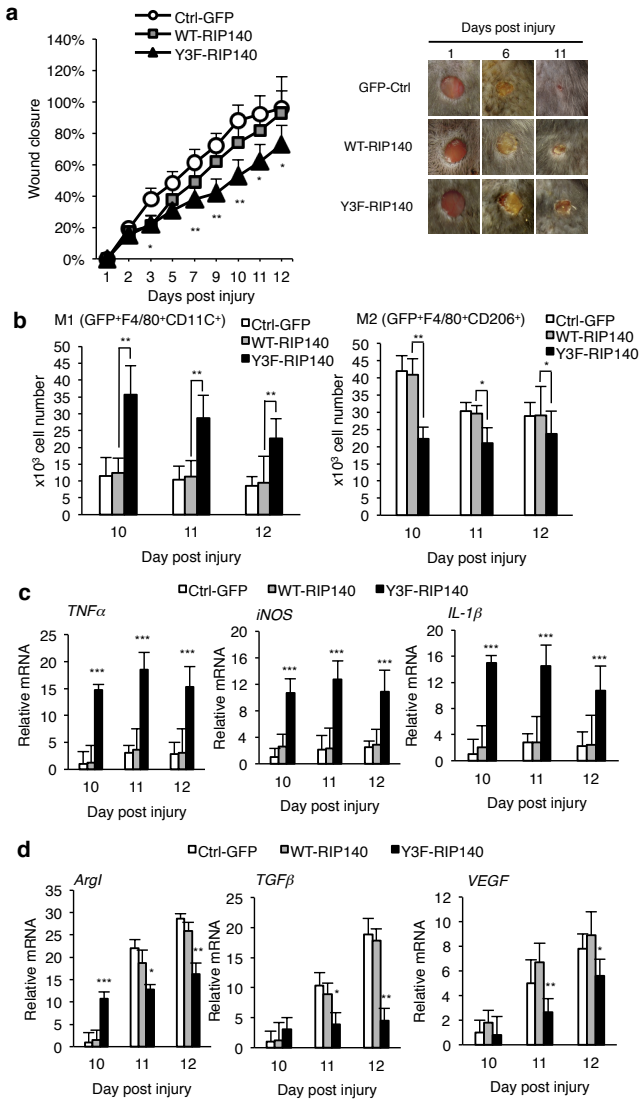
a
Ctrl-GFP
WT-RIP140
Y3F-RIP140
Wound closure
Days post injury
GFP-Ctrl
WT-RIP140
Y3F-RIP140
b
M1 (GFP+F4/80+CD11C+)
M2 (GFP+F4/80+CD206+)
x10^5 cell number
Day post injury
c
TNFα
iNOS
IL-1β
Relative mRNA
d
Arg1
TGFβ
VEGF

Figure 3-3. Preventing RIP140 degradation delays wound healing by inhibiting M1–M2 switch. a Daily record of wound closure in mice receiving WT-GFP-, WT-RIP140- or Y3F-RIP140-expressing cells. A one-way ANOVA test was used * $p < 0.05$; * * $p < 0.01$. **b.** FACS analyses of M1 and M2 populations normalized to the wound mass (cell numbers/mg). **c , d.** qPCR of M1 and M2 marker expression in the wounds of 3 experiments. Student's t test (n = 3) was used. * $p < 0.05$; * * $p < 0.01$; * * * $p < 0.001$ (WTRIP140 vs. Y3F-RIP140). Ctrl = Control.

Figure 3-4.

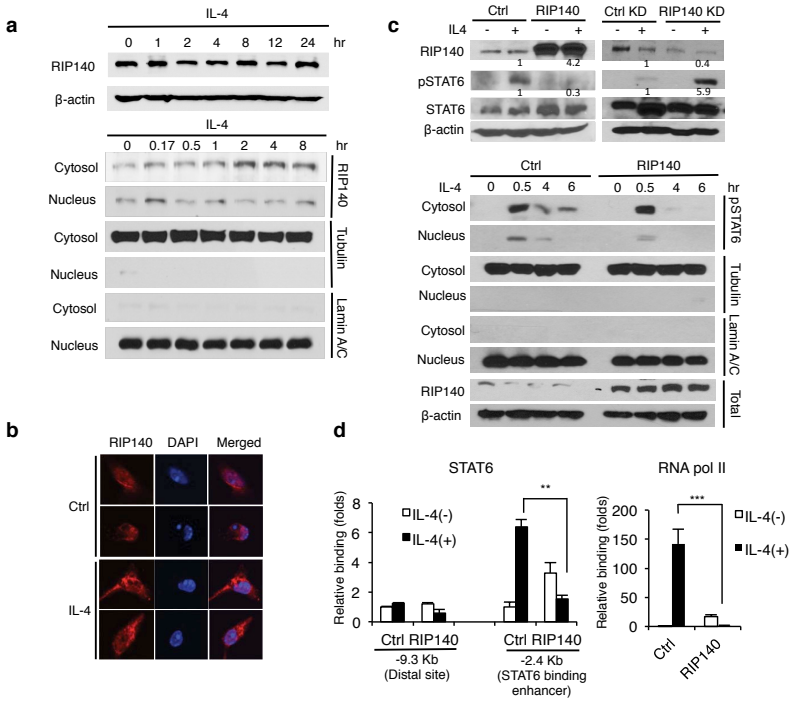

Figure 3-4. RIP140 translocates to the cytosol and suppresses M2 marker gene expression via reducing STAT6 phosphorylation. a. Western blot of endogenous RIP140 from total (top) and the nuclear and cytosolic (bottom) fractions in IL-4-treated RAW264.7. **b.** Immunofluorescence of endogenous RIP140 (red) in IL-4-treated (10 ng / ml) RAW264.7. **c.** Western blot of pSTAT6 and STAT6 in RIP140-overexpression (RIP140) or knockdown (RIP140 KD) RAW264.7, with or without IL-4 treatment (top). Western blot of pSTAT6 and STAT6 in the nuclear and cytosolic fractions (bottom) of RIP140-overexpressing RAW264.7 with IL-4 treatment. **d.** ChIP of STAT6 and RNA pol II on Arg1 promoter in IL-4-treated RAW264.7. Data show 3 experimental results with Student's t test (n = 3). * $p < 0.05$; * * $p < 0.01$; * * * $p < 0.001$. Ctrl = Control.

Figure 3-5.

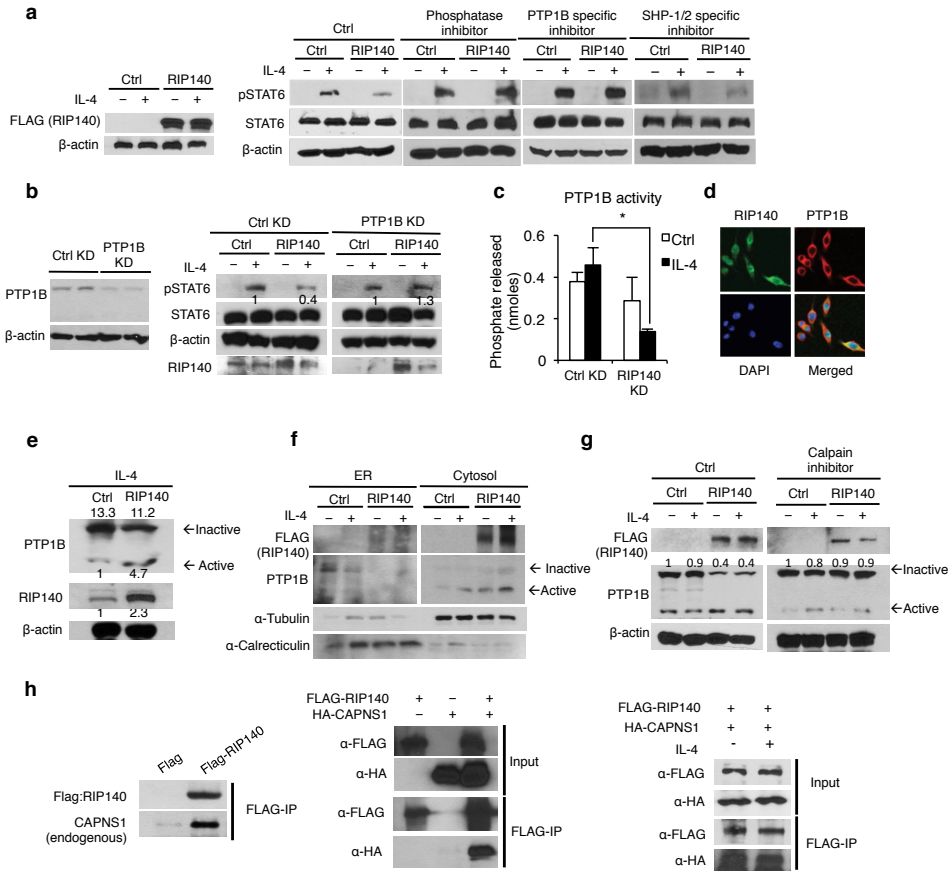
a
Ctrl
RIP140
IL-4
FLAG (RIP140)
β-actin
Phosphatase inhibitor
PTP1B specific inhibitor
SHP-1/2 specific inhibitor
pSTAT6
STAT6
b
Ctrl KD
PTP1B KD
PTP1B
RIP140
c
PTP1B activity
Phosphate released (nmoles)
Ctrl
IL-4
Ctrl KD
RIP140 KD
d
RIP140
PTP1B
DAPI
Merged
e
Inactive
Active
f
ER
Cytosol
α-Tubulin
α-Calreticulin
g
Calpain inhibitor
h
Flag
Flag-RIP140
Flag:RIP140
CAPNS1 (endogenous)
FLAG-IP
FLAG-RIP140
HA-CAPNS1
α-FLAG
α-HA
Input

Figure 3-5. RIP140 suppresses STAT6 phosphorylation by targeting calpain 1/2 to activate PTP1B phosphatase. a. Western blot of pSTAT6 and STAT6 in IL-4-treated control versus RIP140-overexpressing (left) RAW264.7 which were pretreated with a general phosphatase inhibitor, PTP1B specific inhibitor or SHP-1/2 specific inhibitor. **b.** Western blot of PTP1B in control or PTP1Bknockdown RAW264.7 (left). Western blot of pSTAT6 and STAT6 in IL-4-treated control or RIP140-overexpressing RAW264.7 with control or PTP1B knockdown (right). **c.** PTP1B phosphatase activity in RAW264.7 control or RIP140 knockdown, with or without IL-4 treatment. **d.** Immunofluorescence of RIP140 (green), PTP1B (red) and DAPI (blue) in IL-4-treated RAW264.7. e Western blot of PTP1B in control or RIP140-overexpressing IL-4-treated PM. **f.** Western blot of Flag-RIP140, PTP1B, tubulin and calreticulin in ER and cytosolic fractions of RAW264.7 control or IL-4-stimulated, with or without RIP140-overexpressing RAW264.7. **g.** Western blot of PTP1B in the presence (right) or absence (left) of calpain inhibitor. **h.** Co-ip of Flag-RIP140 and endogenous calpain regulatory subunit (CAPNS1) in IL-4-treated RAW264.7 (left), Flag-RIP140 and HA-CAPNS1 in 293TN cells (middle), and Flag-RIP140 and HA-CAPNS1 in IL-4-treated RAW264.7 (right), from 3 experiments. Student's t test (n = 3) was used. * $p < 0.05$; * * $p < 0.01$; * * * $p < 0.001$. Ctrl = Control.

Figure 3-S1.

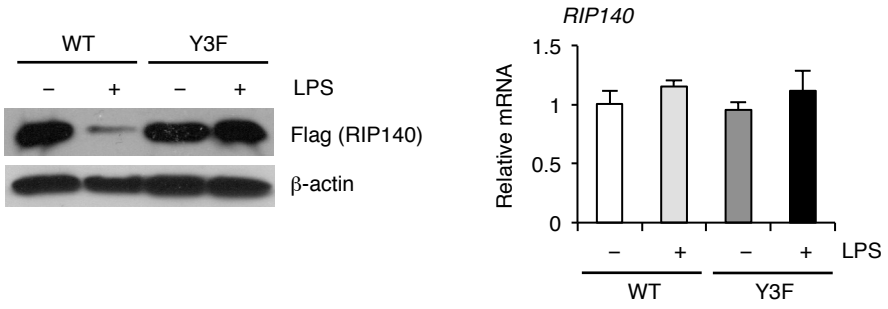

Figure 3-S1. RIP140 expression in PM transfected with WT or Y3F mutant RIP140 followed by control or LPS stimulation.

Protein and mRNA level were analyzed by western blotting and qPCR.

Figure 3-S2.

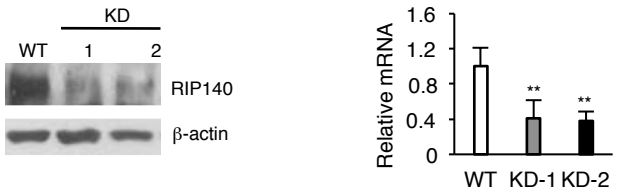

Figure 3-S2. Knockdown efficiency. The expression level of RIP140 protein (left) and mRNA (right) in WT and MφRIP140KD mice.

Figure 3-S3.

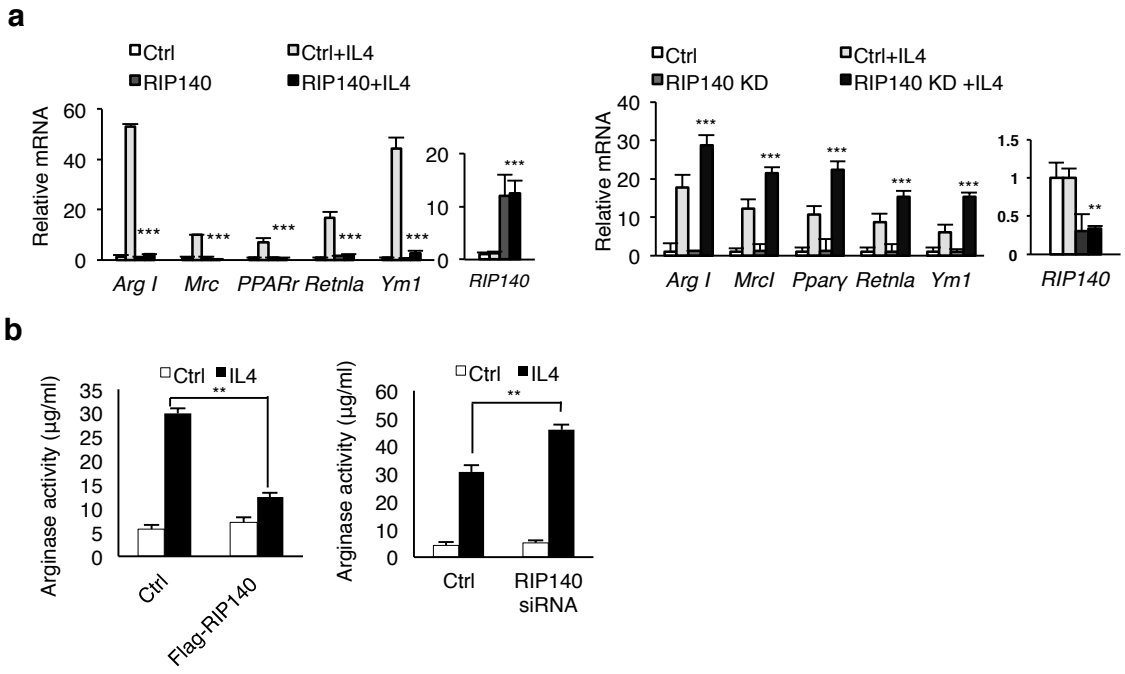

Figure 3-S3. Altering RIP140 levels affects IL4-induced M2 activation.

a. qPCR analyses of M2 gene expression in control vs. RIP140 over-expressing (left) or RIP140-knockdown (right) mouse PM, with or without IL-4 stimulation. b. Arginase activity assay. Data are presented as urea concentrations, and show three experimental results (means±s.d.). Student's t-test (n=3) was used (*P<0.05; **P<0.01; ***P<0.001).

Figure 3-S4.

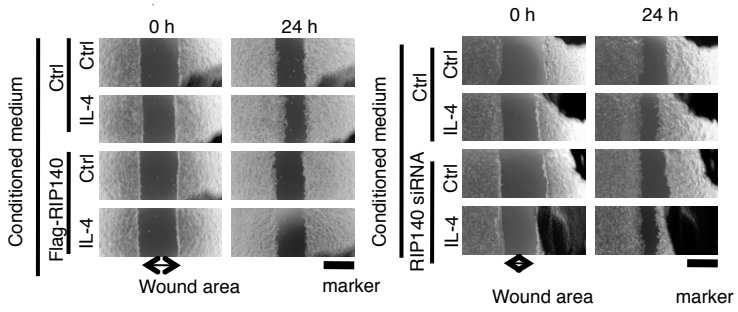

Figure 3-S4. In vitro wound healing assay.

In vitro wound healing was assessed using 293TN cells supplemented with conditioned medium of macrophage with RIP140 over-expression (Flag-RIP140) or RIP140-knockdown (RIP140siRNA). IL-4 was used to trigger M2 polarization of macrophages whereas Ctrl denotes treatment with a control solution without cytokine.

Figure 3-S5.

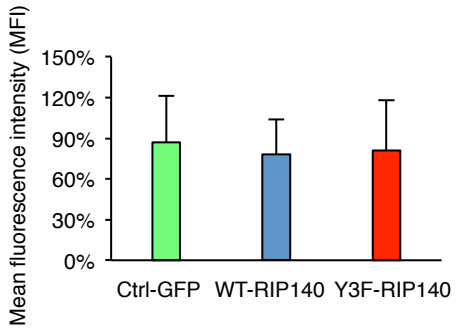

Figure 3-S5. Bone marrow transplantation efficiency validation.

GFP intensity in bone marrow cells of the receiving mice following BMT with cells carrying either Ctrl-GFP, WT-RIP140 or Y3F-RIP140.

Figure 3-S6.

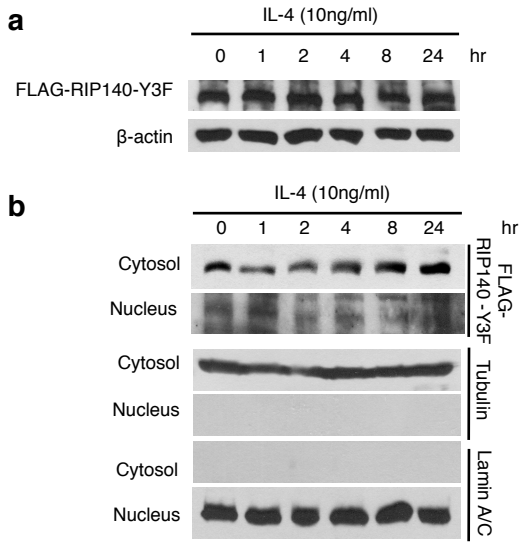

Figure 3-S6. Non-degradable mutant RIP140 (RIP140-Y3F) can also translocate to the cytosol in macrophages upon IL-4 treatment.

a. Western blot analyses of FLAG-RIP140 Y3F from total cell lysate in IL-4 (10ng/ml) treated RAW264.7 cells. b. Western blot analyses of FLAG-RIP140 Y3F from the cytosolic/nuclear fractions of IL-4 (10ng/ml) treated RAW264.7 cells. Data show three experimental results.

Figure 3-S7.

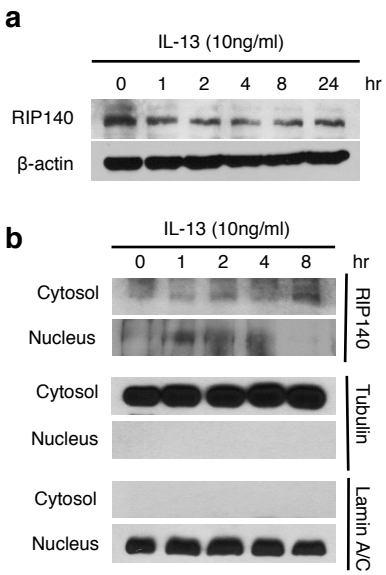

Figure 3-S7. Endogenous RIP140 translocates to the cytosol in macrophages upon IL-13 treatment.

a. Western blot analyses of endogenous RIP140 from total cell lysate in IL-13 (10ng/ml) treated RAW264.7 cells. b. Western blot analyses of RIP140 from the cytosolic/nuclear fractions of IL-13 (10ng/ml) treated RAW264.7 cells. Data show three experimental results.

Figure 3-S8.

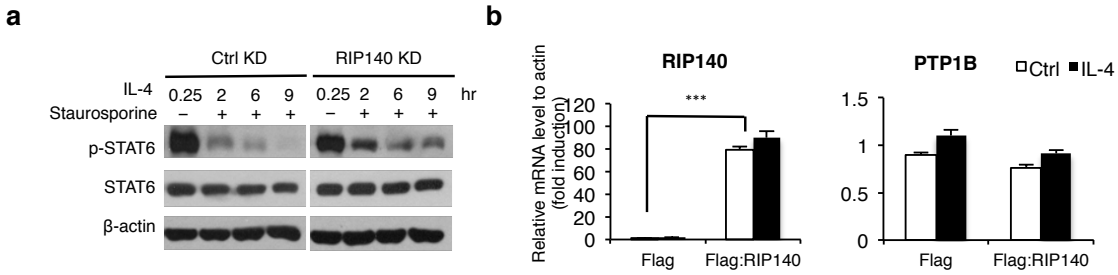

Figure 3-S8. RIP140 knockdown still increases pSTAT6 levels in macrophages treated with kinase inhibitor, but fails to affect PTP1B gene expression.

a. Western blot analyses of phospho-STAT6 and STAT6 levels in IL-4-treated (10ng/ml) control vs. RIP140 knockdown RAW264.7 cells, with or without pretreatment with kinase inhibitor Staurosporine (50ng/ml). b. qRT-PCR analyses of RIP140 and PTP1B mRNA levels in control (flag) vs. RIP140-overexpressing RAW264.7 cells with or without IL-4 treatment (10ng/ml, 6hr). Data show three experimental results (means±s.d.). Student's t-test (n=3) was used (*P<0.05; **P<0.01; ***P<0.001).

Preface

This chapter has not been published, but in preparation for publication:

Bomi Lee[a], Urszula T. Iwaniec[b], Russell T. Turner[b], Bart L. Clarke[c], Anne Gingery[d] and Li-Na Wei[a,]

The affiliations of collaborators for this study are below:

[a]Department of Pharmacology, University of Minnesota Medical School

[b]Skeletal Biology Laboratory, School of Biological and Population Health Sciences, College of Public Health and Human Sciences, Oregon State University

[c]Division of Endocrinology, Diabetes, Metabolism, and Nutrition, Mayo Clinic

[d]Division of Orthopedic Research, Mayo Clinic

*Contribution: B.L., A.G., and L.N.W. designed research. B.L., A.G. performed research, B.L., U.T.I, R.T.T., and A.G. collected data. B.L., U.T.I., R.T.T, B.L.C., A.G., L.N.W. contributed to discussion, reviewed and wrote paper.

Chapter IV

Orphan Nuclear Receptor TR4-Receptor interacting Protein 140 Complex

In Osteoclast Differentiation, Function and Bone Mass

Introduction

Bone homeostasis requires a balance between osteoclast-mediated bone resorption, and osteoblast-mediated bone formation[137,138]. Pathological conditions such as osteoporosis, rheumatoid arthritis and osteolytic bone metastases lead to uncoupling of resorption and bone formation, resulting in bone loss, increased fracture risk and deterioration in bone micro-architecture[139]. It has become increasingly evident that metabolism has a substantial impact on skeletal health and the coupling of bone formation and resorption[140,141].

Multinucleated, mature osteoclasts are derived from the fusion of myeloid osteoclast progenitor cells[142]. Macrophage Colony Stimulating Factor (M-CSF) activation of the M-CSF receptor/colony stimulating factor (c-fms) and Receptor Activator of Nuclear factor Kappa-B Ligand (RANKL) activation of its receptor RANK are important signaling events that trigger osteoclast precursor proliferation and differentiation[143,144]. RANKL signaling activates transcription factors, such as Nuclear Factor of Activated T cells cytoplasmic 1 (NFATc1), and c-fos to upregulate osteoclast functional genes such as Tartrate-Resistant Acid Phosphatase (TRAP, Acp5) and Cathepsin K (Ctsk)[38].

Metabolic effects on skeletal health present an increasingly recognized medical concern, as obesity, metabolic syndrome, and type II diabetes are on the rise[145-147]. It was once thought that increased body mass would be protective to the skeleton, but this has now been put to serious question as adipose tissue, in particular, visceral fat depots have been found to negatively impact bone health[148,149]. For instance, fat and visceral adipose tissue mass are negative predictors of bone quality in overweight and obese patients[150].

Furthermore, women with type 2 diabetes mellitus (T2DM) have a normal or higher bone mineral density; however, they have nearly double the risk of fracture, indicating that overall quality of the bone is impaired[151]. Metabolic disease and obesity induce the accumulation of M1 inflammatory macrophages, resulting in increased inflammation and insulin resistance. In contrast, in lean humans and mice, M2 anti-inflammatory macrophages predominate[152]. We have previously shown that the co-regulator, Receptor Interacting Protein 140 (RIP140) plays an important role in macrophage polarization. RIP140 is a co-activator for NF-κB in pro-inflammatory (M1) macrophages and its degradation mediates resolution of inflammation[36]. RIP140 is also a cytosolic repressor of alternative, anti-inflammatory (M2) polarized macrophages[81]. In mice, lowering macrophage-specific RIP140 expression levels reduces M1 macrophages, increases M2 macrophages, prevents high fat diet-induced insulin resistance, and enhances insulin sensitivity and white adipose tissue browning even under a high fat diet[37].

RIP140 is also a co-repressor of most nuclear receptors including orphan Testicular nuclear Receptor 4 (TR4) [20,153]. A global knockout of TR4 resulted in severe cachexia and spinal kyphosis, with impact both on the skeleton and metabolism[154]. Given that monocytes/macrophages are osteoclast progenitors, that RIP140 plays a significant role in macrophage activation, and that RIP140 co-regulates TR4 activity, we speculated a functional role for TR4/RIP140 complex in osteoclast-affected bone health. Indeed, peripheral blood analyses of osteoporosis patients have indicated a significant penetrance of the RIP140 gene, *Nrip1,* SNPs in osteoporosis patients[155].

Here we present evidence for a physiological role for TR4/RIP140 complex in bone homeostasis, which suggests a potential for targeting RIP140 in the development of therapeutics for bone diseases.

Materials and Methods

Reagents

Reagent sources: mouse RANKL (Biolegend, #577102), mouse M-CSF (Sigma-Aldrich, #M9170). Antibody sources: α-HA (sc-7392), α-NFATc1 (sc-13033), α-TR4 (sc-9086), α-pMEK1/2 (sc-7995), α-MEK1/2 (sc-436), α-p65 (sc-372), α-β-actin (sc-47778) from Santa Cruz. α-FLAG (F3165) from Sigma-Aldrich. α-RIP140 (ab42126) from Abcam. α-pERK1/2 (#9101), α-ERK1/2 (#9102) and α-pp65 (#3033) are from Cell signaling.

Immunoprecipitation and Mass spectrometry

FLAG-RIP140 cells were treated with or without doxycycline (250 ng/ml) for 6 hr. Cells were washed with PBS and harvested. Nuclear extract was prepared using hypotonic buffer, low salt buffer and high salt buffer. Benzonase nuclease (Sigma) was treated, and nuclear extract was dialyzed in BC300[156]. After pre-clearing with mouse IgG-agarose beads, nuclear extract was immunoprecipitated with anti-FLAG M2 magnetic beads (Sigma) and washed with 0.1% NP-40-contained BC300. FLAG-RIP140-bound proteins were eluted with FLAG peptides (Sigma), and samples were sent to the Taplin Biological Mass Spectrometry Facility at Harvard Medical School for mass spectrometry analysis. FLAG-RIP140 binding proteins were validated with western blot analysis using specific antibodies.

Cell culture and conditioned medium (CM) experiment

For primary osteoclasts, bone marrow cells were isolated from mouse femurs and tibias by flushing bone marrow with PBS. After lysing red blood cells, bone marrow cells were plated and incubated with α-MEM media overnight. Non-adherent cells were plated with M-CSF (25ng/ml) and RANKL (100ng/ml) for 5 days. MC3T3-E1 cells were cultured in α-MEM medium supplemented with 10% FBS and 1% antibiotics. RAW264.7 cells were cultured in DMEM medium supplemented with 10% FBS and 1% antibiotics. For the conditioned medium (CM), FBS-contained fresh α-MEM media was added to primary osteoclasts differentiated with M-CSF and RANKL for 5~6 days. After 24 hr incubation, CM was collected and added to MC3T3-E1 cells or primary osteoblasts for 3 days with ascorbic acid (50μg/ml) for osteoblast differentiation.

DNA constructs lentivirus production and transduction

WT-RIP140 and Y3F-RIP140 expression lentivirus constructs were as described[36]. Doxycycline-inducible FLAG-HA-RIP140 expression lentivirus construct was made as described[157]. Viruses were generated by transfection of lentivirus constructs and packaging plasmids in HEK293T cells. Incubated medium including viruses was harvested on 3 days after transfection, and filtered to remove flowing 293T cells. Filtered viruses were concentrated with Lenti-X (Clontech, #631232) overnight. Viruses are collected by centrifugation and saved in -80 degree. For virus transduction in cells, viruses were incubated in Polybrene (EMD Millifore)-contained media for 3 days.

RNA isolation and gene expression analysis

Total RNA was isolated using TRIzol (Invitrogen). Reverse transcription (RT) was performed using High-Capacity cDNA Reverse Transcription Kit (Applied Biosystems). Quantitative real-time PCR (qPCR) was performed with SYBR enzyme mix (Thermo Scientific, #K0253). Each gene expression experiment was performed triplicate. Expression levels were normalized to β-actin mRNA level.

Western blot analysis

RAW264.7 cells were lysed with cell lysis buffer (20mM Tris-HCl pH7.5, 150mM NaCl, 1mM EDTA, 1mM EGTA, 2.5mM Sodium Pyrophosphate, 1mM glycerophosphate, 1% NP40, 1% deoxy cholate), and cell lysates were mixed with SDS loading dye and loaded to a SDS-PAGE gel to separate proteins after protein quantification using a Bradford method. Separated proteins in a SDS-PAGE gel are transferred to a western blot membrane and blotted with primary and secondary antibodies.

Chromatin-immunoprecipitation (ChIP) assay

RAW264.7 cells were crosslinked with 1% formaldehyde, lysed, sonicated and immunoprecipitated with antibodies overnight. Magnetic beads (EDM Millipore, #16-663) were added to pull down antibody-protein-DNA complex. After 4 hr incubation, beads were washed with low salt, high salt, LiCl buffer and TE buffer according to the instruction from EZ-ChIP (EMD Millipore, #17-371). Following reverse-crosslinking, DNA was isolated and analyzed by qPCR.

In vitro TRAP (tartrate-resistant acid phosphatase) assay/ALP (alkaline phosphatase)/Calcium assay

TRACP and ALP assay kit was purchased from Takara (#MK301). For TRAP assay, bone marrow-derived primary osteoclasts or RAW264.7 cells were plated in a 96 well plate and lysed with extraction solution. Cells were immediately incubated with pNPP-contained substrate solution for 60 min, and then stop solution (0.5N NaOH) was added to measure the absorbance at 405nm. For ALP assay, serum was collected from mice blood, and then samples were incubated with substrate, as similar to TRAP assay except for the buffer condition. Calcium concentration in mouse serum was detected using calcium reagent set (#503-Teco diagnostics). The buffers provided from the kit were mixed with serum, and the color change was detected by the absorbance at 570nm.

Animal

All studies were carried out using male C57BL/6J mice maintained in the animal facility of the of Minnesota. 9 week-old male mice (n=9-10/group) were injected with the fluorochrome calcein (12.5 mg/kg; Sigma Chemical) 4 days and 1 day prior to sacrifice to label mineralizing bone. Animal studies were approved by the University of Minnesota IACUC. MϕRIP140KD mice were generated as described[36,81].

Microcomputed Tomography

Microcomputed tomography (μCT) was used for nondestructive 3-dimensional evaluation of bone volume and architecture as previously described[158]. In brief femora were scanned in 70% ethanol using a Scanco μCT40 scanner (Scanco Medical AG, Basserdorf, Switzerland) at a voxel size of 12 x 12 x 12 μm (55 kVp x-ray voltage, 145 μA intensity, and 200 ms integration time). For the femoral diaphysis, 20 consecutive slices (240 μm) of bone were evaluated and cross-sectional volume (cortical and marrow

volume, mm^3), cortical volume (mm^3), marrow volume (mm^3), cortical thickness (μm) were measured. Polar moment of inertia was determined as a surrogate measure of bone strength in torsion. Analysis of the lumbar vertebra included the entire region of cancellous bone between the cranial and caudal growth plates (151 ± 2 slices, 1,812 ± 24 μm). Direct cancellous bone measurements included cancellous bone volume fraction (bone volume/tissue volume, %), connectivity density (mm-3), trabecular number (mm-1), and trabecular thickness (μm). Further details are provided in *SI Materials and Methods.*

Histomorphometry

Methods used for measuring static and dynamic bone histomorphometry have been described[159]. In brief, distal femora were dehydrated in a graded series of ethanol and xylene, and embedded undecalcified in modified methyl methacrylate. Longitudinal sections (4 μm thick) were cut with a vertical bed microtome (Leica 2065) and affixed to slides precoated with 1% gelatin solution. All data were collected using the OsteoMeasure System (OsteoMetrics, Inc.). Fluorochrome-based measurements of bone formation included 1) mineralizing perimeter 2) mineral apposition rate and 3) bone formation rate. Cell-based measurements included osteoblast perimeter and osteoclast perimeter. All bone histomorphometric data are reported using standard nomenclature[160].

Reference point indentation

The material properties of the anterior surface of the tibia mid-diaphysis were assessed using ex vivo reference point indentation (RPI) (BioDent Hfc; Active Life Scientific). Tibias were rehydrated in PBS prior to testing, and all tests were conducted in PBS. A

reference force of ~550 N was applied to each femur. Measurements consisted of 10 cycles at 4 N. 3 to 5 measurements were collected per tibia sample, with a distance of at least 250 μm between sampling sites. RPI metrics, including first cycle indentation distance, total indentation distance, first cycle energy dissipated, and first cycle unloading slope, were obtained using the manufacturer's software.

Statistics

In vitro experiments were performed at least three times and results were presented as means ± SD. Student's t-test was used. P values of 0.05 or less were considered statistically significant (*P<0.05; **P<0.01; ***P<0.001).

Results

TR4/RIP140 complex formation and repression of osteoclast gene expression

Given RIP140's early expression and biological activity in the monocyte-macrophage lineage, and that osteoclasts differentiate from the monocyte/macrophage lineage, we speculated a functional role for RIP140 in osteoclast differentiation and activity. We first sought to identify the RIP140 complex involvement in early phases of osteoclast differentiation by examining RIP140-containing complexes in a murine preosteoclastic cell line RAW264.7[161]. We introduced a FLAG-RIP140 vector into RAW264.7 cells and immunoprecipitated nuclear FLAG-RIP140 complexes. Mass spectrometry data revealed TR4 (*Nr2c2*), a previously reported orphan receptor that acts primarily to repress genes[153,162], with the greatest number of unique reads (Fig. 4-1A). TR4/RIP140 complex formation was confirmed by co-immunoprecipitation assays (Fig.

4-1B, C). Interestingly, TR4 mRNA and protein expression was down-regulated in RANKL-stimulated osteoclast cultures (Fig. 4-1D). We then performed TR4 knockdown (KD) in RAW264.7 cells under RANKL stimulation and found elevated expression of *Nfatc1, Ctsk* and *Acp5*, markers of osteoclast differentiation (Fig. 4-1E). In contrast, overexpression of TR4 in RANKL-stimulated RAW264.7 cells rendered significant or nearly significant down regulation of osteoclast genes (supplementary Fig. 4-S1A), which further supports a repressive activity of the TR4 complex in osteoclast differentiation (see later for the co-repressive activity of RIP140). We also validated TR4 binding to endogenous osteoclast marker gene promoters. This binding was reduced by RANKL treatment, which was recovered by elevating RIP140 expression (Fig. 4-1F). Taken together, these data reveal that RIP140 forms a complex with TR4 in preosteoclastic cells, and the TR4/RIP140 complex exerts a repressive effect on osteoclast differentiation through directly targeting promoter regions of genes critical for osteoclast differentiation or activity.

RIP140's repressive activity and its protein degradation in RANKL-stimulated osteoclast differentiation

To determine the functional role of RIP140 in osteoclast differentiation, we first performed a gain-of-function study in RANKL-stimulated RAW264.7 cells. Elevating RIP140 levels dampened expression of differentiation markers (Fig. 4-2A), confirming the co-repressive activity of RIP140 in RANKL-induced osteoclast differentiation. Interestingly, RANKL stimulation decreased RIP140 protein level without altering *RIP140* mRNA expression (Fig. 4-2B and 4-2C) suggesting post-transcriptional

regulation to lower RIP140 protein level by RANKL stimulation. We previously identified Syk, a non-receptor tyrosine kinase, that stimulated a RIP140 protein ubiquitination/degradation pathway in M1 polarized macrophages[36]. Interestingly, Syk inhibition reduced RANKL-stimulated osteoclast gene expression and RIP140 protein degradation (Fig. 4-2B and 4-2D). To provide further evidence for the significance of RIP140 degradation in this process, lentiviruses carrying either wild type (WT) or a non-degradable RIP140 mutant (Y3F) were introduced into bone marrow-derived mononuclear cells, which were then treated with M-CSF and RANKL for osteoclast differentiation. As predicted, differentiation markers were reduced by expressing WT RIP140, and completely blocked by expressing Y3F (Fig. 4-2E). Thus, RIP140 exerts a co-repressive activity for RANKL-stimulated osteoclast differentiation markers, and RIP140 is degraded over time by RANKL treatment during differentiation. Accordingly, we conclude that the TR4/RIP140 complex exerts a repressive activity in osteoclast differentiation. RANKL signal triggers TR4 mRNA down-regulation and RIP140 protein degradation, providing a physiological break to terminate the potent repressive activity of TR4/RIP140 complex on osteoclast differentiation.

RIP140 suppresses RANKL signaling and activation of osteoclastogenic genes

RANKL signaling activates NF-κB and MAPK to induce osteoclast differentiation[163-165]. We monitored the effect of RIP140 on kinetic changes in the endogenous signaling components following RANKL treatment. As shown in Fig. 4-3A, RANKL-induced MEK1/2, ERK1/2 and p65 phosphorylation within 30 minutes, which was abolished by over-expressing RIP140 in RAW264.7 cells. Consistently, RANKL

induced Tartrate-Resistant Acid phosphatase (TRAP) was dose-dependently reduced by expressing RIP140 (Fig. 4-3B). To confirm the effects of RIP140 on osteoclastogenic gene activation, we performed chromatin immunoprecipitation (ChIP) assay to monitor transcription factors binding to the principal TR4-regulated osteoclastogenic gene *Nfatc1* in HA-RIP140 expressing RAW264.7 cells. Fig. 4-3C left panel shows reduced recruitment of RIP140 to *Nfatc1* upon RANKL stimulation. TR4 binding was significantly enhanced by overexpressing RIP140 in unstimulated cells, however upon RANKL treatment the complex was significantly reduced, supporting TR4/RIP140 repressive complex formation on *Nfatc1*, a key pre-osteoclast differentiation gene. In the later (24 hrs) phase of RANKL-stimulation, the repressor TR4 no longer bound to this gene as predicted (Fig. 4-3C, second left panel). *Nfatc1* promoter was bound by major activating transcription factors NFATc1 itself and PU.1 in unstimulated cells, which was enhanced by RANKL treatment. But overexpressing RIP140 reduced binding of these activating transcription factors for both unstimulated and RANKL-stimulated cells (Fig. 4-3C, two central panels), confirming the suppressive effect of RIP140 on osteoclastogenic program. Consistently, RANKL-triggered transcription activation marks such as H3 acetylation was dampened and transcription silencing markers such as H3K9 tri-methylation was enhanced by increasing RIP140 expression (Fig. 4-3C, two right panels). Together, these data confirm a suppressive role for TR4/RIP140 transcription complex in the osteoclastogenic differentiation program.

Enhancing osteoclast differentiation/activity by reducing RIP140 in animals.

Bone remodeling involves coupling of osteoclast-mediated bone resorption and osteoblast-mediated bone formation. To examine the functional relevance of RIP140 in bone homeostasis in animals, we examined the bone phenotype of a monocyte/macrophage-specific RIP140 KD transgenic mouse model, mϕRIP140KD. We first carried out *in vitro* osteoclast differentiation using bone-marrow cells from tibias and femurs of WT and mϕRIP140KD mice, stimulated with RANKL and M-CSF for 2 days. The expression of osteoclast marker genes *Nfatc1, Ctsk and Acp5* in WT cultures was elevated following RANKL treatment; this was further enhanced in cultures collected from mϕRIP140KD mice (Fig. 4-4A) because of the deletion of RIP140-mediated suppression in this primary osteoclast differentiation system. RIP140 KD efficiency was confirmed (Fig. 4-4A, right). The mature osteoclast functional indicator such as TRAP activity was increased, whereas the osteoblast functional indicators such as alkaline phosphatase and calcium concentration were significantly reduced in mϕRIP140KD mice (Fig. 4-4B), further confirming that the coupling has been affected by reducing RIP140 expression to enhance osteoclastogenesis. Conditioned medium (CM) from osteoclast cultures derived from WT or mϕRIP140KD mouse bone marrow-derived mononuclear cells was applied to MC3T3-E1 osteoblast cells to assess *in vitro* coupling of osteoclast to bone formation responses. Markers of osteoblast differentiation *Runx2, Osterix* and *Alkaline phosphatase* were assessed by quantitative PCR. Consistent with the result of osteoblast activity in mouse serum, osteoblast marker gene expression was substantially diminished by treatment with CM of osteoclasts derived from mϕRIP140KD mice (Fig.

4-4C). These data further support the functional consequence of depleting RIP140 in osteoclasts *in vivo*, that depleting RIP140 enhances osteoclast differentiation and activity, which inhibits osteoblast differentiation and results in uncoupling of osteoclasts and osteoblasts.

Loss of RIP140 *in vivo* results in decreased cancellous volume

To further validate RIP140's functional role in osteoclastogenesis suppression *in vivo*, we performed μCT and histomorphometric analysis of bones of WT and mϕRIP140KD mice. A representative μCT image (Fig 4-5A) of the femoral diaphysis and metaphysis shows cortical and cancellous bone volume fraction in control and mϕRIP140KD mice. Significant differences in cortical bone parameters in the femur diaphysis were not detected with genotype (Fig. 4-5B). Additionally, reference point indentation material properties assessed *ex vivo* on the tibia of control and mϕRIP140KD mice were not significantly different (supplementary Fig. 4-S2A). In contrast, bone volume fraction (BV/TV) at both the distal femur metaphysis (37%) and the L5 vertebra (15%) was significantly lower in mϕRIP140KD mice compared to WT mice (Fig. 4-5C and D). The reduction in bone volume fraction in the femur metaphysis was associated with a reduction in connectivity density (Fig. 4-5C, two left panels). However, significant differences in trabecular number, thickness, or spacing were not detected with genotype in the femur metaphysis (Fig. 4-5C, three right panels). In contrast, vertebrae in mϕRIP140KD mice showed reduced connectivity density, trabecular thickness and increased trabecular spacing (Fig. 4-5D).

Bone resorption and formation indices were significantly altered with loss of RIP140.

Mineralizing perimeter and bone formation rate were both significantly reduced (-46% and -54%, respectively) in the femur metaphysis of mϕRIP140KD mice as compared to control (Fig. 4-6A, two left panels). Significant differences in mineral apposition rate were not detected with genotype (Fig. 4-6A, middle panel). Consistent with *in vitro* results, osteoclast perimeter/bone perimeter was significantly increased (+46%) with a concomitant decrease (-90%) in osteoblast perimeter/bone perimeter, indicating uncoupling of osteoclast and osteoblast formation (Fig. 4-6A, two right panels). The effects of genotype on bone formation (incorporation of label into mineralizing bone) and bone resorption (osteoclast perimeter) can be appreciated in Fig. 6B.

Discussion

In this study, we uncovered that TR4 and RIP140 form a transcriptional repressor complex to suppress osteoclast differentiation. With RANKL treatment this repressive complex is dampened as a result of reduction in TR4 mRNA and RIP140 protein levels, providing a physiological brake to terminate this important repressive control of osteoclastogenesis. The TR4/RIP140 complex targets key genes for osteoclast differentiation and activity including *Nfatc1, Ctsk* and *Acp5*. The physiological significance of this is demonstrated in a monocyte/macrophage lineage-specific RIP140 KD mouse model, which exhibits an osteopenic phenotype with increased osteoclast and

reduced osteoblast numbers, ultimately resulting in decreased bone formation rate and trabecular bone volume, similar to what is seen in many conditions of pathologic bone loss. Consistent with *in vivo* studies, osteoblastic MC-3T3 cells cultured with conditioned medium from mϕRIP140KD primary osteoclasts had significantly reduced osteoblast marker gene expression. This indicates that RIP140 can be an important regulator of osteoclast-mediated coupling with osteoblasts.

Of interest, RANKL-stimulated cells utilize different mechanisms to down-regulate the TR4/RIP140 repressive complex. While TR4 expression is reduced mainly at the level of mRNA, RIP140 protein is rapidly degraded by RANKL-induced, Syk-mediated phosphorylation. Thus, targeting and maintaining RIP140 protein stability/quality provides a potential therapeutic strategy for various bone destructive diseases. To this end, several reports have indicated RIP140 as a candidate gene associated with bone-related traits and osteoporosis in microarray, multilocus single nucleotide polymorphisms (SNPs) analysis. RIP140 gene expression in hematopoietic cells was found to have a correlation with bone mineral density[166]. Further, analysis with estrogen-related genes in Spanish postmenopausal women detected genetic interactions between RIP140 and other estrogen-related genes such as *ESR2* and *BMP15* loci, and the involvement of RIP140 in osteoporosis[155,167]. Recently, it has also been reported that RIP140 is involved in estrogen's effect on osteoclast differentiation and bone resorption[168]. These studies further support our conclusion that RIP140 plays a critical role in maintaining bone health and is a potential therapeutic target for bone diseases such as osteoporosis.

Whole body TR4 knockout leads to postnatal mortality and growth retardation, impaired reproduction and maternal behavior in female mice[154], and impaired skeletal development including osteoporosis with reduced osteoblast activity[169]. This further supports our monocyte/macrophage lineage-specific KD of RIP140 mouse model, which displays an osteopenic phenotype in the skeletal system.

Increased osteoclast number and bone resorption are characteristic of bone destructive diseases such as osteoporosis, osteolytic bone metastases, and rheumatoid arthritis. Therefore, an important therapeutic strategy for these diseases is to maintain the coupled resorption and formation that is found in healthy bone remodeling. Specifically targeted therapeutics that can regulate osteoclast activity would be an important leap forward in therapeutic design, rather than relying on substantial inhibition of osteoclast activity or survival. In osteoclast differentiation, there are well known RANKL-stimulated positive signaling components such as MAPK, NF-κB and calcium-dependent signal transduction[170], as well as negative regulators such as Ids, Mafb, Irf8 and Bcl6[53-55,171,172]. Our study reveals a master transcriptional regulator complex for osteoclastogenesis; importantly, this complex is regulated by rapid RIP140 degradation, which provides a new target for therapeutic intervention and preventive care for various bone diseases. However, endogenous signaling molecules that mediate the coupling of osteoclasts and osteoblasts to maintain bone homeostasis remain to be identified.

Another major function of the skeleton is accommodating the hematopoietic niche which is the origin of immune cells, including monocytes/macrophages and dendritic cells[173]. Given the prominent expression and function of RIP140 in the monocyte-

macrophage lineage, mϕRIP140KD mice indeed exhibit multiple phenotypes all related to disruption in macrophage differentiation/activation such as inflammation[36], wound healing[81], type 2 diabetes[37], atherosclerosis[174] and osteopenia (this current study). It is not surprising that these metabolic disease conditions can easily be accompanied by bone destruction or osteoporosis. Our results show a specific mechanism of osteoclast regulation that may be an important and novel therapeutic target for osteolytic diseases. Questions remain as to the degree of other systemic effects caused by reducing RIP140 in the monocyte-macrophage lineage which may also contribute to overall bone metabolism. In summary, our results reveal a critical role for the TR4/RIP140 transcription regulatory complex in osteoclast differentiation, activity and bone remodeling.

Figures

Figure 4-1.

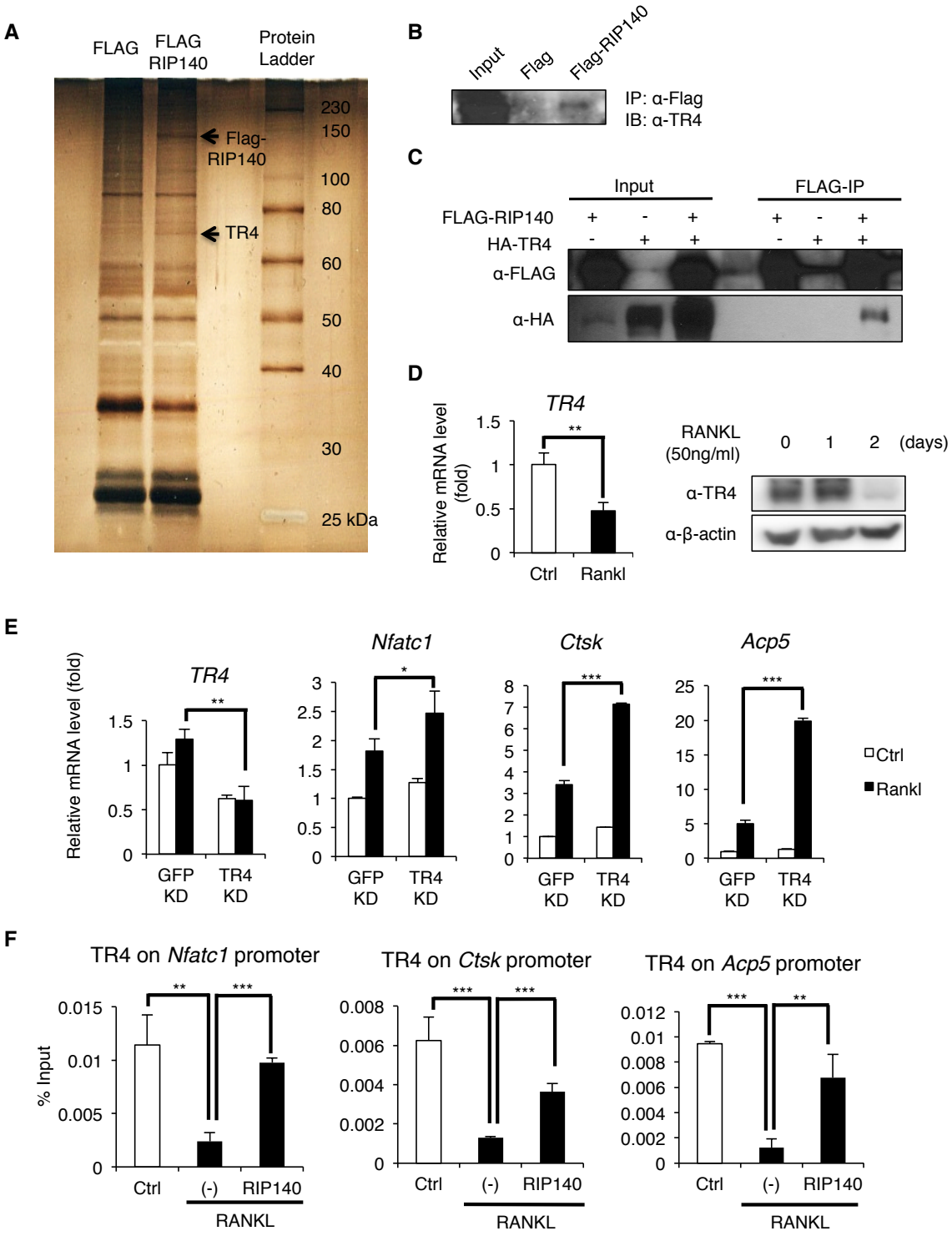

Figure 4-1. TR4/RIP140 complex formation and repressive activity in osteoclast differentiation.

A. Silver stained of FLAG-RIP140 associated proteins. **B.** Western blot analysis of RIP140/TR4 complex. **C.** Co-immunoprecipitation (IP) of FLAG-RIP140/HA-TR4 from HEK293T. **D.** qRT-PCR and western analyses of TR4 after RANKL stimulation for 2 days. **E.** qRT-PCR analysis of osteoclast marker genes in control (GFP KD) vs. TR4 (TR4 KD) knockdown RAW264.7 cells with or without RANKL treatment for 24 hr. **F.** ChIP assay of TR4 on osteoclast marker gene promoters in RAW264.7 cells treated with RANKL stimulation for 30 min. Data are representative of three experimental repeats (mean ± s.d). Student's t-test (n=3) was used (*P<0.05; **P<0.01; ***P<0.001).

Figure 4-2.

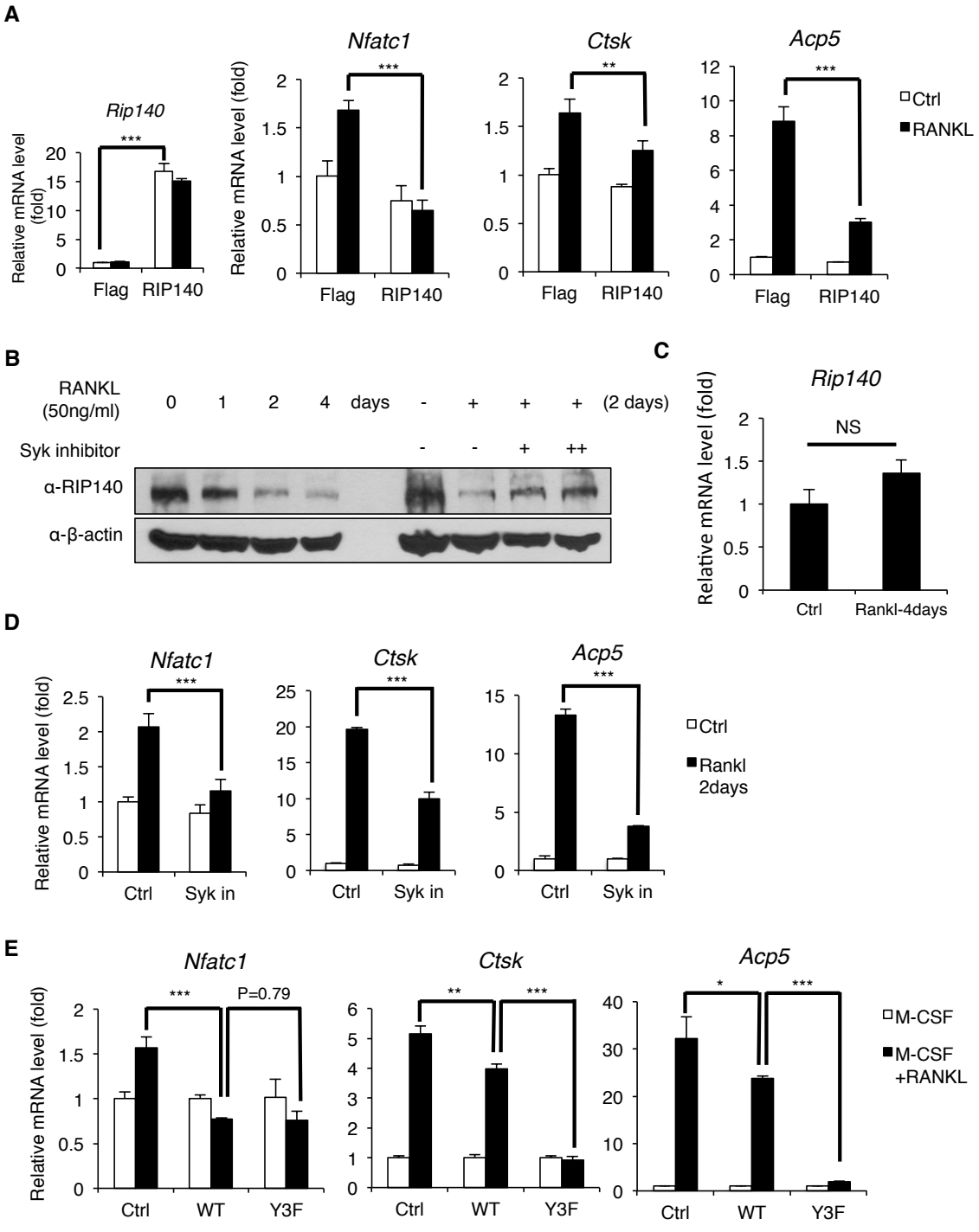
A
Rip140
Relative mRNA level (fold)
Flag
RIP140
Nfatc1
Relative mRNA level (fold)
Ctsk
Acp5
Ctrl
RANKL
B
RANKL (50ng/ml)
0 1 2 4 days - + + + (2 days)
Syk inhibitor
- - + ++
α-RIP140
α-β-actin
C
Rip140
NS
Relative mRNA level (fold)
Ctrl
Rankl-4days
D
Nfatc1
Ctsk
Acp5
Relative mRNA level (fold)
Ctrl
Syk in
Ctrl
Rankl 2days
E
Nfatc1
Ctsk
Acp5
P=0.79
Relative mRNA level (fold)
Ctrl
WT
Y3F
M-CSF
M-CSF +RANKL

Figure 4-2. RIP140 represses osteoclast differentiation and is degraded by RANKL treatment in osteoclast differentiation.

A. qRT-PCR analyses of osteoclast markers in control (FLAG) or FLAG-RIP140-overexpressing RAW264.7 cells treated with RANKL for 2 days. **B.** Western blot analyses of RIP140 in RAW264.7 cells treated with RANKL for indicated time periods with or without Syk (non-receptor tyrosine kinase) inhibitor pretreatment. **C.** qRT-PCR analyses of RIP140 in RAW264.7 cells with or without RANKL treatment for 4 days. **D.** qRT-PCR analyses of osteoclast markers in RAW264.7 cells treated with RANKL for 2 days with or without Syk inhibitor pre-treatment. **E.** qRT-PCR analyses. Bone marrow-derived osteoclasts were differentiated with M-CSF and RANKL for 3 days following transduction with lentiviruses carrying control (Ctrl), wild type RIP140 (WT) or non-degradable mutant RIP140 (Y3F). Data are representative of three experimental repeats (mean ± s.d). Student's t-test (n=3) was used (*P<0.05; **P<0.01; ***P<0.001).

Figure 4-3.

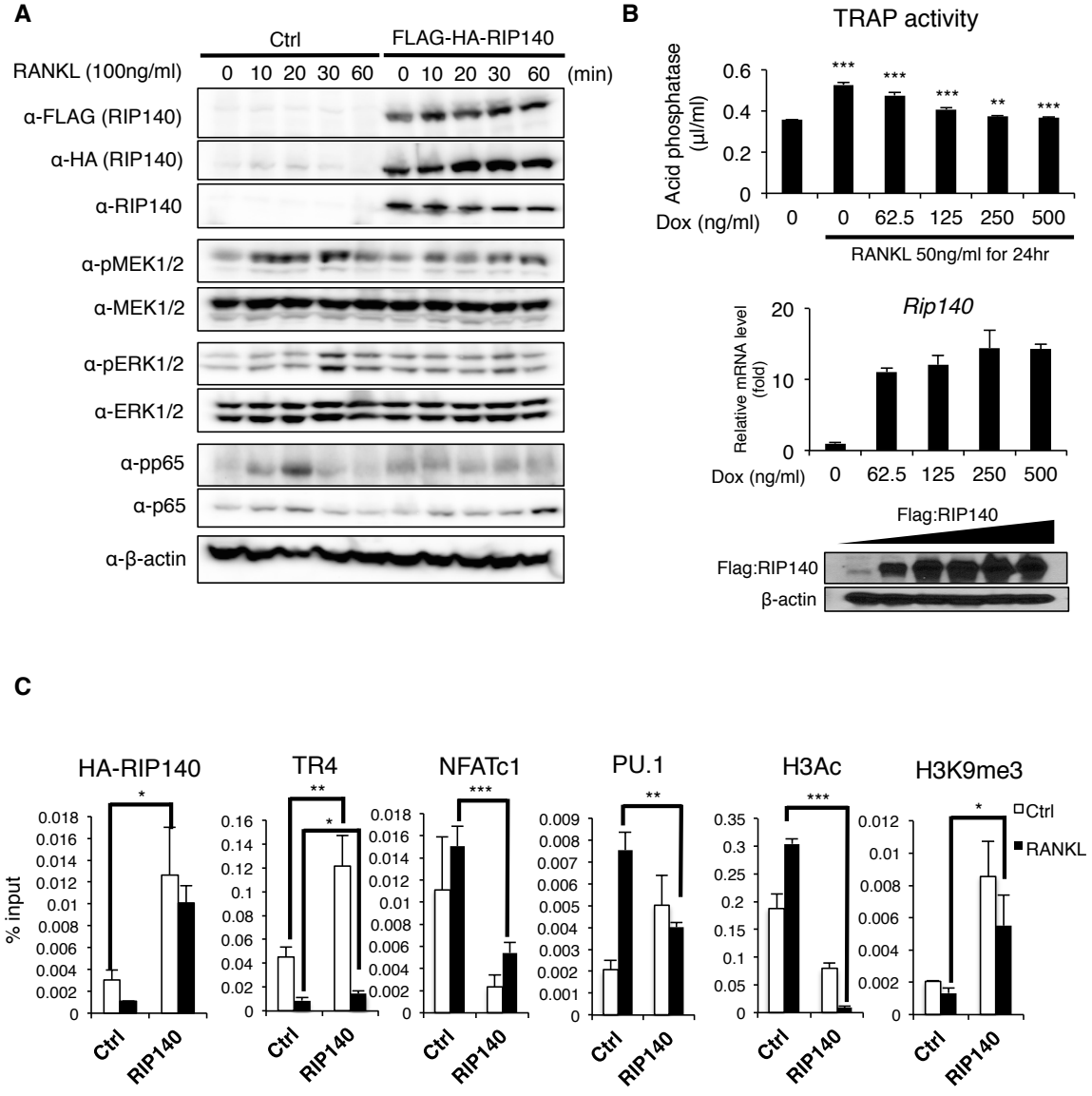
A
Ctrl
FLAG-HA-RIP140
RANKL (100ng/ml)
0 10 20 30 60 0 10 20 30 60 (min)
α-FLAG (RIP140)
α-HA (RIP140)
α-RIP140
α-pMEK1/2
α-MEK1/2
α-pERK1/2
α-ERK1/2
α-pp65
α-p65
α-β-actin
B
TRAP activity
Acid phosphatase (μl/ml)
Dox (ng/ml) 0 0 62.5 125 250 500
RANKL 50ng/ml for 24hr
Rip140
Relative mRNA level (fold)
Dox (ng/ml) 0 62.5 125 250 500
Flag:RIP140
Flag:RIP140
β-actin
C
HA-RIP140
TR4
NFATc1
PU.1
H3Ac
H3K9me3
Ctrl
RANKL
% input
Ctrl
RIP140

Figure 4-3. RIP140 suppresses RANKL signaling and transcription activation of osteoclastogenic genes

A. Western blot analyses of Flag-HA-RIP140 and MAPK/NF-kB signaling components in control vs. RIP140 overexpressing RAW264.7 cells treated with RANKL at indicated times. **B.** TRAP activity in doxycycline-induced RIP140-expressing RAW264.7 cells. **C.** ChIP assay of HA-RIP140, TR4, NFATc1, PU.1, H3Ac and H3K9me3 on Nfatc1 promoter in RANKL-treated RIP140-expressing RAW264.7 cells. Data are representative of three experimental repeats (mean ± s.d). Student's t-test (n=3) was used (*P<0.05; **P<0.01; ***P<0.001).

Figure 4-4.

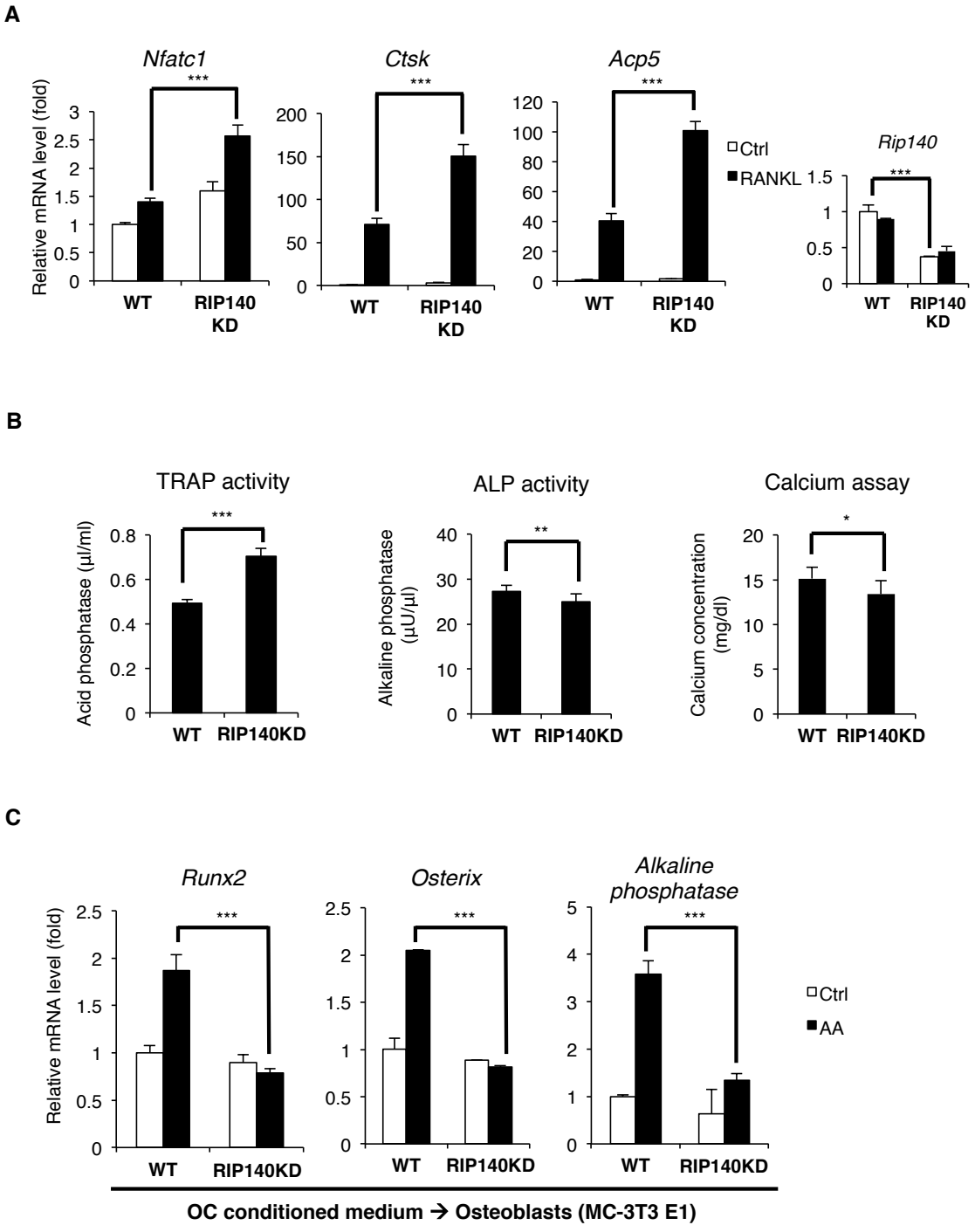
A
Nfatc1
Ctsk
Acp5
Rip140
Relative mRNA level (fold)
Ctrl
RANKL
WT
RIP140 KD
B
TRAP activity
ALP activity
Calcium assay
Acid phosphatase (μl/ml)
Alkaline phosphatase (μU/μl)
Calcium concentration (mg/dl)
WT
RIP140KD
C
Runx2
Osterix
Alkaline phosphatase
Relative mRNA level (fold)
Ctrl
AA
WT
RIP140KD
OC conditioned medium → Osteoblasts (MC-3T3 E1)

Figure 4-4. Enhancing osteoclast differentiation/activity by reducing RIP140 in animals.

A. qRT-PCR analyses of osteoclast markers in bone marrow-derived osteoclasts from WT and mϕRIP140KD mice with or without RANKL treatment. **B.** TRAP activity in bone marrow-derived osteoclasts from WT and mϕRIP140KD mice after RANKL and M-CSF treatment for 5 days (left). Serum levels of ALP (alkaline phosphatase) activity (middle) and calcium concentration (right) in WT and mϕRIP140KD mice. **C.** qRT-PCR analyses of osteoblast markers in osteoclasts differentiated (5 days) from bone marrow cells of WT and mϕRIP140KD mice. MC-3T3 E1 cells were incubated with conditioned medium from osteoclast culture, with or without ascorbic acid (AA, 50μg/ml) treatment for 3 days. Data are representative of three experimental repeats (mean ± s.d), and Student's t-test (n=3) was used (*P<0.05; **P<0.01; ***P<0.001).

Figure 4-5.

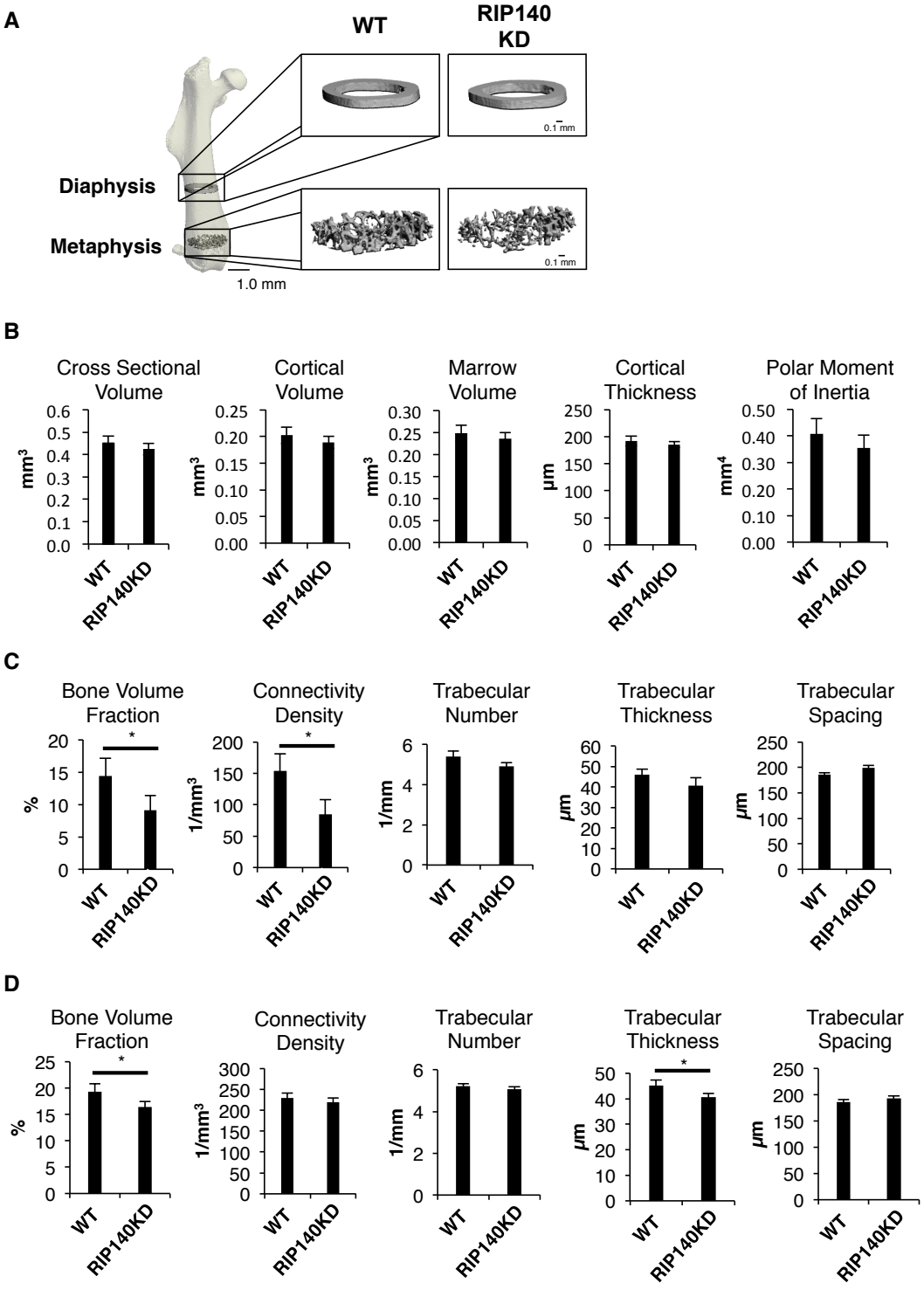
A
WT
RIP140 KD
Diaphysis
Metaphysis
0.1 mm
1.0 mm
B
Cross Sectional Volume
Cortical Volume
Marrow Volume
Cortical Thickness
Polar Moment of Inertia
mm3
mm4
µm
WT
RIP140KD
C
Bone Volume Fraction
Connectivity Density
Trabecular Number
Trabecular Thickness
Trabecular Spacing
%
1/mm3
1/mm
µm
*
D
Bone Volume Fraction
Connectivity Density
Trabecular Number
Trabecular Thickness
Trabecular Spacing

Figure 4-5. Femoral and vertebral trabecular bone is significantly decreased in mice with reduced RIP140 expression

A. Representative micro-CT images of the femoral diaphysis and metaphysis illustrating differences in trabecular bone volume fraction in 9-week-old WT and mϕRIP140KD mice. **B**. Micro-CT analysis of cortical bone in the femur diaphysis; cross-sectional volume, cortical volume, marrow volume, cortical thickness, and polar moment of inertia. **C**. Micro-CT analysis of cancellous bone in the distal femur metaphysis; bone volume fraction, connectivity density, trabecular number, thickness and spacing. **D**. Micro-CT analysis of cancellous bone in L5 vertebra; bone volume fraction, connectivity density, trabecular number, thickness and spacing. Data are presented as means ± SD (* denotes significance at $P<0.05$ n = 9–10/group).

Figure 4-6.

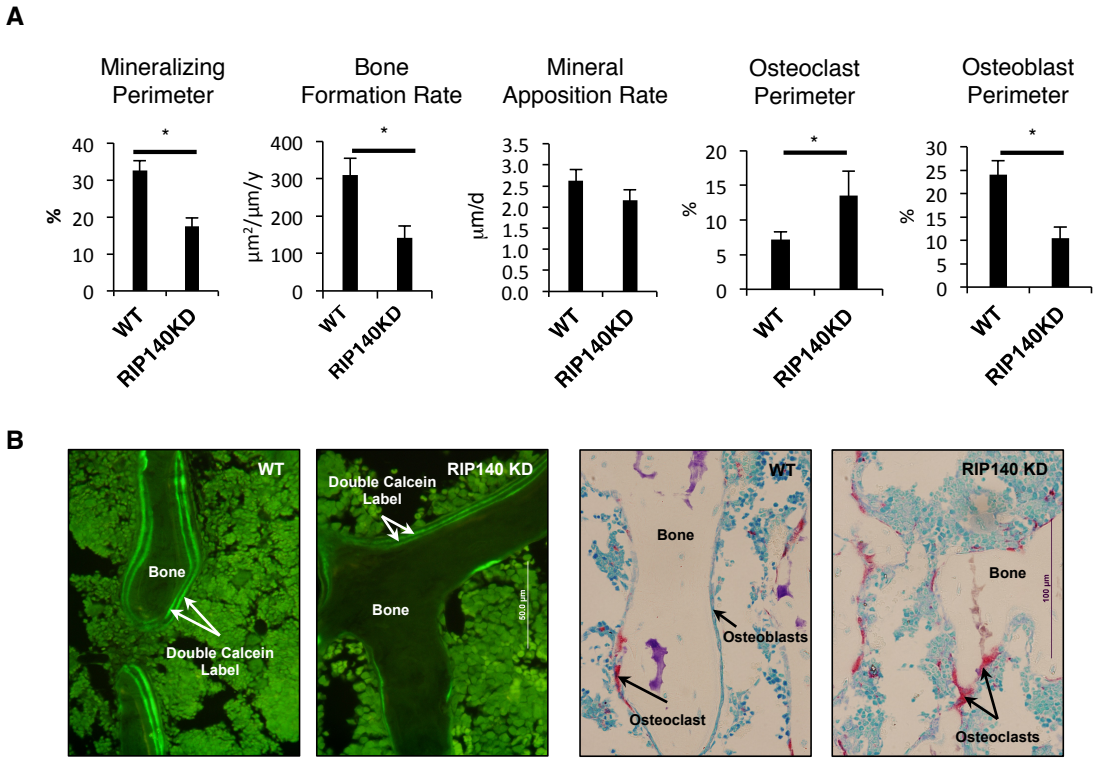

Figure 4-6. Indices of bone formation are reduced, and bone resorption increased in mice with reduced RIP140 expression

A. Indices of bone formation (mineralizing perimeter, bone formation rate, mineral apposition rate, osteoblast perimeter) and of bone resorption (osteoclast perimeter) in control and mϕRIP140KD mice at 9 weeks of age. Data are presented as mean ± SD (* denotes significance at $P<0.05$ n = 9–10/group). B. Photomicrographs illustrating differences in fluorochrome label incorporation and osteoclast perimeters in control and mϕRIP140KD mice.

Figure 4-S1.

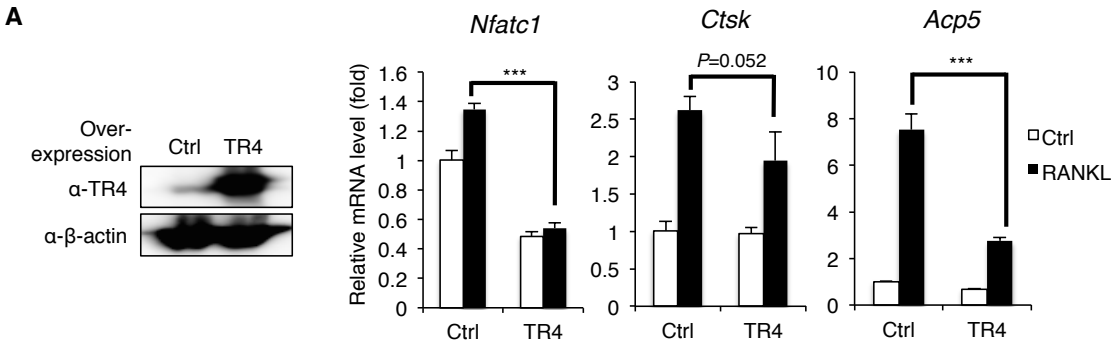

Figure 4-S1.

A. Western blot analysis of TR4 overexpression in RAW264.7 cells (left). qRT-PCR analysis of osteoclast marker genes in control overexpressing (Ctrl) or TR4 overexpressing (TR4) RAW264.7 cells with or without RANKL treatment (50ng/ml) for 24 hrs (right). Data are representative of three experimental repeats (mean ± SD), and Student's t-test (n=3) was used (*P<0.05; **P<0.01; ***P<0.001).

Figure 4-S2.

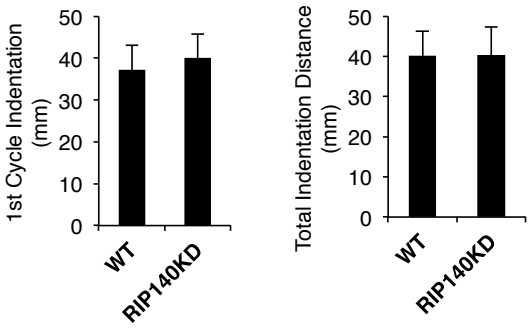

Figure 4-S2.

Reference point indentation of the tibia in WT (n=10) and mφRIP140KD (n=9) mice at 9 weeks of age. Data are mean ± SD.

Chapter V

Conclusion and Future Studies

Vitamin A and its metabolites have a variety of biological functions, thus it is not surprising RA and its derivatives have been used as therapeutics for various diseases including inflammation and cancer[175,176]. The crucial role of RA in immunity has been extensively studied in cell differentiation and functional activities of dendritic cells, T cells and B cells[11]. Moreover, the effect of RA has been reported in wound healing and anti-inflammatory responses[62]. However, the mechanistic details and the connection between functional roles and a physiological impact of RA in macrophages remain to be elucidated. Thus, the main purpose in one of my studies was to elucidate a functional role of RA in anti-inflammatory macrophages. The findings regarding the role of RA in macrophages are, 1) topical application of RA on skin improves wound healing process with increased anti-inflammatory macrophage signals, 2) RA synergistically increases Arg1 gene expression and activity with IL-4 treatment, 3) the synergism of Arg1 activation by RA and IL-4 is through MED25 that modulated chromatin remodeling and enhanced the coupling of transcription initiation and elongation, which result in the acceleration of Arg1 gene expression[177]. The provided mechanism for the synergistic activation of Arg1 by RA and IL-4 through MED25 does not exclude the idea that this synergism might also involve pre-mRNA processing. Current reports suggest that pre-mRNA splicing occurs in concert with transcription in various organisms including mammalian cells[178,179]. Key evidence for the coupling between pre-mRNA splicing and transcription is that a number of transcription factors have been functionally and physically associated with splicing altering mRNA/protein expression[180]. It will be interesting to study whether RAR and STAT6 associate with splicing factors that can be

recruited in response to IL-4 and RA signaling in order to modulate transcriptional pre-mRNA splicing process.

Recent studies uncovered that RIP140 acts as a key immune modulator affecting various cellular signaling in macrophages[22,36,37]. In these cells, RIP140 is mostly located in the nucleus and its expression is modulated by different extracellular signaling molecules including cholesterol and LPS[36,122]. One of the important findings about RIP140 in my studies is the modulatory function in macrophage phenotype switch. Based on previous studies about RIP140's role as a positive regulator in M1 macrophages, we discovered that the failure to establish RIP140 degradation-mediated ET prevents M2 activation, and the reduced RIP140 level facilitates an M1 to M2 phenotype switch improving wound repair process. These data prompted us to speculate whether RIP140 also modulates M2 macrophages during wound healing. We finally uncovered the novel function of RIP140 in IL-4-stimulated STAT6 signaling cascade in M2 macrophages; First, RIP140 translocates to the cytoplasm upon IL-4 stimulation to form a complex with cytosolic cysteine proteinase, CAPNS1. The activated calpain 1/2 by CAPNS1 then enhances PTP1B activity to dephosphorylate STAT6 resulting in suppressed M2 activation. In this study, the detailed mechanisms still remain to be proved; such as how the IL-4 signal triggers RIP140's export to the cytosol and how RIP140/CAPNS1 complex alters PTP1B activity. As we have discovered various post-translational modifications (PTMs) of RIP140 through different signaling molecules in previous studies[121], identification of RIP140-associating proteins and the altered PTMs by biochemical methods including mass spectrometry may provide more details to unravel

these questions. Moreover, RIP140's expression and dynamic functional roles in different types of macrophages arouses the possibility that it may play a role in other macrophage phenotypes, for example, tumor-associated macrophages (TAM). Given that the functional roles of RIP140 in different types of cancer have been identified[181-183], it would be interesting to study RIP140's role in TAM and TAM-medicated tumor microenvironment whether it affects tumor progression.

RIP140 functions in macrophages as a key regulator for inflammatory responses[36,81] and lipid metabolism[37,174]. Interestingly, many clinical studies have shown that patients with higher inflammatory markers or metabolic dysfunction are easily accompanied by increased bone fractures[184,185]. Moreover, numerous bone diseases, such as osteoporosis and rheumatoid arthritis, are characterized by excessively activated osteoclasts differentiated from hematopoietic macrophage/monocyte lineage cells[42]. Based on this evidence, it was hypothesized that RIP140 may have a functional role in osteoclast differentiation and activity. First, I found RIP140 formed a complex with TR4, which exerted a suppressive role for osteoclastogenesis. This repressive mechanism was validated with macrophage/monocyte-specific RIP140 KD (mϕRIP140KD) mice, which revealed an osteopenic phenotype characterized by significantly decreased trabecular bone mass, increased osteoclast number and activity, and reduced osteoblast number and activity indicating the uncoupling of osteoclasts and osteoblasts. This study uncovered a critical functional role of RIP140 in osteoclast biology contributing to the understanding of molecular mechanism in bone homeostatic control. Lastly, I conclude this study by addressing following remaining questions; first, what molecules mediate the uncoupling

of osteoclasts and osteoblasts? Second, are there any other genes targeted by TR4/RIP140 in preosteoclasts? Third, does RIP140 also have a role in osteoblasts? In order to provide evidence for these questions, these experiments are suggested; 1) Identification of the secretome from conditioned medium cultured with RIP140 overexpressed or knockdown osteoclasts by proteomics techniques including mass spectrometry, 2) whole-genome chromatin immunoprecipitation sequencing to identify RIP140's binding sites across the entire genome regions, and 3) examination of RIP140's function in preosteoblasts/osteoblasts by using RIP140 knockdown cells or osteoblasts lineage-specific RIP140 knockout mice.

The data and results generated from all these three studies shed light on the functional impact of RA and RIP140 in macrophages by providing molecular mechanisms as well as their physiological relevance in wound healing, inflammation and osteopenia. These studies will provide new insights and fundamental knowledge of RA and RIP140 in the context of biological functions in macrophages, which may fill the gaps in knowledge of macrophage biology and contribute to new therapeutic strategies for related diseases.

Bibliography

1. van Amerongen, M. J., Harmsen, M. C., van Rooijen, N., Petersen, A. H. & van Luyn, M. J. A. Macrophage depletion impairs wound healing and increases left ventricular remodeling after myocardial injury in mice. *The American Journal of Pathology* **170,** 818–829 (2007).
2. Duffield, J. S. *et al.* Selective depletion of macrophages reveals distinct, opposing roles during liver injury and repair. *Journal of Clinical Investigation* **115,** 56–65 (2005).
3. Lucas, T. *et al.* Differential roles of macrophages in diverse phases of skin repair. *The Journal of Immunology* **184,** 3964–3977 (2010).
4. Mantovani, A., Sozzani, S., Locati, M., Allavena, P. & Sica, A. Macrophage polarization: tumor-associated macrophages as a paradigm for polarized M2 mononuclear phagocytes. *Trends in Immunology* **23,** 549–555 (2002).
5. Diegelmann, R. F. & Evans, M. C. Wound healing: an overview of acute, fibrotic and delayed healing. *Front. Biosci.* **9,** 283–289 (2004).
6. Deonarine, K. *et al.* Gene expression profiling of cutaneous wound healing. *J Transl Med* **5,** 11 (2007).
7. Novak, M. L. & Koh, T. J. Macrophage phenotypes during tissue repair. *Journal of Leukocyte Biology* **93,** 875–881 (2013).
8. Wolf, G. A history of vitamin A and retinoids. *FASEB J.* **10,** 1102–1107 (1996).
9. Clagett-Dame, M. & DeLuca, H. F. The role of vitamin A in mammalian reproduction and embryonic development. *Annu. Rev. Nutr.* **22,** 347–381 (2002).
10. Duester, G. Retinoic acid synthesis and signaling during early organogenesis. *Cell* **134,** 921–931 (2008).
11. Hall, J. A., Grainger, J. R., Spencer, S. P. & Belkaid, Y. The role of retinoic acid in tolerance and immunity. *Immunity* **35,** 13–22 (2011).
12. Pino-Lagos, K., Guo, Y. & Noelle, R. J. Retinoic acid: A key player in immunity. *BioFactors* **36,** 430–436 (2010).
13. Geissmann, F. *et al.* Retinoids regulate survival and antigen presentation by immature dendritic cells. *J. Exp. Med.* **198,** 623–634 (2003).
14. Svensson, M. *et al.* Retinoic acid receptor signaling levels and antigen dose regulate gut homing receptor expression on CD8+ T cells. *Mucosal Immunol* **1,** 38–48 (2008).
15. Sun, C.-M. *et al.* Small intestine lamina propria dendritic cells promote de novo generation of Foxp3 T reg cells via retinoic acid. *J. Exp. Med.* **204,** 1775–1785 (2007).
16. Molenaar, R. *et al.* Expression of retinaldehyde dehydrogenase enzymes in mucosal dendritic cells and gut-draining lymph node stromal cells is controlled by dietary vitamin A. *The Journal of Immunology* **186,** 1934–1942 (2011).
17. Broadhurst, M. J. *et al.* Upregulation of retinal dehydrogenase 2 in alternatively activated macrophages during retinoid-dependent type-2 immunity to helminth infection in mice. *PLoS Pathog* **8,** e1002883 (2012).
18. Na, S. Y. *et al.* Retinoids inhibit interleukin-12 production in macrophages

through physical associations of retinoid X receptor and NFkappaB. *J. Biol. Chem.* **274,** 7674–7680 (1999).
19. Cavaillès, V. *et al.* Nuclear factor RIP140 modulates transcriptional activation by the estrogen receptor. *EMBO J.* **14,** 3741–3751 (1995).
20. Lee, C. H., Chinpaisal, C. & Wei, L. N. Cloning and characterization of mouse RIP140, a corepressor for nuclear orphan receptor TR2. *Mol. Cell. Biol.* **18,** 6745–6755 (1998).
21. Lee, C. H. & Wei, L. N. Characterization of receptor-interacting protein 140 in retinoid receptor activities. *J. Biol. Chem.* **274,** 31320–31326 (1999).
22. Zschiedrich, I. *et al.* Coactivator function of RIP140 for NF B/RelA-dependent cytokine gene expression. *Blood* **112,** 264–276 (2008).
23. Ho, P.-C. & Wei, L.-N. Biological activities of receptor-interacting protein 140 in adipocytes and metabolic diseases. *Curr Diabetes Rev* **8,** 452–457 (2012).
24. Nautiyal, J., Christian, M. & Parker, M. G. Distinct functions for RIP140 in development, inflammation, and metabolism. *Trends Endocrinol. Metab.* (2013). doi:10.1016/j.tem.2013.05.001
25. Thenot, S., Charpin, M., Bonnet, S. & Cavaillès, V. Estrogen receptor cofactors expression in breast and endometrial human cancer cells. *Molecular and Cellular Endocrinology* **156,** 85–93 (1999).
26. Kerley, J. S., Olsen, S. L., Freemantle, S. J. & Spinella, M. J. Transcriptional activation of the nuclear receptor corepressor RIP140 by retinoic acid: a potential negative-feedback regulatory mechanism. *Biochem. Biophys. Res. Commun.* **285,** 969–975 (2001).
27. Ho, P. C., Chang, K. C., Chuang, Y. S. & Wei, L. N. Cholesterol regulation of receptor-interacting protein 140 via microRNA-33 in inflammatory cytokine production. *The FASEB Journal* **25,** 1758–1766 (2011).
28. Vo, N., Fjeld, C. & Goodman, R. H. Acetylation of nuclear hormone receptor-interacting protein RIP140 regulates binding of the transcriptional corepressor CtBP. *Mol. Cell. Biol.* **21,** 6181–6188 (2001).
29. Gupta, P. Regulation of Co-repressive Activity of and HDAC Recruitment to RIP140 by Site-specific Phosphorylation. *Molecular & Cellular Proteomics* **4,** 1776–1784 (2005).
30. Huq, M. D. M., Tsai, N. P., Lin, Y.-P., Higgins, L. & Wei, L.-N. Vitamin B6 conjugation to nuclear corepressor RIP140 and its role in gene regulation. *Nat Chem Biol* **3,** 161–165 (2007).
31. Gupta, P. *et al.* PKCε Stimulated Arginine Methylation of RIP140 for Its Nuclear-Cytoplasmic Export in Adipocyte Differentiation. *PLoS ONE* **3,** e2658 (2008).
32. Ho, P.-C. *et al.* Modulation of lysine acetylation-stimulated repressive activity by Erk2-mediated phosphorylation of RIP140 in adipocyte differentiation. *Cellular Signalling* **20,** 1911–1919 (2008).
33. Ho, P.-C., Lin, Y.-W., Tsui, Y.-C., Gupta, P. & Wei, L.-N. A Negative Regulatory Pathway of GLUT4 Trafficking in Adipocyte: New Function of RIP140 in the Cytoplasm via AS160. *Cell Metabolism* **10,** 516–523 (2009).

34. White, R. *et al.* The nuclear receptor co-repressor nrip1 (RIP140) is essential for female fertility. *Nat Med* **6,** 1368–1374 (2000).
35. Leonardsson, G. *et al.* Nuclear receptor corepressor RIP140 regulates fat accumulation. *Proc. Natl. Acad. Sci. U.S.A.* **101,** 8437–8442 (2004).
36. Ho, P.-C., Tsui, Y.-C., Feng, X., Greaves, D. R. & Wei, L.-N. NF-κB-mediated degradation of the coactivator RIP140 regulates inflammatory responses and contributes to endotoxin tolerance. *Nat Immunol* **13,** 379–386 (2012).
37. Liu, P.-S. *et al.* Reducing RIP140 expression in macrophage alters ATM infiltration, facilitates white adipose tissue browning, and prevents high-fat diet-induced insulin resistance. *Diabetes* **63,** 4021–4031 (2014).
38. Boyle, W. J., Simonet, W. S. & Lacey, D. L. Osteoclast differentiation and activation. *Nature* **423,** 337–342 (2003).
39. Seeman, E. Bone modeling and remodeling. *Crit. Rev. Eukaryot. Gene Expr.* **19,** 219–233 (2009).
40. Sims, N. A. & Martin, T. T. J. Coupling the activities of bone formation and resorption: a multitude of signals within the basic multicellular unit. *BoneKEy Reports* **3,** 1–10 (2014).
41. Parfitt, A. M. Quantum concept of bone remodeling and turnover: implications for the pathogenesis of osteoporosis. *Calcif. Tissue Int.* **28,** 1–5 (1979).
42. Rodan, G. A. & Martin, T. J. Therapeutic approaches to bone diseases. *Science* **289,** 1508–1514 (2000).
43. Theill, L. E., Boyle, W. J. & Penninger, J. M. RANK-L and RANK: T cells, bone loss, and mammalian evolution. *Annu. Rev. Immunol.* **20,** 795–823 (2002).
44. Wiktor-Jedrzejczak, W. *et al.* Total absence of colony-stimulating factor 1 in the macrophage-deficient osteopetrotic (op/op) mouse. *Proc. Natl. Acad. Sci. U.S.A.* **87,** 4828–4832 (1990).
45. Ross, F. P. & Teitelbaum, S. L. alphavbeta3 and macrophage colony-stimulating factor: partners in osteoclast biology. *Immunol. Rev.* **208,** 88–105 (2005).
46. Asagiri, M. & Takayanagi, H. The molecular understanding of osteoclast differentiation. *Bone* **40,** 251–264 (2007).
47. Franzoso, G. *et al.* Requirement for NF-kappaB in osteoclast and B-cell development. *Genes & Development* **11,** 3482–3496 (1997).
48. Tondravi, M. M. *et al.* Osteopetrosis in mice lacking haematopoietic transcription factor PU.1. *Nature* **386,** 81–84 (1997).
49. Weilbaecher, K. N. *et al.* Linkage of M-CSF signaling to Mitf, TFE3, and the osteoclast defect in Mitf(mi/mi) mice. *Molecular Cell* **8,** 749–758 (2001).
50. Johnson, R. S., Spiegelman, B. M. & Papaioannou, V. Pleiotropic effects of a null mutation in the c-fos proto-oncogene. *Cell* **71,** 577–586 (1992).
51. Asagiri, M. *et al.* Autoamplification of NFATc1 expression determines its essential role in bone homeostasis. *J. Exp. Med.* **202,** 1261–1269 (2005).
52. Vaira, S. *et al.* RelB is the NF-kappaB subunit downstream of NIK responsible for osteoclast differentiation. *Proceedings of the National Academy of Sciences* **105,** 3897–3902 (2008).
53. Lee, J. *et al.* Id helix-loop-helix proteins negatively regulate TRANCE-mediated

osteoclast differentiation. *Blood* **107,** 2686–2693 (2006).
54. Kim, K. *et al.* MafB negatively regulates RANKL-mediated osteoclast differentiation. *Blood* **109,** 3253–3259 (2007).
55. Zhao, B. *et al.* Interferon regulatory factor-8 regulates bone metabolism by suppressing osteoclastogenesis. *Nat Med* 1–7 (2009). doi:10.1038/nm.2007
56. Sommer, A. Vitamin a deficiency and clinical disease: an historical overview. *J. Nutr.* **138,** 1835–1839 (2008).
57. Carman, J. A., Pond, L., Nashold, F., Wassom, D. L. & Hayes, C. E. Immunity to Trichinella spiralis infection in vitamin A-deficient mice. *J. Exp. Med.* **175,** 111–120 (1992).
58. Smith, S. M., Levy, N. S. & Hayes, C. E. Impaired immunity in vitamin A-deficient mice. *J. Nutr.* **117,** 857–865 (1987).
59. Verma, A. K. Retinoids in chemoprevention of cancer. *J. Biol. Regul. Homeost. Agents* **17,** 92–97 (2003).
60. Malkovský, M. *et al.* Enhancement of specific antitumor immunity in mice fed a diet enriched in vitamin A acetate. *Proc. Natl. Acad. Sci. U.S.A.* **80,** 6322–6326 (1983).
61. ABDELMALEK, M. & SPENCER, J. Retinoids and Wound Healing. *Dermatol Surg* **32,** 1219–1230 (2006).
62. Hunt, T. K. Vitamin A and wound healing. *J. Am. Acad. Dermatol.* **15,** 817–821 (1986).
63. Ulland, A. E., Shearer, J. D., Coulter, C. & Caldwell, M. D. Altered wound arginine metabolism by corticosterone and retinoic acid. *J. Surg. Res.* **70,** 84–88 (1997).
64. Ross, A. C. Vitamin A and retinoic acid in T cell-related immunity. *Am. J. Clin. Nutr.* **96,** 1166S–72S (2012).
65. Ross, A. C., Chen, Q. & Ma, Y. Vitamin A and retinoic acid in the regulation of B-cell development and antibody production. *Vitam. Horm.* **86,** 103–126 (2011).
66. Mora, J. R. *et al.* Generation of gut-homing IgA-secreting B cells by intestinal dendritic cells. *Science* **314,** 1157–1160 (2006).
67. Mucida, D. *et al.* Reciprocal TH17 and regulatory T cell differentiation mediated by retinoic acid. *Science* **317,** 256–260 (2007).
68. Iwata, M. *et al.* Retinoic acid imprints gut-homing specificity on T cells. *Immunity* **21,** 527–538 (2004).
69. Zhu, B. *et al.* IL-4 and retinoic acid synergistically induce regulatory dendritic cells expressing Aldh1a2. *The Journal of Immunology* **191,** 3139–3151 (2013).
70. Chang, J. *et al.* Retinoic acid promotes the development of Arg1-expressing dendritic cells for the regulation of T-cell differentiation. *Eur. J. Immunol.* **43,** 967–978 (2013).
71. Eriksen, A. B. *et al.* Retinoic acid enhances the levels of IL-10 in TLR-stimulated B cells from patients with relapsing-remitting multiple sclerosis. *J. Neuroimmunol.* **278,** 11–18 (2015).
72. Malik, S. & Roeder, R. G. The metazoan Mediator co-activator complex as an integrative hub for transcriptional regulation. *Nat Rev Genet* **11,** 761–772 (2010).

73. Taatjes, D. J. The human Mediator complex: a versatile, genome-wide regulator of transcription. *Trends in Biochemical Sciences* **35,** 315–322 (2010).
74. Yuan, C. X., Ito, M., Fondell, J. D., Fu, Z. Y. & Roeder, R. G. The TRAP220 component of a thyroid hormone receptor- associated protein (TRAP) coactivator complex interacts directly with nuclear receptors in a ligand-dependent fashion. *Proc. Natl. Acad. Sci. U.S.A.* **95,** 7939–7944 (1998).
75. Park, J. M. *et al.* Signal-induced transcriptional activation by Dif requires the dTRAP80 mediator module. *Mol. Cell. Biol.* **23,** 1358–1367 (2003).
76. Lee, H.-K., Park, U.-H., Kim, E.-J. & Um, S.-J. MED25 is distinct from TRAP220/MED1 in cooperating with CBP for retinoid receptor activation. *EMBO J.* **26,** 3545–3557 (2007).
77. Mikita, T., Campbell, D., Wu, P., Williamson, K. & Schindler, U. Requirements for interleukin-4-induced gene expression and functional characterization of Stat6. *Mol. Cell. Biol.* **16,** 5811–5820 (1996).
78. Gordon, S. Alternative activation of macrophages. *Nat. Rev. Immunol.* **3,** 23–35 (2003).
79. Pourcet, B. & Pineda-Torra, I. X. S. Transcriptional regulation of macrophage arginase 1 expression and its role in atherosclerosis. *Trends in Cardiovascular Medicine* **23,** 143–152 (2013).
80. Gray, M. J., Poljakovic, M., Kepka-Lenhart, D. & Morris, S. M. Induction of arginase I transcription by IL-4 requires a composite DNA response element for STAT6 and C/EBPbeta. *Gene* **353,** 98–106 (2005).
81. Lin, Y.-W., Lee, B., Liu, P.-S. & Wei, L.-N. Receptor-Interacting Protein 140 Orchestrates the Dynamics of Macrophage M1/M2 Polarization. *J Innate Immun* (2015). doi:10.1159/000433539
82. Wu, C.-Y., Feng, X. & Wei, L.-N. Coordinated repressive chromatin-remodeling of Oct4 and Nanog genes in RA-induced differentiation of embryonic stem cells involves RIP140. *Nucleic Acids Res* **42,** 4306–4317 (2014).
83. Singh, J. & Padgett, R. A. Transcription rate nsmb.1666 2009. *Nat. Struct. Mol. Biol.* **16,** 1128–1133 (2009).
84. Murray, P. J. & Wynn, T. A. Protective and pathogenic functions of macrophage subsets. *Nature Publishing Group* **11,** 723–737 (2011).
85. Fuda, N. J., Ardehali, M. B. & Lis, J. T. Defining mechanisms that regulate RNA polymerase II transcription in vivo. *Nature* **461,** 186–192 (2009).
86. Weber, C. M. & Henikoff, S. Histone variants: dynamic punctuation in transcription. *Genes & Development* **28,** 672–682 (2014).
87. Wen, H. *et al.* ZMYND11 links histone H3.3K36me3 to transcription elongation and tumour suppression. *Nature* **508,** 263–268 (2014).
88. Kim, J., Guermah, M. & Roeder, R. G. The human PAF1 complex acts in chromatin transcription elongation both independently and cooperatively with SII/TFIIS. *Cell* **140,** 491–503 (2010).
89. Elias, P. M. Epidermal effects of retinoids: supramolecular observations and clinical implications. *J. Am. Acad. Dermatol.* **15,** 797–809 (1986).
90. Hevia, O., Nemeth, A. J. & Taylor, J. R. Tretinoin accelerates healing after

trichloroacetic acid chemical peel. *Arch Dermatol* **127,** 678–682 (1991).
91. Popp, C., Kligman, A. M. & Stoudemayer, T. J. Pretreatment of photoaged forearm skin with topical tretinoin accelerates healing of full-thickness wounds. *Br. J. Dermatol.* **132,** 46–53 (1995).
92. Bronte, V., Serafini, P., Mazzoni, A., Segal, D. M. & Zanovello, P. L-arginine metabolism in myeloid cells controls T-lymphocyte functions. *Trends in Immunology* **24,** 301–305 (2003).
93. Bronte, V. & Zanovello, P. Regulation of immune responses by L-arginine metabolism. *Nat. Rev. Immunol.* **5,** 641–654 (2005).
94. Munder, M. Arginase: an emerging key player in the mammalian immune system. *Br. J. Pharmacol.* **158,** 638–651 (2009).
95. Benedit, P. *et al.* PTOV1, a novel protein overexpressed in prostate cancer containing a new class of protein homology blocks. *Oncogene* **20,** 1455–1464 (2001).
96. Mittler, G. *et al.* A novel docking site on Mediator is critical for activation by VP16 in mammalian cells. *EMBO J.* **22,** 6494–6504 (2003).
97. Boube, M., Joulia, L., Cribbs, D. L. & Bourbon, H.-M. Evidence for a mediator of RNA polymerase II transcriptional regulation conserved from yeast to man. *Cell* **110,** 143–151 (2002).
98. Rana, R., Surapureddi, S., Kam, W., Ferguson, S. & Goldstein, J. A. Med25 is required for RNA polymerase II recruitment to specific promoters, thus regulating xenobiotic and lipid metabolism in human liver. *Mol. Cell. Biol.* **31,** 466–481 (2011).
99. Jonkers, I. & Lis, J. T. Getting up to speed with transcription elongation by RNA polymerase II. *Nat. Rev. Mol. Cell Biol.* **16,** 167–177 (2015).
100. Liu, X., Kraus, W. L. & Bai, X. Ready, pause, go: regulation of RNA polymerase II pausing and release by cellular signaling pathways. *Trends in Biochemical Sciences* **40,** 516–525 (2015).
101. Nock, A., Ascano, J. M., Barrero, M. J. & Malik, S. Mediator-regulated transcription through the +1 nucleosome. *Molecular Cell* **48,** 837–848 (2012).
102. Gordon, S. & Taylor, P. R. Monocyte and macrophage heterogeneity. *Nat. Rev. Immunol.* **5,** 953–964 (2005).
103. Galli, S. J., Borregaard, N. & Wynn, T. A. Phenotypic and functional plasticity of cells of innate immunity: macrophages, mast cells and neutrophils. *Nature Publishing Group* **12,** 1035–1044 (2011).
104. Sica, A. & Mantovani, A. Macrophage plasticity and polarization: in vivo veritas. *Journal of Clinical Investigation* **122,** 787–795 (2012).
105. Mosser, D. M. & Edwards, J. P. Exploring the full spectrum of macrophage activation. *Nat. Rev. Immunol.* **8,** 958–969 (2008).
106. Mantovani, A., Biswas, S. K., Galdiero, M. R., Sica, A. & Locati, M. Macrophage plasticity and polarization in tissue repair and remodelling. *J. Pathol.* **229,** 176–185 (2013).
107. McNelis, J. C. & Olefsky, J. M. Macrophages, immunity, and metabolic disease. *Immunity* **41,** 36–48 (2014).

108. Stearns-Kurosawa, D. J., Osuchowski, M. F., Valentine, C., Kurosawa, S. & Remick, D. G. The Pathogenesis of Sepsis. *Annual Review of Pathology: Mechanisms of Disease, Vol 6* **6,** 19–48 (2011).
109. Mantovani, A. Cancer: Inflaming metastasis. *Nature* **457,** 36–37 (2009).
110. Lawrence, T. & Natoli, G. Transcriptional regulation of macrophage polarization: enabling diversity with identity. *Nat. Rev. Immunol.* **11,** 750–761 (2011).
111. Liao, X. *et al.* Krüppel-like factor 4 regulates macrophage polarization. *Journal of Clinical Investigation* **121,** 2736–2749 (2011).
112. Krausgruber, T. *et al.* IRF5 promotes inflammatory macrophage polarization and T. *Nat Immunol* **12,** 231–238 (2011).
113. Satoh, T. *et al.* Critical role of Trib1 in differentiation of tissue-resident M2-like macrophages. *Nature* **495,** 524–528 (2013).
114. Angus, D. C. & van der Poll, T. Severe Sepsis and Septic Shock. *N. Engl. J. Med.* **369,** 840–851 (2013).
115. Russell, J. A. Drug therapy: Management of sepsis. *N Engl J Med* **355,** 1699–1713 (2006).
116. Biswas, S. K. & Lopez-Collazo, E. Endotoxin tolerance: new mechanisms, molecules and clinical significance. *Trends in Immunology* **30,** 475–487 (2009).
117. West, M. A. & Heagy, W. Endotoxin tolerance: A review. *Crit. Care Med.* **30,** S64–S73 (2002).
118. Chan, C., Li, L., McCall, C. E. & Yoza, B. K. Endotoxin tolerance disrupts chromatin remodeling and NF-kappaB transactivation at the IL-1beta promoter. *J. Immunol.* **175,** 461–468 (2005).
119. Nomura, F. *et al.* Cutting edge: Endotoxin tolerance in mouse peritoneal macrophages correlates with down-regulation of surface Toll-like receptor 4 expression. *J. Immunol.* **164,** 3476–3479 (2000).
120. Kobayashi, K. *et al.* IRAK-M is a negative regulator of toll-like receptor signaling. *Cell* **110,** 191–202 (2002).
121. Huq, M. D. M., Gupta, P. & Wei, L.-N. Post-translational modifications of nuclear co-repressor RIP140: A therapeutic target for metabolic diseases. *Curr. Med. Chem.* **15,** 386–392 (2008).
122. Ho, P. C., Chang, K. C., Chuang, Y. S. & Wei, L. N. Cholesterol regulation of receptor-interacting protein 140 via microRNA-33 in inflammatory cytokine production. *The FASEB Journal* **25,** 1758–1766 (2011).
123. Pena, O. M., Pistolic, J., Raj, D., Fjell, C. D. & Hancock, R. E. W. Endotoxin tolerance represents a distinctive state of alternative polarization (M2) in human mononuclear cells. *J. Immunol.* **186,** 7243–7254 (2011).
124. Porta, C. *et al.* Tolerance and M2 (alternative) macrophage polarization are related processes orchestrated by p50 nuclear factor kappaB. *Proc. Natl. Acad. Sci. U.S.A.* **106,** 14978–14983 (2009).
125. Nathan, C. & Ding, A. Nonresolving inflammation. *Cell* **140,** 871–882 (2010).
126. Chen, J. & Ivashkiv, L. B. IFN-γ abrogates endotoxin tolerance by facilitating Toll-like receptor-induced chromatin remodeling. *Proceedings of the National*

Academy of Sciences **107,** 19438–19443 (2010).
127. Lu, X. *et al.* PTP1B is a negative regulator of interleukin 4-induced STAT6 signaling. *Blood* **112,** 4098–4108 (2008).
128. Cortesio, C. L. *et al.* Calpain 2 and PTP1B function in a novel pathway with Src to regulate invadopodia dynamics and breast cancer cell invasion. *The Journal of Cell Biology* **180,** 957–971 (2008).
129. Kuchay, S. M., Kim, N., Grunz, E. A., Fay, W. P. & Chishti, A. H. Double knockouts reveal that protein tyrosine phosphatase 1B is a physiological target of calpain-1 in platelets. *Mol. Cell. Biol.* **27,** 6038–6052 (2007).
130. Arthur, J. S., Elce, J. S., Hegadorn, C., Williams, K. & Greer, P. A. Disruption of the murine calpain small subunit gene, Capn4: calpain is essential for embryonic development but not for cell growth and division. *Mol. Cell. Biol.* **20,** 4474–4481 (2000).
131. Zimmerman, U. J., Boring, L., Pak, J. H., Mukerjee, N. & Wang, K. K. The calpain small subunit gene is essential: its inactivation results in embryonic lethality. *IUBMB Life* **50,** 63–68 (2000).
132. Feng, X. *et al.* Receptor-interacting protein 140 attenuates endoplasmic reticulum stress in neurons and protects against cell death. *Nature Communications* **5,** 4487 (2014).
133. Chernoff, J. Protein tyrosine phosphatases as negative regulators of mitogenic signaling. *J. Cell. Physiol.* **180,** 173–181 (1999).
134. Bence, K. K. *et al.* Neuronal PTP1B regulates body weight, adiposity and leptin action. *Nat Med* **12,** 917–924 (2006).
135. Lantz, K. A. *et al.* Inhibition of PTP1B by trodusquemine (MSI-1436) causes fat-specific weight loss in diet-induced obese mice. *Obesity (Silver Spring)* **18,** 1516–1523 (2010).
136. Cho, H. Protein tyrosine phosphatase 1B (PTP1B) and obesity. *Vitam. Horm.* **91,** 405–424 (2013).
137. Parfitt, A. M. The coupling of bone formation to bone resorption: a critical analysis of the concept and of its relevance to the pathogenesis of osteoporosis. *Metab Bone Dis Relat Res* **4,** 1–6 (1982).
138. Martin, T. J. & Sims, N. A. Osteoclast-derived activity in the coupling of bone formation to resorption. *Trends Mol Med* **11,** 76–81 (2005).
139. Cummings, S. R. *et al.* Risk factors for hip fracture in white women. Study of Osteoporotic Fractures Research Group. *N Engl J Med* **332,** 767–773 (1995).
140. Lecka-Czernik, B. & Rosen, C. J. Energy Excess, Glucose Utilization, and Skeletal Remodeling: New Insights. *J. Bone Miner. Res.* **30,** 1356–1361 (2015).
141. Compston, J. E. *et al.* Relationship of weight, height, and body mass index with fracture risk at different sites in postmenopausal women: the Global Longitudinal study of Osteoporosis in Women (GLOW). *J. Bone Miner. Res.* **29,** 487–493 (2014).
142. Teitelbaum, S. L. Bone Resorption by Osteoclasts. *Science* **289,** 1504–1508 (2000).
143. Yoshida, H. *et al.* The murine mutation osteopetrosis is in the coding region of

the macrophage colony stimulating factor gene. *Nature* **345,** 442–444 (1990).
144. Dougall, W. C. *et al.* RANK is essential for osteoclast and lymph node development. *Genes & Development* **13,** 2412–2424 (1999).
145. Cornier, M.-A. *et al.* The Metabolic Syndrome. *Endocrine Reviews* **29,** 777–822 (2008).
146. Alberti, K. G. M. M. *et al.* Harmonizing the metabolic syndrome: a joint interim statement of the International Diabetes Federation Task Force on Epidemiology and Prevention; National Heart, Lung, and Blood Institute; American Heart Association; World Heart Federation; International Atherosclerosis Society; and International Association for the Study of Obesity. in **120,** 1640–1645 (2009).
147. Kaur, J. A Comprehensive Review on Metabolic Syndrome. *Cardiology Research and Practice* **2014,** 1–21 (2014).
148. Vestergaard, P. Discrepancies in bone mineral density and fracture risk in patients with type 1 and type 2 diabetes - a meta-analysis. *Osteoporos Int* **18,** 427–444 (2007).
149. Kawai, M., de Paula, F. J. A. & Rosen, C. J. New insights into osteoporosis: the bone-fat connection. *J. Intern. Med.* **272,** 317–329 (2012).
150. Zhang, P., Peterson, M., Su, G. L. & Wang, S. C. Visceral adiposity is negatively associated with bone density and muscle attenuation. *Am. J. Clin. Nutr.* **101,** 337–343 (2015).
151. Krakauer, J. C. *et al.* Bone loss and bone turnover in diabetes. *Diabetes* **44,** 775–782 (1995).
152. Lumeng, C. N., Bodzin, J. L. & Saltiel, A. R. Obesity induces a phenotypic switch in adipose tissue macrophage polarization. *Journal of Clinical Investigation* **117,** 175–184 (2007).
153. Huq, M. D. M., Gupta, P., Tsai, N. P. & Wei, L.-N. Modulation of testicular receptor 4 activity by mitogen-activated protein kinase-mediated phosphorylation. *Mol. Cell Proteomics* **5,** 2072–2082 (2006).
154. Collins, L. L. *et al.* Growth retardation and abnormal maternal behavior in mice lacking testicular orphan nuclear receptor 4. *Proc. Natl. Acad. Sci. U.S.A.* **101,** 15058–15063 (2004).
155. Morón, F. J. *et al.* Multilocus analysis of estrogen-related genes in Spanish postmenopausal women suggests an interactive role of ESR1, ESR2 and NRIP1 genes in the pathogenesis of osteoporosis. *Bone* **39,** 213–221 (2006).
156. van den Berg, D. L. C. *et al.* An Oct4-Centered Protein Interaction Network in Embryonic Stem Cells. *Stem Cell* **6,** 369–381 (2010).
157. Choi, S. H. *et al.* DUX4 recruits p300/CBP through its C-terminus and induces global H3K27 acetylation changes. *Nucleic Acids Res* **44,** 5161–5173 (2016).
158. Philbrick, K. A., Turner, R. T., Branscum, A. J., Wong, C. P. & Iwaniec, U. T. Paradoxical effects of partial leptin deficiency on bone in growing female mice. *Anat Rec (Hoboken)* **298,** 2018–2029 (2015).
159. Iwaniec, U. T., Wronski, T. J. & Turner, R. T. Histological analysis of bone. *Methods Mol. Biol.* **447,** 325–341 (2008).
160. Dempster, D. W. *et al.* Standardized nomenclature, symbols, and units for bone

histomorphometry: a 2012 update of the report of the ASBMR Histomorphometry Nomenclature Committee. *J. Bone Miner. Res.* **28,** 2–17 (2013).
161. Cuetara, B. L. V., Crotti, T. N., O'Donoghue, A. J. & McHugh, K. P. Cloning and characterization of osteoclast precursors from the RAW264.7 cell line. *In Vitro Cell. Dev. Biol. Anim.* **42,** 182–188 (2006).
162. Lee, Y. F., Young, W. J., Burbach, J. P. & Chang, C. Negative feedback control of the retinoid-retinoic acid/retinoid X receptor pathway by the human TR4 orphan receptor, a member of the steroid receptor superfamily. *J. Biol. Chem.* **273,** 13437–13443 (1998).
163. Gingery, A. *et al.* TGF-beta coordinately activates TAK1/MEK/AKT/NFkB and SMAD pathways to promote osteoclast survival. *Exp. Cell Res.* **314,** 2725–2738 (2008).
164. Takayanagi, H. *et al.* Induction and activation of the transcription factor NFATc1 (NFAT2) integrate RANKL signaling in terminal differentiation of osteoclasts. *Dev. Cell* **3,** 889–901 (2002).
165. Kim, H.-H. *et al.* Association of sustained ERK activity with integrin beta3 induction during receptor activator of nuclear factor kappaB ligand (RANKL)-directed osteoclast differentiation. *Exp. Cell Res.* **289,** 368–377 (2003).
166. Chen, Y. & Xia, R. G. Screening and functional microarray analysis of differentially expressed genes related to osteoporosis. *Genet. Mol. Res.* **13,** 3228–3236 (2014).
167. Mendoza, N. *et al.* Estrogen-related genes and postmenopausal osteoporosis risk. *Climacteric* **15,** 587–593 (2012).
168. Piao, H., Chu, X., Lv, W. & Zhao, Y. Involvement of receptor-interacting protein 140 in estrogen-mediated osteoclasts differentiation, apoptosis, and bone resorption. *J Physiol Sci* (2016). doi:10.1007/s12576-016-0447-2
169. Lin, S.-J. *et al.* Reduced osteoblast activity in the mice lacking TR4 nuclear receptor leads to osteoporosis. *Reprod. Biol. Endocrinol.* **10,** 43 (2012).
170. Novack, D. V. & Mbalaviele, G. Osteoclasts-Key Players in Skeletal Health and Disease. *Microbiol Spectr* **4,** (2016).
171. Miyauchi, Y. *et al.* The Blimp1-Bcl6 axis is critical to regulate osteoclast differentiation and bone homeostasis. *J. Exp. Med.* **207,** 751–762 (2010).
172. Zhao, B. & Ivashkiv, L. B. Negative regulation of osteoclastogenesis and bone resorption by cytokines and transcriptional repressors. *Arthritis Res. Ther.* **13,** 234 (2011).
173. Mundy, G. R. Osteoporosis and inflammation. *Nutr. Rev.* **65,** S147–51 (2007).
174. Lin, Y.-W., Liu, P.-S., Adhikari, N., Hall, J. L. & Wei, L.-N. RIP140 contributes to foam cell formation and atherosclerosis by regulating cholesterol homeostasis in macrophages. *Journal of Molecular and Cellular Cardiology* **79,** 287–294 (2015).
175. Stephensen, C. B. V ITAMINA, I NFECTION, ANDI MMUNEF UNCTION*. *Annu. Rev. Nutr.* **21,** 167–192 (2001).
176. Coco, Lo, F., Pelicci, P. G. & Biondi, A. Clinical relevance of the PML/RAR-a

gene rearrangement in acute promyelocytic leukaemia. *Leuk. Lymphoma* **12,** 327–332 (1994).
177. Lee, B., Wu, C.-Y., Lin, Y.-W., Park, S. W. & Wei, L.-N. Synergistic activation of Arg1 gene by retinoic acid and IL-4 involves chromatin remodeling for transcription initiation and elongation coupling. *Nucleic Acids Res* (2016). doi:10.1093/nar/gkw392
178. Brugiolo, M., Herzel, L. & Neugebauer, K. M. Counting on co-transcriptional splicing. *F1000Prime Rep* **5,** 9 (2013).
179. Pandya-Jones, A. Pre-mRNA splicing during transcription in the mammalian system. *WIREs RNA* **2,** 700–717 (2011).
180. Montes, M., Becerra, S., Sánchez-Álvarez, M. & Suñé, C. Functional coupling of transcription and splicing. *Gene* **501,** 104–117 (2012).
181. Rosell, M. *et al.* Complex formation and function of estrogen receptor α in transcription requires RIP140. *Cancer Res.* **74,** 5469–5479 (2014).
182. Lapierre, M. *et al.* The emerging role of the transcriptional coregulator RIP140 in solid tumors. *Biochim. Biophys. Acta* **1856,** 144–150 (2015).
183. Zhang, D. *et al.* Downregulation of RIP140 in hepatocellular carcinoma promoted the growth and migration of the cancer cells. *Tumour Biol.* **36,** 2077–2085 (2015).
184. Schwartz, A. V. *et al.* Older women with diabetes have an increased risk of fracture: a prospective study. *J. Clin. Endocrinol. Metab.* **86,** 32–38 (2001).
185. Cauley, J. A. *et al.* Inflammatory markers and incident fracture risk in older men and women: the Health Aging and Body Composition Study. *J. Bone Miner. Res.* **22,** 1088–1095 (2007).